UNIVERSIDAD DE GUANAJUATO

CAMPUS IRAPUATO-SALAMANCA
DIVISIÓN DE INGENIERÍAS

"Emotion Recognition Using Electroencephalogram Signals Through Bicomplex Quaternion-Based Processing"

TESIS

QUE PARA OBTENER EL GRADO DE:

DOCTOR EN INGENIERÍA ELÉCTRICA

PRESENTA:

M. I. OSCAR ALMANZA-CONEJO

Director:

Dr. Mario Alberto Ibarra Manzano

Codirector:

Dr. Arturo García Pérez

Salamanca, Guanajuato **Septiembre, 2025**

Dedication

A mis Padres:
Por tan valiosas lecciones y
fortaleza durante toda mi vida.

Personal acknowledgements

Saber que existe el dolor no es aterrador.
Lo que es aterrador es saber que no puedes volver
a la felicidad que desperdiciaste.
Matsumoto Rangiku, Bleach.

A mis padres: ¿de qué manera agradecer treinta y tres años de vida? No alcanzan las palabras; todo cuanto soy es por ustedes. Gracias por su fortaleza, dedicación, trabajo y la formación que me dieron. Gracias en esta y en todas mis vidas. Gracias por cada día. Gracias por el techo que hubo siempre sobre mí durante tantos años. Pero sobre todas las cosas, les agradezco que sigan con vida, sobre todo a ti Mamá; has luchado como siempre lo hiciste, FUERTE. Papá, gracias por darme el ejemplo de una vida de trabajo. Es debido a ello que hoy estoy aquí bajo todos estos pequeños éxitos. Gracias a ambos.

Gracias a mi hermana y a mi sobrino Gael que complementan mi vida. Gracias Karen por tanto y tanto apoyo, tengo que agradecerte que indirectamente has unido a la familia, al dar a luz al ser humano más maravilloso que hay en esta familia. Gracias por las peleas y las risas al ser cómplices de una vida.

Agradezco profundamente también a toda mi familia. A los colegas que se volvieron amigos y a los amigos que se volvieron familia. Gracias por todo. Agradecimientos especiales a los compañeros con los que he compartido gratos momentos desde la maestría; todos forman parte esencial en este viaje. Mención especial para mis colegas Verónica Hernández, Marco Antonio Contreras Terán, Fernando Daniel Hernández y Juan José Cárdenas, quienes me han apoyado en todo momento y han estado ahí en las buenas y en las malas. Gracias por su amistad y por su apoyo incondicional.

Finalmente, gracias al Dr. Mario Alberto porque más allá de ser un excelente profesor y asesor, eres un gran ser humano. Gracias por creer en mí.

Profesional acknowledgements

En primer lugar, agradezco profundamente a mi director de tesis, Dr. Mario Alberto Ibarra Manzano, por su guía rigurosa, su paciencia y su confianza en mi trabajo. Sus observaciones puntuales, su visión crítica y su ejemplo de integridad académica fueron determinantes para dar forma a cada etapa de esta investigación. Gracias por abrirme espacios de discusión, por impulsar altos estándares y por enseñarme que la ciencia se hace con método, curiosidad y ética.

Deseo expresar un reconocimiento especial al Dr. Juan Gabriel Aviña Cervantes, cuyas clases y tutorías me proporcionaron técnicas clave de investigación y un sólido desarrollo metodológico para el cumplimiento de las investigaciones realizadas en esta etapa. Su orientación fortaleció la estructura de este trabajo, mejoró la calidad de los resultados y me inculcó disciplina, claridad conceptual y rigor en cada decisión metodológica.

Extiendo mi gratitud a los y las sinodales de este trabajo de tesis: Dr. Juan Carlos Gómez Carranza, Dr. José Ruiz Pinales, Dr. Carlos Andrés Pérez Ramírez y la Dra. Laura Ivoone Garay Jiménez, por la lectura minuciosa del manuscrito, sugerencias y recomendaciones que enriquecieron sustancialmente la claridad teórica, metodológica y experimental de este estudio.

A mis profesoras y profesores del programa, les debo una formación sólida. Los cursos y seminarios bajo su enseñanza ampliaron mis horizontes y me brindaron las herramientas para abordar el problema de investigación. Aprecio en particular los aprendizajes del Dr. José Amparo Andrade Lúcio, Dr. Oscar Ibarra Manzano, Dr. Arturo García Pérez, y demás implicados en esta formación, cuyas clases y consejos siguen orientando mi práctica académica.

Este logro es, en buena medida, fruto del esfuerzo compartido con una comunidad que apuesta por el conocimiento con responsabilidad social. Me comprometo a honrar ese legado en mi desempeño profesional, procurando contribuir con rigor, colaboración y respeto a nuestra disciplina.

Institutional Acknowledgements

This thesis project was partially funded by the

- **Secretaría de Ciencia, Humanidades, Tecnología e Innovación (SECIHTI)** for supporting my doctoral studies with funding under the scholarship number **CVU: 1007303**.

Ciencia y Tecnología
Secretaría de Ciencia, Humanidades, Tecnología e Innovación

- **To the Division of Engineering, Irapuato-Salamanca Campus** of the University of Guanajuato for providing the necessary tools to accomplish this study. Special thanks to the Graduate Program in Electrical Engineering and Eelectronics Engineering department. To the Digital Signal Processing and Telematics laboratories for the workspace and equipment provided in the development of this thesis work.

UNIVERSIDAD DE GUANAJUATO

Abstract

By the time when our predecessors learned to walk upright, a human evolution process began and the social context get stronger until the *Homo sapiens* evolved and interacted in social events. This social behaviour affected the biology of the humans' brain until presented a drastic change in the subcortical limbic structure emerging new capacities for the nervous system. Nowadays, human emotions significantly influence individual and social interactions, becoming crucial in medical, security, psychological, psychiatric, and educational environments. In this study, an emotion recognition approach is proposed by using a modify Quaternion Signal Analysis algorithm following the bicomplex quaternion form introduced by Cayley-Dixon. This Bicomplex Quaternion Signal Analysis (bQSA) is developed by taking the electroencephalogram (EEG) information of five different emotion recognition databases. Following a channel selection method to find the top-four effective channels per dataset, the bQSA is constructed in order to propose a novel EEG signal processing method and computing their statistical features to feed several machine learning models and testing the performance in two quaternion produc types: (1) the bicomplex and (2) the quaternion. As results, this method highlights that bicomplex product is slightly accurate than the quaternion form in three out of five tested datasets, achieving the kNN and Tree-based kernels as the top classifiers in eight out of ten (two product types signal processing per dataset) cross-validation models. A tree-way Analysis of Variance test suggested that the interaction among product type, machine learning model, and dataset significantly affects classification performance ($p < 0.00001$). Finally, prior literature typically emphasizes fronto-temporal brain regions as crucial for emotion recognition, this approach identifies a significant relationship among fronto-temporal-parietal regions based on the selected effective channels. Numerical results followed a 10-fold cross-validation to increase the reliability of the Bicomplex Quaternion Signal Analysis and positioning this electroencephalogram signal processing method as one of the top approaches in the current state-of-the-art.

Contents

List of Figures

List of Tables

Chapter 1

Introduction

A detailed understanding of the emotional brain has been made since *Homo* lineage started to pronounce a complex consciousness (LeDoux and Brown (2017)). Communication and decision-making are highly influential aspects of daily life that significantly shape human behavior. In this regard, neurophysiological response plays an essential role in a survival and evolutionary context (Gupta et al. (2019)). According to LeDoux and Brown (2017), emotions like fear elicit a physiological response primarily centered in the amygdala in the presence of threats. Accordingly, it is also important to emphasize that emotions are highly affected by the psychological state of a subject, yielding negative or positive emotions. For instance, Silard and Dasborough (2021) remarks that negative emotions are highly associated with physical or psychological distress. In contrast, positive emotions are related to mental states of high arousal and high emotional valence.

According to Egger et al. (2019), both non-physiologic —– words, facial expressions, vocal tone, and body language —– and physiologic modalities — as heart rate, skin conductance, retinal motion, and brain activity — reflect emotional states that can be measured with sensors and cameras, among others. Non-psychological modalities have been broadly used in Emotion Recognition (ER) applications due to their capacity to capture humans' superficial behaviour; accurate applications have been developed in fields such as computer vision (Naga et al. (2023)), speech recognition (Singh and Goel (2022)), and motion analysis (Ahmed et al. (2020)). However, physiological modalities have been limited due to their complexity by capturing Central Nervous System (CNS) and Peripheral Nervous System (PNS) information. In a neurological sense, Šimić et al. (2021) remarked the influence of CNS and PNS; the former remarks the importance of a continuous physiological collection,

processing, and integration of the internal body state of humans — temperature, heart rate, blood pressure, among others — to keep homeostasis internal behavior to survive. The latter is responsible for sensoring information such as pain, heat, or cold to trigger and transmit those stimuli to the CNS. Here, the Somatic Maker Hypothesis (SMH) by Damasio (1996) where it is mentioned that the amygdala is the key place where CNS triggers somatic states — bodily conditions in response to emotional stimuli — to produce more accurate emotions than just the primary ones. In the words of Ekman (1992b), the primary emotions theory is based on a culture and demographic independence; anger, fear, joy, sadness, disgust, and surprise are the somatic states listed in Ekman's theory and expressed in the first six months of a newborn's life. These primary emotions considered the following distinctive characteristics: (1) emotions must be instinctive; (2) people in the environment present the same emotions; (3) people express these basic emotions similarly; finally, (4) the physiological pattern remains in dissimilar people when one of the primary emotions is triggered. Consequently, analyzing physiologic signals is essential due to their ability to record central and peripheral nervous system changes. In this regard, Electroencephalogram (EEG) signals have been used to classify accurately the primary and primitive emotions with Machine Learning (ML) and Deep Learning (DL) applications (Hosseini et al. (2021)) by recording the neurophysiological bioelectrical potential for human's brain using, typically, a 10-20 electrode scalp.

In order to create a novel approach to studying human emotions, two types of ER model frameworks have been introduced: the primary and primitive. The former is presented above — such as happiness and fear emotions — and the latter involves the hedonic pleasantness or unpleasantness of emotions — valence — and the physiological arousal at the stimuli response (see Jackson et al. (2019)). In general, primitive emotion techniques are based on classifying the subjects' self-assessed magnitude of valence and arousal stimuli, and some other studies propose operating the stimuli subjects' domain. Recently, Işık et al. (2023) suggested a Valence-Arousal-Dominance (VAD) classification space for analyzing unbalanced feature data for denoising EEG. Besides, Doma and Pirouz (2020) chunk the EEG record into four sets per minute, improving the classification results in a VAD space. Similarly, Islam et al. (2021) performed a channel correlation matrix based on the α, β, and γ EEG sub-frequency bands of the Pearson coefficient to reduce the feature matrix dimension and computational complexity in a 2-D space Valence-Arousal (VA) DL architecture. In close connection, Fang et al. (2021) analyzed the novel tendency to use raw EEG as input to a deep forest classifier, concluding that such a framework does not substantially increase the accuracy rate, suggesting a prior feature extraction from EEG to feed the deep forest architecture. These studies were designed

and validated using the Database for Emotion Analysis Using Physiological Signals (DEAP) dataset (developed by Koelstra et al. (2012)). Conversely, the Affect, Personality, and Mood Research on Individuals and Groups (AMIGOS) dataset by Miranda-Correa et al. (2021) recently performed similar studies to record EEG signals from 40 subjects to measure emotional activity and become the baseline for recent research. Employing this dataset, V. and Bhat. (2022) highlighted the advantages of using ResNet-18 as a feature extractor to target a 3D classification space for VAD using T7, T8, F7, and F8 electrodes as input to the AdaBoost Decision Tree (EBT). Similarly, Topic and Russo (2021) in the VA space, highlighting the use of topographic and holographic spectral distribution images from EEG in future applications for people with disabilities and neuroimaging.

In a similar context to primitive emotions, primary or discrete emotions are triggered and modulated by the amygdala and hippocampus, avoiding the degree of self-assessed stimuli in primitive emotions. In this regard, Yang et al. (2020) showed a high correlation of the γ band (> 30 Hz) with increased brain activity in EEG. This Gamma Band Activity (GBA) is highly correlated with the amygdala, Orbitofrontal Cortex (OFC), and ventromedial Prefrontal Cortex (vmPFC) in affective studies. Indeed, the amygdala showed an increased magnitude in the γ-band during the emotion stimuli (Sonkusare et al. (2022)). Besides, Bechara and Damasio (2005) used the SMH to emphasize the amygdala's role and vmPFC in generating secondary emotions. Hence, the subjects' experience is based on physio-psychological previous events and provides information to develop a more accurate emotion than the primary ones. Alternatively, Albert et al. (2010) established the importance of the FC1 and CZ electrodes scalp in EEG for emotional stimuli detection.

All these previous ER techniques provides a specific research goal based on different ER-EEG databases, signal processing, feature extraction, and Artificial Intelligence (AI) approaches. In this respect, this research introduces a novel signal processing technique based on the quaternion algebra proposed initially by Hamilton (1844), denoted as $\{q \in \mathbb{H}\}$, where $q = a + b\boldsymbol{i} + c\boldsymbol{j} + d\boldsymbol{k}$, with $\{a, b, c, d \in \mathbb{R}\}$, and $\{\boldsymbol{i}, \boldsymbol{j}$, and $\boldsymbol{k} \in \mathbb{C}\}$ following up the classical complex variable algebra. To mention a couple of quaternion approaches, Contreras-Hernandez et al. (2019) proved the Quaternion Signal Analysis (QSA) performance by computing the $q(t)$ and $q(t + \Delta t)$ quaternion sequence as well as performing a rotation to classify three different induction motor failure states. Similarly, Batres-Mendoza et al. (2016) achieved high binary classification using an efficient feature extractor based on the quaternion rotation for the left and right motor imagery experiments. In this order of ideas, this protocol takes the Bicomplex Quaternion Signal Analysis (bQSA) product criteria proposed by Ell

et al. (2014), following the Cayley-Dickson form, by using a subset of four Effective Channels (EC) of an emotion recognition dataset. The method will be explained widespread in the following sections.

This brief introduction to ER will be taken in extensive in the following background section, where sociology, neuroscience, signal processing, and AI influence to ER will be discussed. In this respect, the justification, hypothesis, and research objectives are outlined below.

1.1 Justification

In recent years, the number of individuals experiencing emotional or mental disorders has significantly increased. To overcome the limitations of non-physiological signals, such as facial expressions, motion, or voice recognition —— which are susceptible to subjects' self-production, lack accurate physiological information, and research bias —— primary human subject-based emotion recognition studies using EEG focus on analyzing peripheral and central nervous system information. This approach provides more reliable data for mental or emotional disorders, stress, and anxiety early diagnosis. Conditions like Alzheimer's and Parkinson's disease, which can alter emotional and brain activity, may also be detected and studied using electroencephalograms. Emotion recognition applications extend beyond healthcare. For instance, monitoring students' emotions can help to improve and personalize learning tasks, preventing disengagement and frustration episodes from an early age. Similarly, adaptive media and brain responses to music, videos, virtual reality, or gaming experiences can be optimized based on emotional feedback. High-security applications, such as biometric authentication, lie detection, and deception detection, also stand to benefit significantly from emotion recognition technologies.

These examples highlight the need for emotion-recognition scientific tools to identify the emotions that a person genuinely experiences under specific conditions or scenarios. Consequently, developing more accurate emotion recognition technologies is essential to reduce personal or social risks.

1.2 Hypothesis

The combination of digital signal processing and quaternion algebra techniques applied to EEG signals will improve the machine learning performance of emotion recognition in comparison to the state-of-the-art methods.

1.3 Objectives

1.3.1 Overall objective

Develop and design a methodology based on digital signal processing and quaternion algebra applied to electroencephalogram signals and a machine learning or deep learning model to classify human emotions.

1.3.2 Specific objectives

1. Find and use an EEG database that models human emotions based on the acquisition of brain's bioelectrical potential activity in test subjects.
2. Find a reduced set of electroencephalogram channels to construct a quaternion-based signal processing algorithm for emotion recognition databases.
3. Identify the most relevant brain's lobes according to the channel selection method and encompass the results with the literature information.
4. Adapt and apply the digital signal processing and quaternion algebra to a set of EEG signals in the context of human emotions recognition.
5. Evaluate the performance of digital signal processing and quaternion algebra in multiple artificial intelligence algorithms.
6. Evaluate and perform the feature extraction on EEG signals using time-frequency domain features or CNNs.

1.4 Background

Discussing human evolution encompasses events before sociology. Initially, hominids moved using arms and legs. Later, an upright stance was needed to see prey and predators, which eventually led hands-free to pick up, hold, and carry food. Then, the Turner (1996) research unveils that, after years of evolution, the neocortex presented a dramatic size increasing and complexity, developing a limbic system, where emotions are activated as a rapid response to social interactions. According to Turner (2000), once social environments became part of hominids' daylife, their brains suffered subcortical limbic structure changes to learn a wide variety of emotions. Taking a crucial advantage from other hominids and evolving to the *Homo* lineage.

Then, moving forward in time to more recent years, in the last century Ekman (1992a) described a theory of six basic emotions based on facial expression studies: happiness, surprise, fear, sadness, anger, and disgust, as the primary ones. However, before introducing this primary emotions in Ekman's theory, more topics are needed to board related emotion recognition theory.

First, people use the words "emotions" and "feelings" in the same way and, even if they are related, are not the same. According to Pace-Schott et al. (2019), there are some important definitions and differences between both; the former has been defined by Damasio and Carvalho (2013) as programmed neural response evolved as an adaptive function to trigger changes in the brain. An emotion shapes as feeling, stimuli, cognition, or cognitive process. The latter is referred to as a subjective experience perception of a particular emotion that comes from afferent information triggered by peripheral receptors (temperature, pain, among others). In the same order of ideas, Hansen (2005) pointed out emotions as primitive, fast, and unconscious mechanisms that controls individual stimuli-responses to different situations. In contrast, he established feelings as cognitive perceptions to describe a non-cognitive emotional stimuli. Another confusion comes when "emotion" and "mood" are called; here, Pace-Schott takes the Kaplan et al. (2016) theory, remarking that their main differences is the duration and magnitude, bearing emotion as a *phasic* (fast and concise) response. However, it is not possible to compute a threshold between them. In short, emotions are fast, intrinsic, and unconscious emotional perceptions; meanwhile feeling is the term that can be associated with a conscious perception and an easier nomenclature for describing them.

Now, if the language and culture is taken in count, the emotion, feeling, and mood terms take a higher context. As introduced previously, cultural evolution outperforms the emotional

context, yielding a robust meaning for that kind of stimuli. Hence, related to culture expansion, the language influence is remarkable, making language promising for analyzing how similar or different the emotional experiences are for different subjects. Jackson et al. (2019) introduced a study based in *colexification* — instances where two or more concepts are expressed with the same word —– showing a global colexification network. The study found that words like "joy," "happy," "love," "sad," "worry," "fear," "surprise," and "anxiety" have stronger network connections, indicating that several cultures or linguistic families possess a higher degree of colexification associated with these emotional terms. Also, their findings suggested that most family languages worldwide differ in emotions in a concept of valence and activation (arousal) — known as primitive emotions.

Primitive emotions reflect the neurophysiological response to an stimuli. The valence and arousal are the principal approaches when a scientist is introduced to ER, and EEG is one of the most used methods to capture that neurophysiological response. According to Hosseini et al. (2021), EEG is a non-invasive method, which is safe and painless as it does not penetrate the body, for testing or recording the brain's bioelectrical potential, presenting high non-Gaussian, non-stationary, and non-linearity properties. EEG are commonly used in eHealth applications in treatments like neurological diseases, epilepsy, sleep disorders, tumors, and depression (Subha et al. (2008)). Firstly discovered by Richard Caton in 1875 by studying the monkey's and rabbit's brain activity, the EEGs are taken by placing electrodes on the scalp, achieving a bioelectrical pattern that can be fragmented into different frequency bands:

- $\rightarrow$ δ (0.5-4 Hz): associated with deep sleep and brain's slow activity,
- $\rightarrow$ θ (4-8 Hz): linked to relaxation, creativity, drowsy, and light sleep,
- $\rightarrow$ α (8-13 Hz): relaxed and calm state,
- $\rightarrow$ β (13-30 Hz): associated with active thinking, problem-solving, physical motion, and focus,
- $\rightarrow$ γ ($>$ 30 Hz): related to cognitive and emotion processing or higher mental activities,

then, one of the first pre-processing tasks for every scientist in ER is the noise and artifacts reduction in EEG signals. In this regard, Dadebayev et al. (2022) suggested that the most common techniques are based on the Fourier Transform (FT) and Wavelet Transform (WT). Moreover, Torres et al. (2020) conducted a comprehensive study from 2015 to 2020, evaluating several spectral analysis techniques for feature extraction, yielding FT and WT as the top ones. In particular, Xie and Oniga (2020) mentioned the contribution of wavelet transform and decomposition of EEGs. Consequently, He et al. (2020) used a wavelet decomposition to

reach the $\delta, \theta, \alpha, \beta$, and γ sub-frequencies, achieving significant noise reduction and leveraging these sub-frequencies for feature extraction.

One of the first ER-EEG developed datasets is introduced by Soleymani et al. (2012) — A Multimodal Database for Affect Recognition and Implicit Tagging (MANHOB-HCI) — where a multimodal study of 27 subjects ($\mu_{age} = 26.06, \sigma^2_{age} = 2.09$), collected the EEG, face, body, eye, and audio stimuli responses. According to the Web of Science Core Collection (WOS), MANHOB-HCI has received 961 cites (WOS = 961), positionating it as a well-known multimodal ER dataset. By the same time, Koelstra et al. (2012) published the DEAP dataset (WOS = 2960) — also multimodal — where CNS and PNS different signals where collected and recorded from 32 subjects ($\mu_{age} = 27.19, \sigma^2_{age} = 19.77$).

The main approach in ER based on primitive emotions is to classify VA/VAD space; then, based on Koelstra's study, multiple techniques have been developed. Mentioning a few, the combination of Empirical Mode Decomposition (EMD), Intrinsic Mode Functions (IMFs), Discrete Wavelet Transform (DWT), and ML in Zhuang et al. (2017) framework showed a higher performance through EC selection along the electrode scalp perimeter. Published in 2017, this approach demonstrated its effectiveness in binary classification by using dedicated models for each primitive emotion, showcasing significant advancements in classification accuracy and model efficiency considering the publication year. After that, several publications increased the performance of ER by using EEG signals. For instance, Farashi and Khosrowabadi (2020) found that V is more related to γ EEG band, while A is more related to α, achieving a higher accuracy rate in comparison with the former one, following the binary classification method per primitive emotion. Hence, a multimodel ML approach is proposed by Doma and Pirouz (2020) where EEG raw is segmented into four sets per minute. After feeding a Principal Component Analysis (PCA) with a set of features, the study concluded that the $[30 - 45]$s segment, combined with Support Vector Machine (SVM), achieved a superior classification performance into VAD space. These approaches are based on binary classification, where the primitive emotions are classified independently. Accordingly, AMIGOS is a novel VA dataset approach introduced by Miranda-Correa et al. (2021). However, ER is not limited to these type of models; The SJTU Emotion EEG Dataset (SEED) dataset by Zheng and Lu (2015) focusing on Positive, Negative, and Neutral (PNN) emotions explore a multimodal dataset for these three classes, which for this document proposes, will be categorized as primitive emotions. Then, more recent and robust datasets are developed for multiclass classification; one of the most reliable was developed for the same authors of SEED, they named it SEED-V (Liu et al. (2022a)). This dataset, also multimodal,

is highlighted as one of the first datasets to get close to primary emotions, including: "happiness," "sadness," "disgust," "fear," and "neutral" emotions (classes). Music, video, image, or gaming modalities are some of the main approaches to trigger an emotion stimuli in subjects to create a more robust dataset, the previously mentioned datasets, along with additional ones, will be discussed in detail in the following chapter.

One of the main challenges in ER is the noise and artifacts in EEG signals. The recent framework by Javidan et al. (2021) proposes a novel channel selection technique to reduce artifacts and classification noise by computing a top EC by measuring each feature and channel significance, highlighting the FC2, F7, F8, T7, T8, and P7 in a Positive and Negative classification task. Following the same method, they found a pair of electrodes with higher performance, F7 and F8, suggesting that the frontal lobe is the main region for emotion processing. In contrast, a Particle Swarm Optimization (PSO) algorithm is applied to a set of spectral features in Yildirim et al. (2021). The method fusioned the Hilbert-Huang Transform (HHT) and Phase Locking Value (PLV) to classify the VA space, highlighting the FP2, AF4, F3, F4, FC5, T7, C3, CP2, PO3, O1, and O2 electrodes, must be located in the frontal lobe. Based on spectral analysis techniques, Bagherzadeh et al. (2024) explored a binary classification performance ("happy" and "sad" classes only) in the SEED datasets series (IV Zheng et al. (2019), V Liu et al. (2022a), GER Liu et al. (2022b), and FRA) by fusing the Synchosqueezing Wavelet Transform (SSWT) and ResNet-18, DL approach, achieving a pair of EC electrodes, T7 and T8 are the most significant for the four datasets. However, the limitation of a binary classification presents a lack of EC generalization for multiclass classification. Finally, a reliable classification task is detailed in Ma et al. (2025) by testing binary or multiclass models using the DEAP and SEED-series datasets. The study remarks the multimodal performance by fusing EEG with peripheral signals — such as Electrooculogram (EOG), Electromyogram (EMG),Electrocardiogram (ECG), Galvanic Skin Response (GSR), among others — to achieve a higher classification rate. The proposal achieved a higher performance in multiclass models than the binary ones, suggesting that binary architectures are unsuitable for multiclass classification.

The studies mentioned above introduce some examples of the state-of-the-art in ER to avoid noise and artifacts in EEG signals. Nevertheless, only a few experiments have studied the synapses, structure or signal energy distribution in human's brain, and their influence on EEGs. It has been proved that some specific EEG frequencies have a special role in emotion processing and decision-making, being necessary to process the information in a deep sense. For instance, Celeghin et al. (2017) stabilized that the co-activation of brain

structures may change the emotional response depending on the current activity of a subject. This inner response produces a two-way effect in the amygdala: in the former, the stimuli are categorized as negative or positive (in a valance sense); in the latter, the stimuli activate the SMH to produce more accurate emotions than just the primary ones. The SMH by Bechara and Damasio (2005) established that the amygdala is the key place in the CNS where all secondary emotions are produced.

According to above, the following studies supported Damasio (1996) theory where given supraliminal or subliminal stimuli — perception in shaping an individual consciousness of emotion — the amygdala is connected to primary emotions and Somatic states, which subsequently activate the vmPFC to generate secondary emotions. Similarly, Šimić et al. (2021) revealed that emotional stimuli are processed as external factors in different brain regions, where their meaning and relevance are evaluated by the Autonomic Nervous System (ANS) to determine an appropriate response. Under the SMH, Damasio (1996) theorized that primary emotions are triggered in the amygdala, latterly supported by Pessoa (2017); Phelps and LeDoux (2005). Consequently, a musculoskeletal and visceral connection to emotional reactions theory suggested a two-way process in emotional evoking: firstly, primary emotions arise from physical experiences, while a secondary process involves the vmPFC activating SMH derived from bodily information, triggering secondary emotions. Furthermore, McRae et al. (2011) suggested that the amygdala, vmPFC, and hippocampus form a generative network that processes emotional stimuli through a bottom-up approach. Additionally, Bechara and Damasio (2005) reported that the vmPFC is the only frontal lobe region associated with the ANS and is thus interconnected with the hippocampus and amygdala. Supporting these findings, Sterling (2012) described the amygdala as playing a feedback role within the PFC, influencing subsequent decisions and planning actions.

The Guex et al. (2020); Sonkusare et al. (2022) studies, based on emotional theory, have proposed that the amygdala can be stimulated by using audiovisual, words, and facial expression modalities. Meanwhile, Sander et al. (2003) emphasized the amygdala's role in assessing the significance of events, suggesting that its response may adapt to human behavior based on personal goals or needs. Analyzing the amygdala's pattern, Pourtois et al. (2010) confirmed a trigger response to a current behavior based on the cognitive significance of the stimuli. Moreover, studies with EEG scalp in subjects reported an emotional stimuli response at around 300ms (Albert et al. (2010)), particularly in frontocentral areas (FC1 and CZ). Complementarily, Berboth and Morawetz (2021) showed that the prefrontal region and the amygdala have a reciprocal connection. In addition, Sonkusare et al. (2022) showed

neural activity in the amygdala, Orbitofrontal Cortex (OFC), and medial Prefrontal Cortex (mPFC) by emotional response to elicited images. In addition, the Gamma Band Activity (GBA) presented an increased activity for positive and negative stimuli. Meanwhile, a high Beta Band Activity (BBA) is shown in negative emotional valence stimuli associated with depressive behavior. These studies concluded that emotions interact profoundly with the CNS, with the amygdala playing a pivotal role. Moreover, its activity is intricately connected to specific regions of the PFC, highlighting its integration into broader emotional and cognitive networks.

1.5 Research achievements

In order to achieve the objectives of this work, the emotion recognition task followed several implementation and testing tasks to accomplish the research goals. The first task was to explore the must common datasets and get familiar with them. Then, the digital signal pre- and post-processing and the classification task were very important to explore the limitations and research gap in the ER field. The following task bring us to the channel selection and conflict learning to find the most relevant EC in the EEG signals. In this order of ideas, the bQSA signal processing was possible. Here, the published research papers in JCR high impact journals, and conference papers, that support the research work presented in this document are listed:

REGEEG: A Regression-Based EEG Signal Processing in Emotion Recognition
https://doi.org/10.1109/JBHI.2025.3543729. IEEE Journal of Biomedical and Health Informatics, 29(7), 4748–4757.
Authors: Oscar Almanza-Conejo*, Juan Gabriel Avina-Cervantes, Arturo Garcia-Perez, and Mario Alberto Ibarra-Manzano
IF: 6.8, JFI-RANK: Q1, 92.83 (19/258), 91.71 (15/175), 3/67 (3/67), 92.71 (4/48)

A channel selection method to find the role of the amygdala in emotion recognition avoiding conflict learning in EEG signals
Authors: Oscar Almanza-Conejo, Juan Gabriel Avina-Cervantes, Arturo Garcia-Perez, and Mario Alberto Ibarra-Manzano*. Engineering Applications of Artificial Intelligence, 126(106971), 106971.
https://doi.org/10.1016/j.engappai.2023.106971
IF: 8.0, JFI-RANK: Q1, 91.6 (8/89), 88.0 (25/204), 91.7 (31/366), 97.4 (5/175)

Emotion Recognition in Gaming Dataset to Reduce Artifacts in the Self-Assessed Labeling Using Semi-Supervised Clustering
Authors: Oscar Almanza-Conejo, Juan Gabriel Avina-Cervantes, Arturo Garcia-Perez, and Mario Alberto Ibarra-Manzano*. IEEE Access: Practical Innovations, Open Solutions, 12, 52659–52668.
https://doi.org/10.1109/ACCESS.2024.3387357
IF: 3.6, JFI-RANK: Q2 64.1 (93/258), 65.2 (128/366), 58.8 (50/120)

Emotion recognition in EEG signals using the continuous wavelet transform and CNNs

Authors: Oscar Almanza-Conejo, Dora Luz Almanza-Ojeda, José Luis Contreras-Hernandez, and Mario Alberto Ibarra-Manzano*. Neural Computing & Applications, 35(2), 1409–1422.
https://doi.org/10.1007/s00521-022-07843-9
IF: 4.5, JFI-RANK: Q2 73.9 (52/197)

Emotion Recognition Using Electroencephalogram Signals and a 1D Local Binary Pattern for an ML-Classification-Based Approach

Authors: Oscar Almanza-Conejo, Juan Gabriel Avina-Cervantes, Arturo Garcia-Perez, and Mario Alberto Ibarra-Manzano*. In Lecture Notes in Networks and Systems (pp. 13–23). Springer Nature Singapore.
Proceedings of Eighth International Congress on Information and Communication Technology
https://doi.org/10.1007/978-981-99-3043-2_2.

Emotion Recognition Using Time-Frequency Distribution and GLCM Features from EEG Signals

Authors: Oscar Almanza-Conejo, Dora Luz Almanza-Ojeda, José Luis Contreras-Hernandez, and Mario Alberto Ibarra-Manzano*. In Lecture Notes in Computer Science (pp. 201–211). Springer International Publishing.
14th Mexican Conference on Pattern Recognition 2022
https://doi.org/10.1007/978-3-031-07750-0_19

1.6 Thesis outline

Emotion recognition encompasses a wide spectrum of understanding the human brain and its response to certain environments or stimuli. Researchers are challenged to develop novel and accurate methodologies that satisfy human beings' social, psychological, and physiological needs. In this regard, a novel and exhaustive study about the ER based on EEG signals, focusing on digital signal processing and quaternion algebra to improve classification performance is proposed. This document results from deep research and multiple experiments published in three peer-reviewed indexed journals. Based on these findings, the thesis is structured as follows:

- **State-of-the-art in emotion recognition**: A comprehensive review of several studies based on ER and EEG signals is provided in this chapter. Here, the reader is introduced to a robust collection of methodologies oriented to the pre- and post-processing of ER data. This section includes the most popular or well-known datasets, several noise, and artifacts reduction techniques. Also, some AI oriented approaches to classify primitive or primary emotions according to different ML, DL, or Fussion Learning (FL) models are presented and discussed.
- **Methodology**: Chapter three introduces the digital signal processing and quaternion algebra methodology to outperform the classification performance in ER. The methodology can be divided into three main tasks: (1) the noise reduction using the wavelet transform and the channel selection method to find the EC by adapting the Minimum Redundancy Maximum Relevance (mRMR) algorithm to compute a relevance scores vector associated to each EEG channel per used dataset, (2) adapt the top-four EC to the quaternion algebra and bQSA product criteria to (3) classify the binary or multiclass primitive or primary emotions using a ML or DL models.
- **Numerical results**: Here, statistics and charts collection modeled by the results of the experiment are presented, considering the classification task by applying the bQSA product criteria to four different datasets: DEAP, AMIGOS, SEED-V, and Force, EEG and Emotion-Labelled (FEEL) datasets. The results are compared with the state-of-the-art to validate the performance of the proposed methodology by measuring the accuracy, precision, recall, F1-score, and p-value metrics. This chapter discusses the results obtained in the previous one, highlighting the advantages, limitations, principal findings, and research gap of this proposal. Some limited and closely connected references are compared and discussed directly with the research work presented in this thesis.

- **Conclusions and future work**: The sixth and final chapter summarizes all the previous chapters and provides a comprehensive conclusion of the leading research proposal, including the future work to improve the methodology or the classification performance in ER based on EEG signals.

Chapter 2

State-of-the-art

As the previous chapter introduced, the existing literature on ER is extensive, with a little bit of emphasis on primitive rather than primary emotions. In this regard, a considerable amount of literature has been published related to ER. Here, this document explores several approaches related to physiological and non-physiological signals and their contribution to the area.

Over the past two decades, Affective Computing (AC) overarching the terms used for emotion recognition, sentiment analysis, or similar. The term, initially proposed by Prof. Piccard in 1997, is introduced to make a reference to the emotions or feelings interpreted by computers to identify, express, or respond to human stimuli. Thus far, Wang et al. (2022) highlights the contribution of non-physiological and physiological data; the former describes a portion of 55% of emotions expressed through facial, 38% voice, and 7% for text:

- **Textual Emotion Recognition (TER)**: surveys, such as the one conducted by Deng and Ren (2023), have summarized the principal benefits of text analysis for emotion recognition as its (1) marketing through customer reactions, (2) security for personal or social risk's prevention, (3) psychology and psychiatry in social media for suicide prevention or political decision-making and statistics elections, among others. A binary, ternary, and multiclass primary or primitive datasets are also recompiled and discussed in Deng and Reng's paperwork.
- **Speech Emotion Recognition (SER)**: real-life and time problems like call center, automatic response, spoken dialog, pain and depression recognition are interesting areas for SER researchers. In Ahmed et al. (2020) review, the Berlin Database of Emotional Speech (EMODB) Burkhardt et al. (2005), Interactive emotional dyadic motion capture

database (IEMOCAP) Busso et al. (2008), and The Ryerson Audio-Visual Database of Emotional Speech and Song (RAVDESS) Livingstone and Russo (2018) datasets are highlighted for speech recognition, establishing the former one as the most balanced in classification performance and use. In the same order of ideas, Wani et al. (2021) review concluded the same regarding the balance of classification performance and usefulness of the EMODB and IEMOCAP datasets. However, EMODB is a German speech dataset, which may limit its research applications and scope.

- **Facial Emotion Recognition (FER)**: as the second most useful data after EEG, FER has been introduced in widespread applications. As result, lot of reviews and surveys have been published; however, only a pair of them are mentioned. According to Mehrabian (1968), 93% of the emotional context is partially distributed as: 55% facial, 38% vocal — the way the voice conveys the message —, and 7% is verbal — the context — expressions. This outlines with Ekman's theory about the six primary emotions and their uncultural variation. FER concerns two types of image encoders: dynamic and static. The former is related to a sequence of images, like GIFs of video formats, and the latter to a single image spatial information. According to Guerdelli et al. (2022), to address the limitations of current FER systems, limited by research bias and subject's lacks, the micro- and macro-FER studies were divided. Both dataset collections can be stored in three types of datasets: *act*, *spontaneus*, and *in-the-wild*.
  - *Macro-FER*:

Table 2.1: FER Macro expressions datasets (extracted from Guerdelli et al. (2022) survey. See extended in the paper.)

Number of Subjects	**Macro-Expression Datasets**
≤ 50	TAVER, RAVDESS, BAUM-1, OPEN-EmoRec-II, BP4D-Spontaneous, DISFA, RECOLA, CCDb, MAHNOB Laughter, DEAP, SEMAINE, MAHNOB-HCI, UNBC-McMaster, CAM3D, B3D(AC), MMI-V, AVLC, AvID, AVIC, VAM-faces, ENTERFACE, MMI, MIT, EmoTV, UA-UIUC, 4D CCDb, FreeTalk, IEMOCAP, SAL, iSAFE, ISED
$\in [50, 100]$	GFT, SEWA, BioVid Emo, MAHNOB Mimicry, AVEC'14, PICS-Stirling ESRC, 3D Face Database, Belfast induced (Set2 and Set3), Hi4D-ADSIP, DD, RU-FACS, AAI, Smile dataset

Continued on next page

Table 2.1: FER Macro expressions datasets (extracted from Guerdelli et al. (2022) survey. See extended in the paper.) (Continued)

Number of Subjects	**Macro-Expression Datasets**
$\in [250, 500]$	SFEW, Aff-Wild2, AM-FED+, BAUM-2, AVEC'13 AViD-Corpus, DynEmo, AFEW, UT-Dallas

its existing datasets are categorized according to subject's number, age, ethnicity, camera frames per second, and amount of data. The average time duration for these emotions in facial expression is from 0.5 to 4 seconds. The datasets labels for this FER-type are strictly necessary for the training-validation-testing tasks in act and spontaneous datasets. However, in-the-wild collections requires a ground-truth and experienced annotators to assess the tasks.

– *Micro-FER*: related to unconscious emotional stimuli, micro-expressions are difficult to hide and act. In consequence, capturing with a low-cost camera is challenging due to their fast and spontaneous occurrence (0.04 to 0.2) covering a voluntary and involuntary expression triggering (Zhou et al. (2022)). A summary of datasets is shown in the following table.

Table 2.2: FER Micro expressions datasets (extracted from Guerdelli et al. (2022) survey.)

Number of Subjects	**Macro-Expression Datasets**
≤ 50	SAMM, CAS(ME)2, MEVIEW, CASME II, CASME, SMIC-E, SMIC, YorkDDT
≥ 100	RAF-DB, AffectNet, Aff-Wild, EmotioNet, FER-Wild, FER-2013, HAPPEL, HU-MAINE

However, these approaches presents a lack of accurate emotion stimuli detection in act or spontaneous macro-expressions results. In consequence, researchers have decided to board deeply the FER information due to their influence in ER. However, despite their own computer vision applications, multiple studies have proved that physiological information provides an accurate ER study, avoiding subjects' lack in self-assessed stimuli.

In close connection, basic emotions expressed in the first six months of life in newborns are associated with specific facial expressions. The study in Matsumoto and Ekman (1989) suggests that emotion culture invariance is possible due to the culture homeostasis in the context of pattern, instinct, and stimuli propagation between different subjects in the same

environment. Consequently, there is a clear influence from visual, auditory, and tactile bio-sensorial information in the trigger of an emotional fight-or-flight response (see Damasio (1999)).

In a formal context, the emotion generation involves a parallel processing task; since a rapid activation-action response through complex CNS responses. Based on Šimić et al. (2021) study, as earlier detector stimuli response, the amygdala is the motor and a key part of the limbic system — amygdala, hippocampus, thalamus, hypothalamus, and cingulate gyrus, among others — which plays a crucial role in emotion regulation and memory formation. Also, Guex et al. (2020) suggested that the amygdala evaluates and reevaluates the input stimuli from the environment to produce a two-way response, the early and late activation process:

- **Early activation ($\approx$ 130ms)**: is the initial phase as automatic response. This "bottom-up" — considered as the non-conscious deliberation process — implicates a fast sensory information response to low-level brain structures, including the amygdala. As consequence, Quadt et al. (2022) theorized that changes in heart rate, blood pressure, skin conductance, and other physiological signals are triggered — ANS responses — to help humans to "feel" the emotion, producing a late activation response.
- **Late activation ($\approx$ 220ms and beyond)**: after the early one, the late response is triggered around 220ms or later. It has been theorized that the late activation goal is to act and modify the behaviour. In this process, the amygdala's activity is modulated by the prefrontal cortex, which sums contextual information to outperform an accurate stimulus context and response — referred to as "top-down" response.

In this context, Stolicyn et al. (2024) highlights that the "bottom-up" and "top-down" (early and late responses) are refered to which nervous system is activated first; central, for a fast and unconscious, or anatomic, for an accurate and contextual responses, respectively. The following section introduces a deeper biological context about how human emotion processing is a whole-brain and whole-body task.

2.1 The physiological emotion processing

As it was anticipated above, the human emotion processing is a complex and parallel involved task that outperforms several biological assignments. Here, a brief introduction to the most relevant neuro and physical parts in the emotional processing are sumarized.

- **Amygdala — Thread detector and arousal trigger**: Located in the anterior sections of the medial temporal lobe, the amygdala is the primary neurological component in emotion generation and regulation, particularly in fear and anger responses (see Elvira et al. (2022)). According to Kirstein et al. (2023), several major depression desorders, and structual and functional anomalies have been associated with amygdala's activity; bipolarity, anxiety, epilepsy, schizophrenia, and Alzheimer's disease are some of them.
- **Hippocampus — Contextual information**: As Ekstrom and Hill (2023) wrote, the hippocampus is the central part in memory information and spatial navigation located in the medial temporal lobe. In emotion processing, the hippocampus plays an important role in providing a deeper context to the amygdala's response, see Roesler et al. (2021). What stands out in the hippocampus is the function in helping to distinguish whether a stimuli represents a real threat or merely resembles an experience. This disambiguation process plays a pivotal role in preventing excessive fear-related responses to situations that are similar to negative past experiences but are not actually threatening. Based on Ben-Zion et al. (2024) study, it can be concluded that dysfunction in this hippocampal mechanism may lead to exaggerated responses in individuals with post-traumatic stress disorder (PTSD) or anxiety disorders, impacting their quality of life.
- **Thalamus — Sensory information relay**: is a subcortical structure located in the center of the brain, it gates all sensory input information to the cortex (except olfaction). Additionally, it relays the information between cerebellum, spinal cord, and cerebrum, see Klein et al. (2009). In simple words, the thalamus acts as a relay station that filters information between the brain and body, activating ANS to provide a deeper context in the amygdala (even avoiding the fear-related fast response). A deeper context of the thalamus and hypothalamus can be found in Moini and Piran (2020) study.
- **Hypothalamus — Hormonal response**: is a subcortical structure located below the thalamus and capping the brainstem. Bhagavan and Ha (2015) established that even if the hypothalamus is smaller than the thalamus, its homeostatic functions are crucial for the CNS and ANS. Pointing out some of its functions, Moini and Piran (2020) summarized that the hypothalamus is related to memory, emotions, body temperature, food intake, sleep-wake cycles, and regulation of water balance and thirst (see its Table 8.1 for a deeper context). A non-optimal function of the hypothalamus can lead to important mental health disorders, such as depression and anxiety, affecting

the emotional hub of a person, Bao and Swaab (2019).

- **Prefrontal Cortex (PFC) — Appraisal and response modulation**: is the cortex that receives projections from the mediodorsal nucleus of the thalamus and is located in front of the motor and premotor cortices in the frontal lobe, see Rolls et al. (1996). In Etkin et al. (2015) it is mentioned that the vmPFC, dorsolateral Prefrontal Cortex (dlPFC), and OFC are strongly implicated in emotional processing and regulation, complementing the response of the amygdala. The PFC initiates a multimodal activation across the CNS to attenuate fear-related responses, effectively reevaluating the environment as safe and "halting" the amygdala's threat detection, see Delgado et al. (2008) experiment. From a global brain perspective, neural saturation within the PFC influences whole-brain signal propagation, modulating multisensory integration, emotion recognition, motor execution, memory retrieval, and higher-order cognitive processes, as described in Sherfey et al. (2020). A notable example of PFC and amygdala co-activation network is detailed in De Silva et al. (2012), where they explored the emotional and motivational aspects of several previous studies that suggested an input stimuli triggered by a top-down signal behaviour such as the feeding satiety scenario.
- **Insula — Interoception and subjective feeling perception**: is a subcortical structure associated to high-order functions, as the integration and analysis of gustatory, auditory, and olfactory signals. In addition, Siegel and Sapru (2006) wrote that it plays a pivotal role in memory and emotion processing, suggesting an important role in the complex cognitive and affective processing. The insula is a crucial hub for the regulation of interoception — the internal body signals sense — and internal feeling states. According to Scott and Plata-Salamán (1999), insula connects hypothalamus, OFC, and limbic system. In this order of ideas, it is correct to assume that the ANS and CNS are directly connected and related by the interoception of insula's response.

In short, a summarized overview of the brain's regions involved in emotion processing is presented in Table 2.3.

To date, no neuroscience and neuropsychology studies have accurately performed a theory that determines or locates the exact spatial coordinates of where multiple emotions are processed by the same distinct group of subcortical nuclei of the brain's region. However, in the review by Lim et al. (2024), they set out to explore the activations of the brain regions associated with the stimuli from the primary emotions of different data modalities. Based on the information above, a complex and robust network of brain regions is involved in

the process of emotion generation and regulation. In order to make an approximation, ER researchers have developed EC techniques to reduce the computational and time processing, achieving a reduced subset of channels that are more effective in emotion recognition tasks. The following section introduce a brief overview of the EEG databases and statistically effective channels in the state-of-the-art.

Table 2.3: Brain regions and their influence in the emotion recognition process

Brain region	Role	Functionality	Associated disorders
Amygdala	Threat detection and arousal trigger.	Generates a fast and bottom-up response to emotion stimuli. Main role in fear and anger responses to link the survival instincts.	Anxiety, depression, bipolarity, schizophrenia, epilepsy, and Alzheimer's disease.
Hippocampus	Context and memory-related processing.	It helps to differentiate between a real and fake threat according to the contextualization of previous experiences, modulating amygdala's response.	PSTD and anxiety.
Thalamus	Sensorial information.	Its primary function is the relay of input sensorial information. Feeding the amygdala with a deeper context to avoid a fast and unconscious response.	
Hypothalamus	Hormonal and homeostatic response.	Manage critical bodily functions, including the hormonal emotion-related responses. Temperature, hunger, thirst, sleep, and wake cycles are also included in its functions.	Depression, anxiety, and hormonal dysfunctions.
PFC	Appraisal, decision-making, and emotional response modulation.	Re-evaluates the environment modulating the threats identified by the amygdala, activating a top-down response and enabling complex bodily functions.	Social and psychological disorders.

Continued on next page

Table 2.3: Brain regions and their influence in the emotion recognition process (Continued)

Brain region	Role	Functionality	Associated disorders
Insula	Interoception and subjective feeling.	Integrates the bodily signals, sensorial information, and emotional responses. It hubs the hypothalamus, PFC, OFC, limbic system, ANS, and CNS.	Corrupts the sensorial and emotional modulation, impacting the social behavior and autonomic function.

2.2 Emotion recognition databases

Several ER datasets have been published in the last decade, in order to provide a deeper context and understanding of the human brain. As established, according to the goals of this thesis, the EEG emotion recognition datasets are the most relevant to claim a specific emotion recognition model. Actually, several ER datasets have been published since 2010, being DEAP and MANHOB-HCI some of the old and most used ones. Those datasets are developed in the order of the primitive emotion recognition. The primitive emotions, according to Dadebayev et al. (2022), *valence* is the primitive emotion that reflects the pleasantness or unpleasantness of a stimulus, while *arousal* is defined as the capture of the intensity of the emotional response. Some authors also propose or consider *dominance* as a third dimension that evolves the emotional domain in response to an stimuli. A representation of the VAD space is shown in Fig. 2.1. One of the characteristics of these datasets is that the primitive emotions are usually self-assessed by the subjects of the experiment. This method presents a wide range of applications, as the detection of changes in the emotional state or the frequency of pleasantness. However, the self-assessed method presents a lack of reliability in the data if the idea is to use the EEG or multimodal information to develop an EEG emotion recognition. For the purposes of this study, two primitive emotions datasets to test this approach in primitive and primary datasets are considered: (1) DEAP (see Koelstra et al. (2012)) and (2) AMIGOS (see Miranda-Correa et al. (2021)).

The context of primary emotions was firstly introduced by Ekman (1992a) where he proposed the six basic emotions: happiness, sadness, fear, anger, surprise, and disgust. These emotions are considered culture-invariant and universal. In this context, several datasets are developed multimodal data to capture the CNS and ANS in response to an audiovisual, image, or sound stimuli. These stimuli material is chosen to produce the primary emotion reaction in the human brain. Hence, the primary emotions in EEG or multimodal information present an advantage in contrast to primitive for the ER studies. This study proposes, the

(1) SEED-V dataset (see Liu et al. (2022b)), that accomplished multimodal information of subjects in reaction to audiovisual stimuli material, (2) SEED-VII which stored a set of the six primary emotions and a neutral one (developed by the same research team as SEED-V), and (3) the FEEL dataset (see Cang et al. (2024)) are used too. This last one presents the self-assessed labels modality; however, is a good material to test the presented approach due to the relation and difference between the captured emotions and the self-assessed labels in a big set of emotional targets.

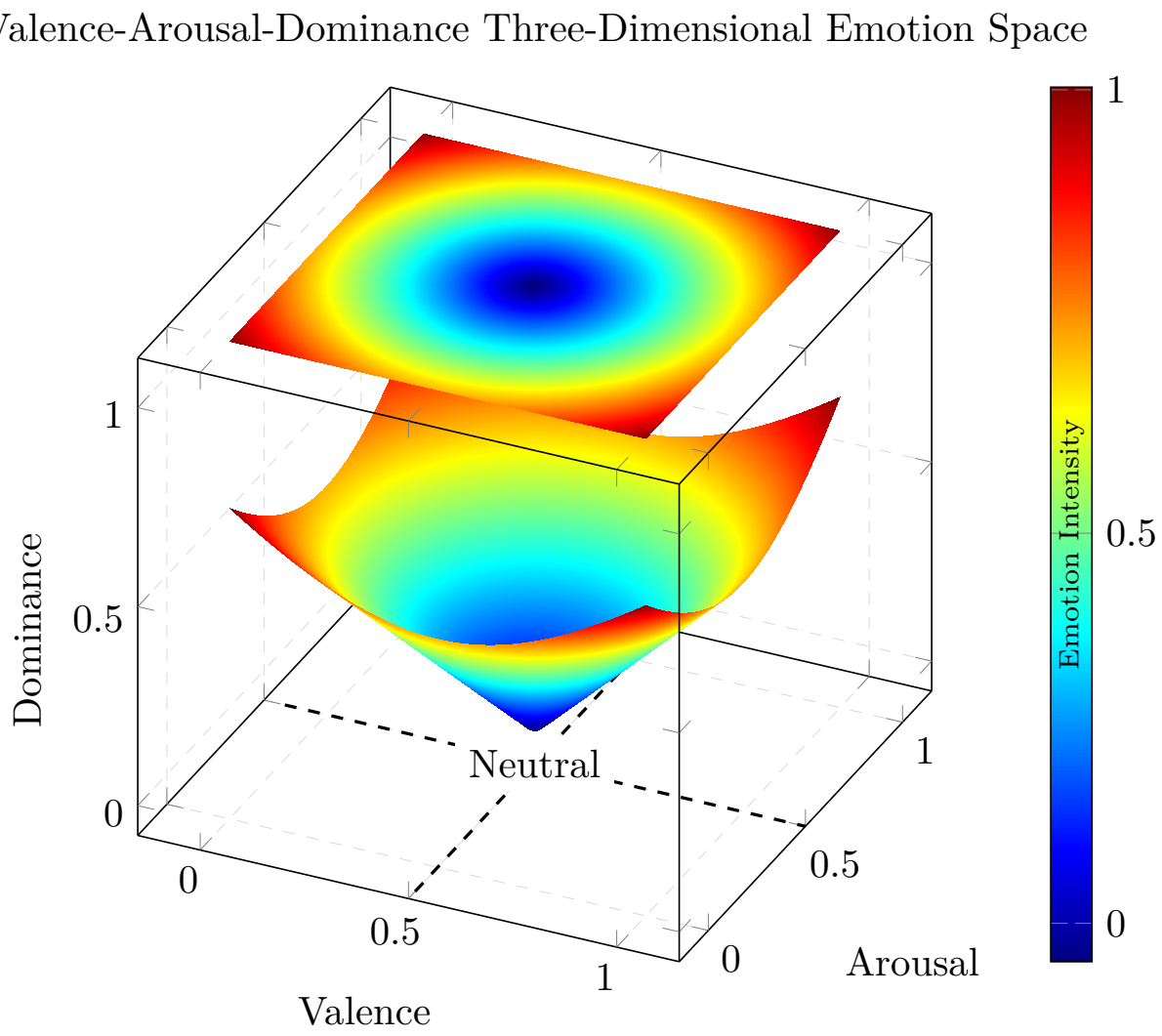

Figure 2.1: Valence-Arousal-Dominance emotion space.

In this regard, an overview of the datasets is detailed in Table 2.4. Almost all datasets follow the 10-20 system (see Fig. 2.2), which is a standardized method for placing electrodes

on the human scalp to record electrical activity from the brain. The number of cites of a few ER datasets until June of 2025 is plotted in Fig. 2.3. The number of cites is extracted from WOS database by searching the title of the publication paper-work of the dataset.

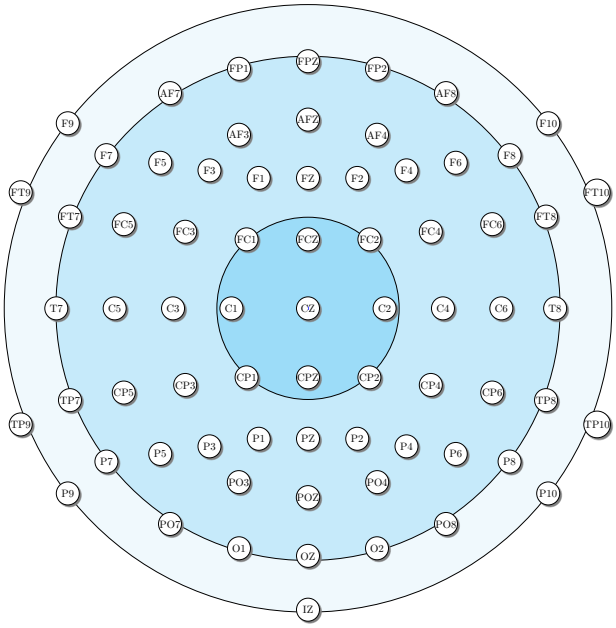

Figure 2.2: 10-20 system diagram of elctrodes positioning.

Table 2.4: EEG-ER datasets

Dataset (Year)	Cites	SN(F/M)[1]	Age ($\mu \pm \sigma^2$)	CN[2]	NSS[3]	RS[4]	f_s[5]
DEAP (Koelstra et al. (2012))	2888	32(16/16)	27.19 ± 19.77	32	40	VAD[6]	128
MAHNOB-HCI (Soleymani et al. (2012))	1018	27(16/11)	26.06 ± 02.09	32	20	VAD	256
SEED (Zheng and Lu (2015))	1430	12(6/6)	23.08 ± 04.08	62	15	PNN[7]	1000
DREAMER (Katsigiannis and Ramzan (2018))	593	23(9/14)	26.65 ± 07.29	14	18	VAD	128
SEED-IV (Zheng et al. (2019))	657	15(8/7)	21.32 ± 02.45	62	3×24	Happy, Neutral, Fear, Sad	1000

Continued on next page

Table 2.4: EEG-ER datasets (Continued)

Dataset (Year)	Cites	SN(F/M)[1]	Age ($\mu \pm \sigma^2$)	CN[2]	NSS[3]	RS[4]	f_s[5]
MPED (Song et al. (2019))	175	30 ()		62	28	Joy, Funny, Anger, Fear, Disgust, Sad, Neutrality	1000
GAMEEMO (Alakus et al. (2020))	91	28(9/19)	23.11 ± 04.69	14	4	Boring, Calm, Happy, and Fear	128
AMIGOS (Miranda-Correa et al. (2021))	361	40(13/27)	28.32 ± 17.82	14	4	HVHA, HVLA, LVHA, LVLA	128
FEEL (Cang et al. (2024))	0	16(8/8)	19-34	64	≈ 13	Anxious, Frustrated, Dread, Satisfied, Hopeful, Accomplished, Alert, Cautious, Curious, Resigned, Threatened	1000
SEED-GER (Liu et al. (2022b))	38	8(1/7)	22.25 ± 03.92	62	20	PNN	1000
SEED-FRA (Liu et al. (2022b))	38	8(2/5)	22.50 ± 07.73	62	21	PNN	1000
SEED-V (Liu et al. (2022a))	167	16(10/6)	21.62 ± 01.62	62	3×15	Happy, Disgust, Neutral, Fear, Sad	1000

[1] Subjects Number (Female/Male), [2] Channel Number, [3] Number of Samples per Subject, [4] Recognition Space, [5] Sampling Frequency, [6] Valence-Arousal-Dominance emotion space (up to 8 classes), [7] Positive, Negative, and Neutral classes.

Based on these datasets, accurate and effective signal processing, feature extraction, and classification models have been developed in order to achieve a ML or DL model to outperform primary or primitive emotions. Meanwhile, Fig. 2.4a introduces a statistical estimation based on the age of the subjects per dataset. Additionally, Fig. 2.4b shows a statistical subjects distribution (top) and the number of stimuli (bottom) per analyzed dataset, beign those exploded slices the ones that are used reliably in this work. In this regard, the following sections introduce a brief overview of the most effective channel selection and AI techniques in the state-of-the-art.

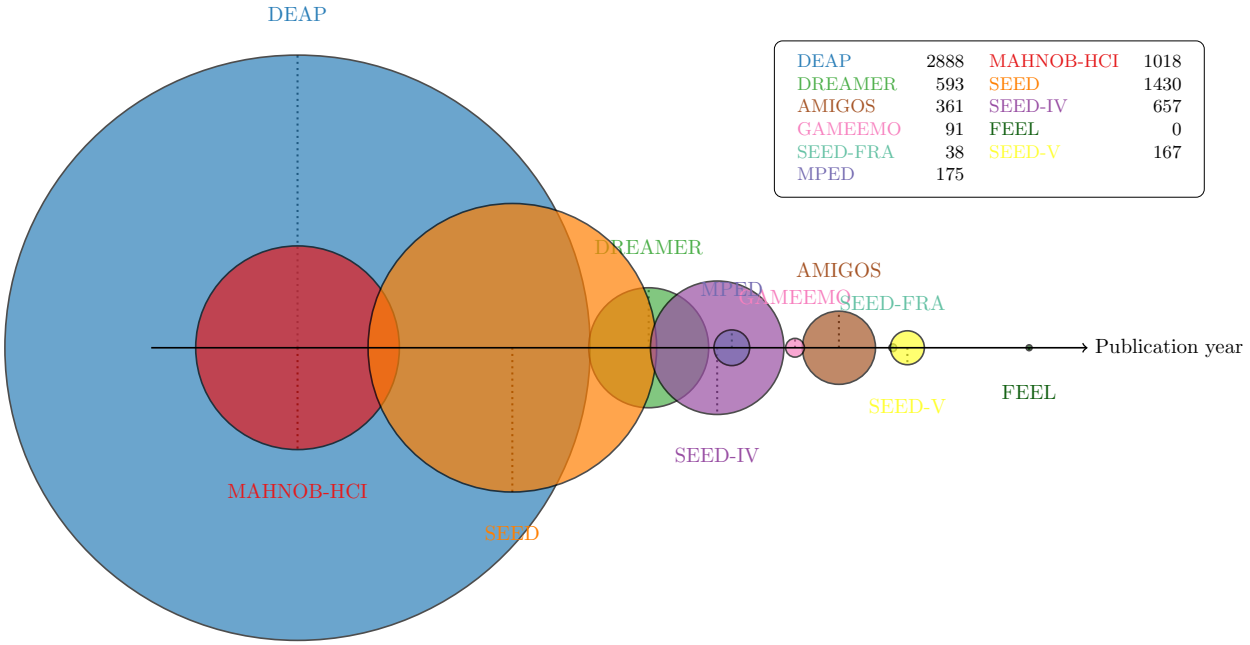

Figure 2.3: Number of cites per year for the most used datasets in emotion recognition.

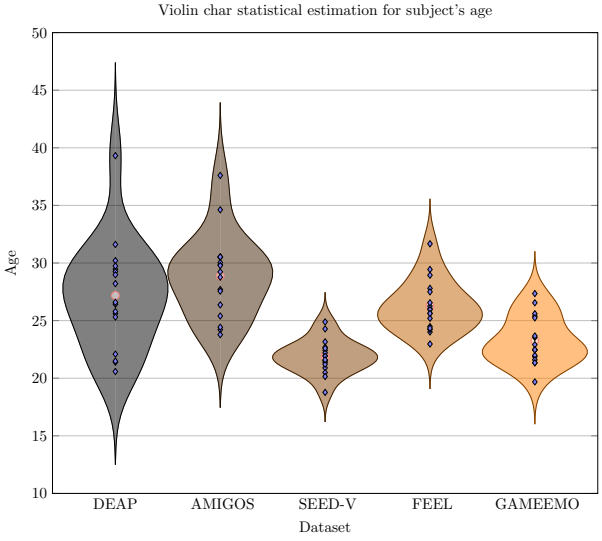

(a) Statistics of the subject's age per dataset.

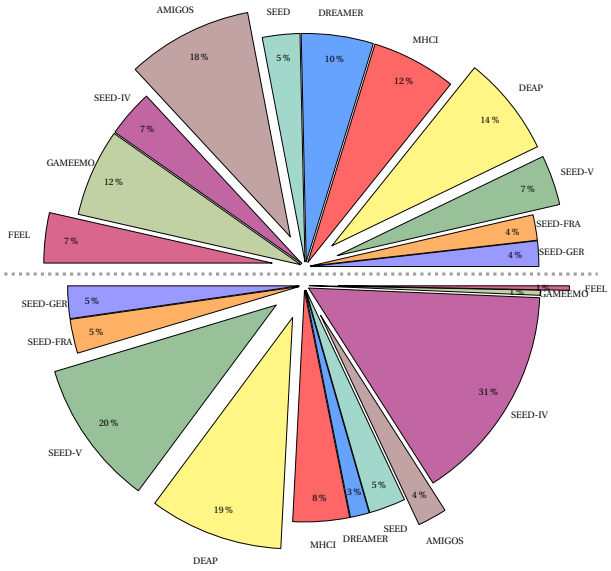

(b) Number of subjects (top) distribution and the number of stimuli (bottom) in emotion recognition analyzed and presented datasets.

2.3 Emotion recognition

The main discussion in this work is the principal advantages, limitations, and challenges in the ER field using EEG as input data. As introduced, EEG signals are complex to interpret and even more challenging to incorporate into the study's proposal. However, the reliability in the acquisition and model performance in order to model the changes in the CNS is unquestionable. Then, the growing interest in the ER field is presented in Fig. 2.5, where the number of publications per year since 2010 is shown. The data was extracted from Web Of Science, and the search was performed using the keywords "EEG" and "ER" in the title, abstract, or keywords. The search was limited to articles published in English and indexed in the Web of Science database.

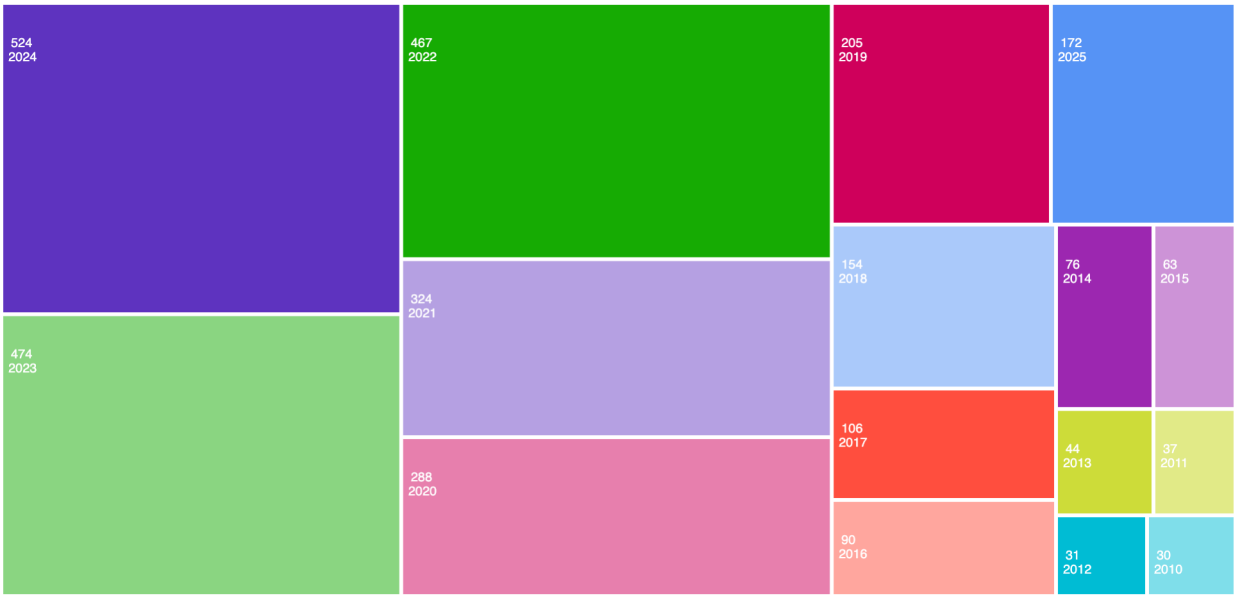

Figure 2.5: Number of publications per year since 2010 in the ER field (extracted from Web Of Science). Indexing: Refine results for emotion recognition EEG and Preprint Citation Index (Exclude – Database) and 2025 or 2024 or 2023 or 2022 or 2021 or 2020 or 2019 or 2018 or 2017 or 2016 or 2015 or 2014 or 2013 or 2012 or 2011 or 2010 (Publication Years).

Based on that TreeMap chart, is unquestionable that the COVID-19 pandemic influenced in mental health and ER research. In this context, neuroscience, psychology, psychiatry, and computer science journals lead the ER field (see Fig. 2.6). Then, the interest to explore EEG signal processing in the ER field is to provide an understanding of the brain's influence or response as a consequence an input emotional stimuli. Since here, this document explores

the principal ER frameworks that have a strong impact in the field and introduces several methodologies or strategies to improve the artificial intelligence performance in order to provide newer and accurate models.

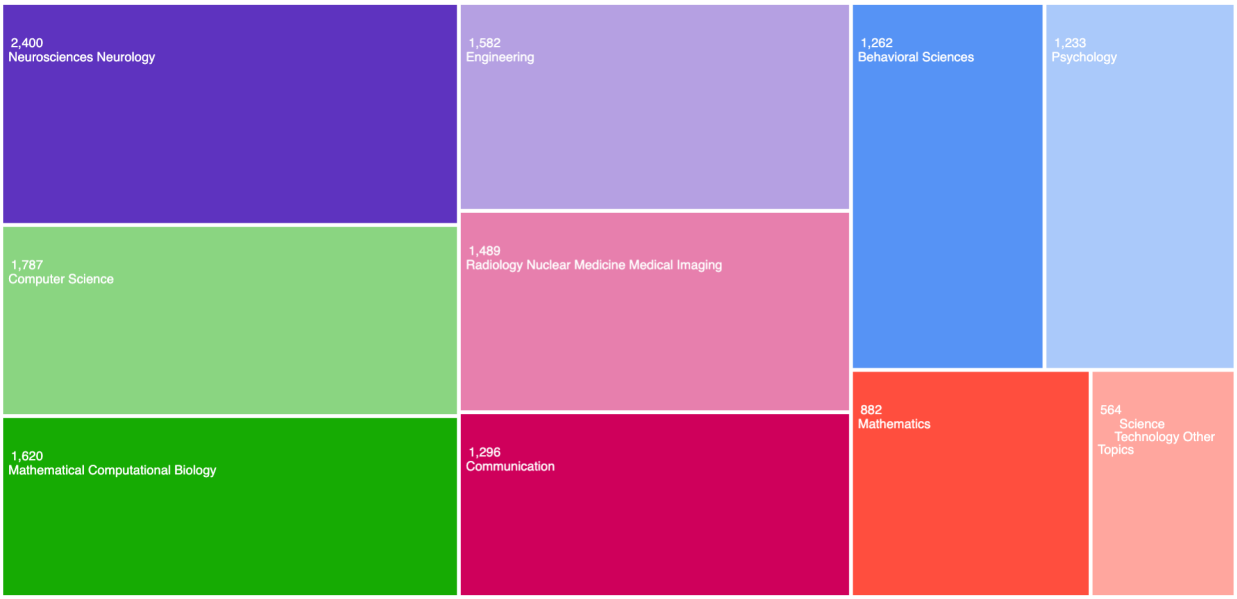

Figure 2.6: Number of publications per area in the ER field (extracted from Web Of Science). Indexing: Refine results for emotion recognition EGG and Preprint Citation Index (Exclude - Database) and Neurosciences Neurology or Psychology or Psychiatry (Research Areas) and 2025 or 2024 or 2023 or 2022 or 2021 or 2020 or 2019 or 2018 or 2017 or 2016 or 2015 or 2014 or 2013 or 2012 or 2011 or 2010 (Publication Years).

2.4 The computer science and artificial intelligence in emotion recognition

In the previous chapter, the ER field is introduced to give you, the reader, a brief overview of different methodologies developed to create and tune algorithms to reduce the gap between the human brain and computer science. Several algorithms aim to provide an accurate and effective model to detect primary or primitive emotions. In this regard, preprocessing EEG signals can be split into three main steps: (1) noise reduction, (2) a novel or improved processing algorithm, and (3) feature extraction. The former can perform some additional tasks, such as frequency decomposition (e.g. EMD or Wavelet Decomposition (WD)) and

channel selection (EC). Both methodologies have shown a substantial impact on classification performance, reaching evaluation metrics as high as the one that can be achieved using all available channels. The middle one has a higher impact and research interest in science. The possible novel or combination applications of the preprocessing task will determine the performance of the proposal methodology. Many applications have been proposed since the last decade, as seen in Fig. 2.5. At last, the latter is also dependent on the research approach; statistical, time-domain, spectral, and entropy features are the most used ones. In this respect, this research documents several methodologies that have proposed interesting applications or algorithms to improve the preprocessing or classification task. The following sections introduce EC, frequency decomposition, feature extraction, and classification methods that strongly impact the ER field. Here, three tables summarize the information provided in each section: (1) the EC and frequency decomposition methodologies, (2) the machine learning, and (3) the deep learning-based models, Tables 2.5 to 2.7, respectively.

2.4.1 Channel selection

A channel selection method, also known as EC, is a technique that effectively reduces the computational complexity in a dataset, significantly improving the processing tasks. It is important to remember that EEGs are a very complex and low signal-to-noise ratio signals. Hence, the EC approach is a key factor to reduce the lack that could be present in datasets by reducing the noise in classification methods, and, in beyond, helping to instrument new and lighter electroencephalogram devices to make the acquisition task more comfortable. In the discussion of the following reviewed frameworks, a statistical approach will be presented to make an inference of the brain regions that locates the major EEG information in response to an emotion stimuli. In this regard, Gupta et al. (2019) explored a subset of 12 channels, chunking the EEG input signals by the first 30 seconds of the recorded data, in the DEAP and SEED datasets. The reported performance in a channel-dependent model showed a notable improvement in classification by the use of ML models and highlighting T7 and T8 channels as the top ones, for both datasets. In the study conducted by Zhuang et al. (2017), half of the channels used in Gupta et al. (2019) study were identified. The former proposes the DEAP's EEG input signals with a five-level IMFs decomposition, associating each IMFs level with a EEG frequency decomposition. In this context, IMF1 showed the higher performance, related to γ-band activity. Then, extracting the IMF1 to a channel's subset (FP1, FP2, F7, F8, T7, T8, P7, and P8), produced almost the same classification performance than the

one yielded by the use of all DEAP channels available. In close connection, V. and Bhat. (2022) suggested the pool location of electrodes in the fronto-temporal region, using the AMIGOS dataset. Here, authors modify the input EEG signal by applying a variational mode decomposition (MVMD) to decompose the input signal, as EMD and WD do, and compute a spectral 2D image distribution to feed a ResNet network to use the extracted features as input matrix to ML algorithms. The model's performance showed a very low accuracy variance by using a subset of two or eight effective channels — both T7 and T8 for the two-channels model and T7, T8, F7, F8, FC5, FC6, AF3, and AF4 for the eight-channels model. A very popular method since the beginning of this decade is to use spectral analysis techniques to convert EEG signals to spectral distribution images and be processed as input images to feed a Convolutional Neural Network (CNN)-DL model. In a self-collected dataset, Zheng et al. (2020) found a 10 EC subset that outperformed a very close accuracy rate to the all-channels performance. Here, the statistics showed a 0.44 ± 0.20 mean and variance difference in a subject-dependent classification. Here, Zheng et al. also reached almost the same classification performance using a single discriminant feature, which they called "The 1st," than with a bigger dimension feature matrix. In a similar way to the last, experimental results in Seal et al. (2020) extracted a set of 10 Time-Domain Statistical-Energy features from $\delta, \theta, \alpha, \beta$ and γ wavelet decomposition from a self-conducted EEG signal acquisition dataset. The model assesses the effectiveness of four pairs of electrodes and the sub-frequency bands. The study concluded that FP1-F7 pair of electrodes are accurate in combination with the γ-band. In Table 2.5, a summary of the channel selection and sub-frequency band performance is detailed. Using the ternary SEED-series dataset, Wagh and Vasanth (2022) tested the positive, negative, and neutral emotions stimuli performance using three different ML models. The method is tested considering the frontal lobe only, assessing five pairs of EEG channels and decomposing the input signal using the Daubechies (db) wavelet-based method. The quantitative evaluation performance suggested that using only two EC (FP1 and FP2) the classification performance overate the 70%. Additionally, they tested the frequency decomposition performance, yielding the γ-band as the most effective one in the use of the ten frontal lobe channels.

One of the most effective works in the ternary evaluation models is developed by Liu et al. (2022b) where the cultural influence in ER is tested in Chinese, German, and French subjects. Here, three experimental models are performed: (1) intraculture subject dependent, (2) intraculture subject independent, and (3) cross-culture subject independent. The performance achieved for the former model indicates that Differential Entropy (DE) feature is highly

superior to other spectral features for the three cultures datasets and the SVM model the top one. Then, a new evaluation is proposed by outperforming the $\delta, \theta, \alpha, \beta,$ and γ classification using the DE and SVM as base for the classification. Results showed that $\beta,$ and γ bands are the most effective ones. However, the combination of the five sub-frequencies achieved a superior performance. Additionally, they proposed a Deep Neural Network (DNN) to contend with ML models using DE as a feature base, obtaining a superior performance in evaluation metrics compared to ML models. These results highlight the importance of the intraculture subject dependent model, where SVM and DNN outperforms the best using the DE as single input feature to the models and concluding the former task of this study. The middle one, the intraculture subject independent model, the Leave-One-Subject-Out Cross-Validation (LOSO-CV) is performed for the three cultures, and the model is evaluated with the single DE feature. The results showed the same bias as the former model. Here, the test is performed using the EEG and EOG signals, showing that EOG information is more effective in the French and German cultures than in the Chinese one. Finally, the cross-culture subject independent model evaluates the influence and performance of EEG in ER by mixing the three cultures. Here, Chinese subjects are used to train the model and German and French subjects are used to test the model, achieving a very low performance in EEG but a superior performance using the EOG. Then, from German to Chinese and French subjects, the performance is very variable; the EEG is superior in German-Chinese and lower in EOG, for the German-French performs as inverse. The bias in the French-Chinese and French-German is the same than in the previous one. The study remarks that German and French share culture-related emotional patterns, in contrast with the Chinese subjects. Even so, they suggested that the lack in the number of test subjects could affect this inference. This study is essential to understand and highlight the cultural influence in the neural patterns for ER in mixing cultures and can take an indirect impact in Ekman's theory of basic emotions.

The use of binary or ternary models in ER is prevalent, particularly for applications like detecting low-valence low-arousal states, or monitoring the frequency of negative emotions in security applications. Additionally, positive emotions and high-valence/high-arousal (HVHA) states are frequently studied to evaluate consumer responses within advertising and marketing domains. Nonetheless, when model architectures rely on stimulus-dependent structures — employing separate models for valence and arousal — achieving real-time emotion recognition becomes substantially more difficult due to the change and frequency of primitive modeling for recognition. Consequently, employing a multiclass approach is crucial to effectively detect rapid and involuntary emotional changes in the brain. Therefore, the multiclass

primitive and primary are some of the most effective AI models to predict the EEG input in emotion recognition. In this type of models, the frequency of chance and the lack of emotional identification is avoided. As a result, the framework introduced by Wu et al. (2022) evaluated binary, ternary, and multiclass classification performances using the DEAP, SEED, and SEED-V datasets, respectively. Their findings indicated a general trend: classification accuracy decreased as the number of classes increased. In this work, Wu et al. explored the functional connectivity between brain regions highlighting the *strength* feature as the best EEG connectivity feature in ER. Here, authors reduced the original set of 62 EEG channels to 18 (the list of channels is not provided) suggesting that the latter subset of channels is sufficient to provide the most relevant brain connection information in the SEED series dataset. The semi-supervised learning in the context of EEG-based emotion recognition has been rarely studied; developing an algorithm that clusters the complexity of EEG signals is a challenging task. Using three SEED-series and AMIGOS datasets, Zhang et al. (2022) tested a semi-supervised clustering algorithm to classify binary, ternary, and multiclass classification models. By evaluating the clustering performance for a set of $\mathbf{S}^{\tau} = \{\mathbb{C}_{\tau} \,|\, \forall \tau = \{1, 3, 5, 7, 10, 25\}\}$ pre-loaded labels per cluster, showed up a significant performance by increasing the labels in the primary emotions dataset; meanwhile, the primitive dataset showed a less sensitive performance by increasing the number of labels per cluster. Recent trends in AI have developed novel and highly accurate deep learning classification techniques for ER. One of the most recent contributions is presented by Dong et al. (2024), who introduced and evaluated an *emotion perceptron*—a spatial feature-processing unit comprising normalization, softmax, and feed-forward layers—and a temporal causal network composed of four interconnected blocks with multi-feedback mechanisms and activation functions (see original publication for details). Here, authors found that the extracted spatial adapter features are validated with the literature about the changes in happy and fear emotions and activation in a distribution map (similar to topography) processed by the spatial unit network. The classification results for the SEED-V dataset showed a precise recognition model with a 94.28 ± 07.51 performance. In the context of brain connections, Valderrama and Sheoran (2025) found that attention weights in some emotions have a strong influence in different brain regions. In general, (1) sadness showed a higher weight in the middle parietal and occipital regions, while (2) neutral is dominant in the right frontal, temporal, and parietal areas. Authors analyzed the SEED-IV and SEED-V datasets, where fear, disgust, and happiness have greater weights in frontal and temporal regions compared to sad and neutral. However, in SEED-IV, fear is stronger in the left temporal-parietal, and

happiness in the right frontal-temporal. Meanwhile, in SEED-V, fear dominates the right frontal-temporal, and happiness the left temporal-parietal.

2.4.2 Frequency decomposition

Using the MAHNOB-HCI, DEAP, and SEED datasets, Li et al. (2019) suggested the feature extraction per $\theta, \alpha, \beta,$ and γ band. The classification performance suggested a competitive ML model using DE-EEG based Network Patterns (ENP) features (see paper for details). The top performance is achieved in the SEED db with the γ band. In DL approach, Ma et al. (2025) includes the ANS contribution instead of using only CNS data. Here, authors made a robust and complex feature extraction by using binary and multiclass classification models, reaching the top accuracy by the use of θ-band in combination with peripheral feature extraction for multiclass models. In the test of binary models, the top performance was reached by the α+peri and β+peri (for feature extraction details go to the research). In a semi-supervised context, Peng et al. (2023) explored that some spatial-frequency patterns are shared across emotions, each emotion exhibits unique patterns, e.g.,: fear and happiness both activate the occipital region, but with different band distributions. Findings remarks that γ band is the most descriptive for the SEED-V dataset, while in a spatial context, prefrontal, temporal, and parietal regions are the most discriminative ones.

A seven-target classification model was developed by Song et al. (2019) by creating their own dataset with: (1) joy, (2) funny, (3) anger, (4) sadness, (5) fear, (6) disgust, and (7) anger emotional stimuli. Here, authors conducted an experimental self-assessed protocol to select 28 different content types of audio-visual stimuli ($[4 \times 7]$, four trials per emotion) in order of 30 Chinese subjects. Using this dataset, Multi-Modal Physiological Emotion Database (MPED), authors conducted three different classification experimental models: a binary, ternary and multiclass. The former compared the performance of positive and negative emotions (joy V anger, joy V fear; funny V anger, funny V fear, and more). The middle assessed a ternary classification clustering negative emotions (anger, sad, disgust, and fear) and positive ones (joy and funny), keeping neutral alone. Finally, the latter performs a subject-dependent multiclass classification. For these models, the feature extraction technique is based on fusing the extracted time-frequency features in order to five Butterworth frequency bands. The performance per model is shown in Table 2.5. An FPGA implementation for the SEED-IV dataset was implemented on an Altera DE2 where a low-resource CNN model was developed by Ezilarasan and Leung (2024). Here, authors reached a significant performance by using the

whole 62 channels and extracting the $\delta, \theta, \alpha, \beta,$ and γ time, frequency, and time-frequency features per band-rythm. Hardware implementation suggested a low resource consumption and a high performance, only requiring 25% of the LUTs and 35% of the DSP units, suggesting a powerful implementation for real-time applications.

Fusion learning combines the use of DL architectures as a feature extractor and ML as the fitting model. In order to extract feature maps from topo- and holo-graphic EEG spectral images, Topic and Russo (2021) created a FL subject-dependent model that outperformed primitive emotions. Here, fusion feature maps are also tested by appending the topo- and holo-graphic CNN features in a single input to the ML, suggesting that the fusion features are not always a better approach, in consequence a higher noise is introduced to the fitted model.

Table 2.5: Effective channels for emotion recognition in the state-of-the-art.

Channel selection					
Author	Dataset	Effective channels	N	Dominant lobe	Effectiviness
Zhuang et al. (2017)	DEAP	FP1, FP2, F7, F8, T7, T8, P7, and P8	8	Frontal, temporal, and parietal	V: $69.10 \pm 06.95^{1,d,*}$ A: $71.99 \pm 07.77^{1,d,*}$
Gupta et al. (2019)	SEED DEAP	T7	1	Temporal	$93.46^{2,a,\star}$ $72.07^{2,a,\bullet}$
Zheng et al. (2020)	Self DEAP	FPZ, AF4, F4, FP1, FC4, O1, PO3, FP2, FZ, and F8	10	Frontal	$91.23 \pm 06.40^{1,b,*}$
Seal et al. (2020)	Self	FP1-F7	2	Frontal	$94.72^{2,c,\bullet}$
Javidan et al. (2021)	DEAP	FC2, F7, F8, T7, T8, and P7	6	Frontal	
Yildirim et al. (2021)	DEAP	FP2, AF4, F3, F4, FC5, T7, C3, CP2, PO3, O1, and O2	11	Frontal	
Wagh and Vasanth (2022)	SEED series	FP1 and FP2	2	Frontal	71.52^{1}
Wu et al. (2022)	SEED-V	NP	18	NP	$84.51 \pm 05.11^{1,a,\bullet}$

Continued on next page

Table 2.5: Effective channels for emotion recognition in the state-of-the-art. (Continued)

Channel selection					
V. and Bhat. (2022)	AMIGOS	T7 and T8	2	Temporal	V: 95.49 A: 95.41 D: 95.49
		T7, T8, F7, F8, FC5, FC6, AF3, and AF4	8	Frontal and temporal	V: 94.56 A: 94.81 D: 95.32
Bagherzadeh et al. (2024)	SEED series	T7 and T8	2	Temporal	
Frequency decomposition					
Author	Dataset	Decomposition	N	Dominant frq	Effectiviness
Li et al. (2019)	MHCI DEAP SEED	Butterworth	4	γ	88.00 ± 07.00
Song et al. (2019)	MPED	Butterworth	5	δ+θ+α+β+γ	$38.74 \pm 07.75^{2,c,\bullet}$
Seal et al. (2020)	Self	Daubechies 8 DWT (db8)	1	γ	$94.72^{2,c,\bullet}$
Wagh and Vasanth (2022)	SEED series	Daubechies 6 DWT (db6)	10	γ	$\approx 70.00^{1}$
Wu et al. (2022)	SEED-V	Butterworth	5	$\beta + \gamma$	$\approx 60.00 \pm 10.00^{1,a,\bullet}$
Peng et al. (2023)	SEED-V	Butterworth	5	δ+θ+α+β+γ	$81.90 \pm 07.07^{1,c,\bullet}$
Ma et al. (2025)	DEAP	Butterworth	5	α	V: $73.67 \pm 07.07^{1,b,*}$ A: $77.03 \pm 03.77^{1,b,*}$
	SEED-IV			β	$41.65 \pm 01.02^{1,b,\star}$
	SEED-V			θ	$71.86 \pm 10.90^{1,b,\bullet}$

[1] Subject dependent model, [2] Subject independent model.

[a] Cross-Validation model, [b] Leave-One-Subject-Out model, [c] Hold-Out Training model, [d] Leave-One-Trail-Out model.

[*] Binary classification model, [⋆] Ternary classification model, [•] Multiclass classification model

The following tables introduce a brief overview of the most effective ML and DL models, some of which are listed in this EC section. However, the analysis is focused on the AI context, advantages, and limitations.

Table 2.6: Machine learning emotion recognition approaches.

Author	Dataset	Method	FE Technique	Classifier	Acc (%)	F1 (%)
Binary classification						
Zhuang et al. (2017)	DEAP	EMD	Spectral	SVM	V: 60.10 ± 06.95, A: 71.99 ± 07.77	$p = 1$
Gupta et al. (2019)	DEAP SEED	FAWT	Information Potential	RF	V: 79.99, A: 79.95, PNN: 90.58	
Farashi and Khosrowabadi (2020)	DEAP	MST	GCF	SVM	V: 81.25, A: 88.28	
Doma and Pirouz (2020)	DEAP	PCA		SVM	V: 63.43, A: 73.75, D: 67.18	V: 77.62, A: 84.73, D: 77.66
Zheng et al. (2020)	Self	WD	Statistical, entropy, and energy	SVM	HS: $91.308^{1,a,*}$	
Javidan et al. (2021)	DEAP	EC	Magnitude Squared Coherence Estimate	SVR	67.45	
Yildirim et al. (2021)	DEAP	PSO	HHT+PLV	RF	60.15 ± 08.94	
V. and Bhat. (2022)	AMIGOS	TF	ResNet	NB	V: $94.56^{2,a,*}$, A: $94.81^{2,a,*}$, D: $95.32^{2,a,*}$	V: $93.71^{2,a,*}$, A: $93.99^{2,a,*}$, D: $93.91^{2,a,*}$
Işık et al. (2023)	DEAP	DWT	Statistical & frequency	RF	100	100
Ternary classification						

Continued on next page

Table 2.6: Machine learning emotion recognition approaches. (Continued)

Author	Dataset	Method	FE Technique	Classifier	Acc (%)	F1 (%)
Liu et al. (2022b)	SEED-CHN SEED-GER SEED-FRA	Butterworth	Differential entropy	SVM	$83.44 \pm 11.10^{1,c,*}$ $65.47 \pm 16.93^{1,c,*}$ $64.84 \pm 13.64^{1,c,*}$	$p < 0.001$ effects of cultures and classifiers
Multiclass classification						
Ezilarasan and Leung (2024)	SEED-IV	Time and Frequency	WD	CNN	87%	
Gupta et al. (2019)	DEAP	FAWT	Information Potential	RF	71.43	
Seal et al. (2020)	Self	WD	Morpho and Statistical	NN	$94.72^{2,c,\bullet}$	94.71

[1] Subject dependent model, [2] Subject independent model.

[a] Cross-Validation model, [b] Leave-One-Subject-Out model, [c] Hold-Out Training model, [d] Leave-One-Trail-Out model.

[*] Binary classification model, [⋆] Ternary classification model, [•] Multi-class classification model.

Functional Analytic Wavelet Transform (FAWT), Random Forest (RF),

Table 2.7: Deep learning emotion recognition approaches.

Author	Dataset	Method	FE Technique	Classifier	Acc (%)	F1 (%)
Binary classification						
Song et al. (2019)	MPED	STFT	Time and frequency	LSTM	$72.93 \pm 13.19^{1,c,*}$	
Topic and Russo (2021)	DEAP	db5-DWT	Spectral	CNN + SVM	V: 74.91 ± 01.93, A: 75.44 ± 02.71	
	SEED				73.11 ± 03.02	
	DREAMER				V: 81.25 ± 01.73, A: 85.10 ± 02.62	
	AMIGOS				V: 79.54 ± 01.26 A: 85.07 ± 02.04	

Continued on next page

Table 2.7: Deep learning emotion recognition approaches. (Continued)

Author	Dataset	Method	FE Technique	Classifier	Acc (%)	F1 (%)
Wu et al. (2022)	DEAP	Brain functional connectivity network	EEG+EOG Connectivity network features	DCCA	V:86.61 ± 03.76[1,a,*] A:85.34 ± 02.90[1,a,*]	
Zhang et al. (2024)	DEAP AMIGOS	TorchEEG$_{EMO}$		CNN	88.94[2,a,*] 90.24[2,a,*]	
Ma et al. (2025)	DEAP	Multimodal	Statistical & Spectral	C2PCI-Net	V: 75.00 ± 06.14[1,b,*], A: 77.33 ± 03.06[1,b,*]	V: 71.24 ± 06.95[1,b,*], A: 73.59 ± 03.04[1,b,*]
	HCI				V: 78.78 ± 17.40[1,b,*], A: 75.38 ± 05.44[1,b,*]	V: 72.39 ± 09.03[1,b,*], A: 70.17 ± 07.44[1,b,*]
			Ternary classification			
Song et al. (2019)	MPED	STFT	Time and frequency	LSTM	71.57[1,c,⋆]	67.74[1,c,⋆]
Liu et al. (2022b)	SEED-CHN	Butterworth	Differential entropy	DCCA-AM	92.79 ± 08.21[1,c,*]	$p < 0.001$ effects of cultures and classifiers
	SEED-GER				88.63 ± 10.87[1,c,*]	
	SEED-FRA				80.71 ± 13.09[1,c,*]	
Wu et al. (2022)	SEED	Brain functional connectivity network	EEG+EOG Connectivity network features	DCCA	95.08 ± 06.42[1,c,⋆]	
Bagherzadeh et al. (2024)	SEED-GER	SSWT	Spectral images	ResNet-18	81.25	
	SEED-FRA				75.00	
Zhang et al. (2024)	SEED	TorchEEG$_{EMO}$		CNN	83.79[2,a,*]	

Continued on next page

Table 2.7: Deep learning emotion recognition approaches. (Continued)

Author	Dataset	Method	FE Technique	Classifier	Acc (%)	F1 (%)
Valderrama and Sheoran (2025)	SEED	NN Extractor	Temporal, spatial, and spectral	DANN	$79.30 \pm 05.80^{1,a,\bullet}$	
			Multiclass classification			
Song et al. (2019)	MPED	STFT	Time and frequency	LSTM	$38.74 \pm 07.75^{1,c,\star}$	
Wu et al. (2022)	SEED-V	Brain functional connectivity network	EEG+EOG Connectivity network features	DCCA	$84.51 \pm 05.11^{1,a,\bullet}$	
Zhang et al. (2024)	SEED-IV	$\text{TorchEEG}_{\text{EMO}}$		CNN	$65.92^{2,a,*}$	
Bagherzadeh et al. (2024)	SEED-IV SEED-V	SSWT	Spectral images	ResNet-18	76.66 78.12	
Dong et al. (2024)	SEED-V	STFT	DE	Emotion perceptron	$94.28 \pm 07.51^{2,c,\bullet}$	
Valderrama and Sheoran (2025)	SEED-V	NN Extractor	Temporal, spatial, and spectral	DANN	$60.70 \pm 15.30^{1,a,\bullet}$	
Ma et al. (2025)	SEED-IV SEED-V	Multimodal	Statistical & spectral	C2PCI-Net	$71.94 \pm 08.80^{1,b,\bullet}$ $84.83 \pm 01.05^{1,b,\bullet}$	$70.82 \pm 09.92^{1,b,\bullet}$ $84.79 \pm 01.03^{1,b,\bullet}$
Ghous et al. (2025)	SEED-V MPED	Spectral and Temporal	Transformed features	Transformed model	90% 79%	90% 79%

[1] Subject dependent model, [2] Subject independent model.

[a] Cross-Validation model, [b] Leave-One-Subject-Out model, [c] Hold-Out Training model, [d] Leave-One-Trail-Out model.

[*] Binary classification model, [⋆] Ternary classification model, [•] Multi-class classification model.

The reviewed literature highlights the effectiveness of ER in the use of EEG signals in the context of binary, ternary, and multiclass classification models. In order of the Table 2.5, the top used channel is the T7 and T8, which are located at the temporal lobe. However, the most used lobe is the frontal one, followed by the temporal (see Table 2.8). Moreover, the γ band resulted as the most effective rhymth in the context of ER in EEG signals, followed by the β and α bands. Finally, in order of classification performance, the DL performance usually overcomes the ML models, however ML models are more effective in the context of real-time applications due to their low computational resources. The DL models are more effective in the context of high-performance applications, where the computational cost is not a limitation. Now, in the context of preprocessing techniques based on Wavelet or Fourier transforms, the former one is the most effective, which is consistent with the literature that suggests that the Wavelet transform is more effective in the context of EEG signals. The use of DWT and db are the most used techniques in the context of ER.

In close connection, the reviewed neuroscience literature highlights the *early* and *late* amygdala's activation process (see Guex et al. (2020)). The formed is related to a "bottom-up" process, where the amygdala is activated by the stimuli and then the ANS is activated. This "bottom-up" is an automatic response in the trigger of the fight-or-flight scenario (see Damasio (1999)) and is presented $\approx$ 130ms after the stimuli. The "top-down" response is activated in 220ms or beyond after the stimuli input. In this process, the amygdala is modulated by the CNS and ANS is order to provide a deeper context to the amygdala, generating an accurate emotional response. According to this theory, Guex et al. (2020) observed that the response to emotional stimuli appears between 100 and 200ms, while Šimić et al. (2021) proposed the *low-road*, where activation occurs between 40 and 140ms.

Table 2.8: Channel frequency analysis (information taken from Table 2.5).

Channel	Count	Dominant Lobe	Channel	Count	Dominant Lobe	Channel	Count	Dominant Lobe
T7	7	Temporal	T8	5	Temporal	F7	4	Frontal
F8	4	Frontal	FP1	4	Frontal	FP2	4	Frontal
AF4	3	Frontal	PO3	2	Parietal	O1	2	Occipital
FC5	2	Frontal	AF3	2	Frontal	F4	2	Frontal
P7	2	Parietal	FC4	1	Frontal	FPZ	1	Frontal
FZ	1	Frontal	C3	1	Central	CP2	1	Central-Parietal

Continued on next page

Table 2.8: Channel frequency analysis (information taken from Table 2.5). (Continued)

Channel	Count	Dominant Lobe	Channel	Count	Dominant Lobe	Channel	Count	Dominant Lobe
F3	1	Frontal	O2	1	Occipital	FC6	1	Frontal

2.4.3 Quaternion Signal Analysis

Based on the reviewed frameworks, this work introduces an adapted version of the quaternion signal processing model that have been used as preprocessing technique. The quaternion algebra was introduced in 1834 by W. R. Hamilton, and it is proposed as an extension of the traditional algebra of complex numbers, given as

$$\mathbb{H} = \{q | q = a + b\boldsymbol{i} + c\boldsymbol{j} + d\boldsymbol{k}, \quad \forall \{a, b, c, d\} \in \mathbb{R}\}, \tag{2.1}$$

where $[\mathbf{1},\ \boldsymbol{i},\ \boldsymbol{j},\ \boldsymbol{k}]$ is the basis for this algebra. The elementary Hamilton multiplication rules for this quadruple are defined as

$$\begin{gathered} \boldsymbol{i}^2 = \boldsymbol{j}^2 = \boldsymbol{k}^2 = -1, \\ \boldsymbol{ij} = -\boldsymbol{ji} = \boldsymbol{k}, \quad \boldsymbol{jk} = -\boldsymbol{kj} = \boldsymbol{i}, \quad \boldsymbol{ki} = -\boldsymbol{ik} = \boldsymbol{j}. \end{gathered} \tag{2.2}$$

In Lian (2018) framework, a deep quaternion-based signal analysis, where a hyper-complex Fourier transform treats multi-channel signals as a quaternion compound was presented. Such a theory establishes the formal mathematics to prove that the two-sided Quaternion Fourier Transform (QFT) is a robust and reliable signal processing method to extract discriminant features. Formally speaking, QFT is defined by

$$F(u, v) = \int_{\mathbb{R}^2} \mathrm{e}^{-2\pi(\boldsymbol{i}xu + \boldsymbol{j}yv)} f(x, y)\, dxdy, \tag{2.3}$$

where $f \in L_1(\mathbb{R}^2, \mathbb{H})$. Accordingly, Bhat et al. (2022) proposed a novel Fourier framework based on windowed signal processing to test the uncertainty principle in the method referred to as the Quaternion Windowed Quadratic-Phase Fourier Transform (QWQPFT), conducting near applications on Wigner distributions.

QSA applied to engineering has shown reliable performance in classification tasks. For instance, Contreras-Hernandez et al. (2019) proved the QSA performance by computing the $q(t)$ and $q(t + \Delta t)$ quaternion sequence as well as performing a rotation to classify three different induction motor failure states. Similarly, Batres-Mendoza et al. (2016) achieved high

binary classification rates using an efficient feature extractor based on the quaternion rotation for the left and right motor imagery experiments. The proposed framework, a novel approach in the field, reached an accurate ML model with 30 samples per quaternion window, offering a fresh perspective on EEG signal analysis and emotion classification. Likewise, Javidi et al. (2011) suggested including multiple EEG channels into a quaternion form to develop a quaternion Fast Independent Component Analysis (q-FastICA), obtaining a substantial reduction in EEG/EOG signal artifacts.

In this context, the presented work proposes an adapted quaternion signal processing by exploring the pre-processing performance using a bicomplex form by applying quaternion and bicomplex product criteria, following the mathematics established in Ell et al. (2014). Hence, the bQSA proposed is adapted to EEG signals for emotion recognition.

Chapter 3

Material and methods

In the preceding sections, an overview of emotion recognition is provided to set a context for the reader, addressing research from neuroscience, biology, data analysis, signal processing (both pre- and post-signal), and AI classification models. With this introduction, this document outlines the principal approach of this study. After extensive experimentation and overcoming several challenges, a highly effective signal pre-processing technique that extracts essential information from EEG signals was developed. Referred to as bQSA, this method provides a pattern that only with statistical features can classify up to six primary emotions (and a neutral one) with 100% of accuracy rate and up to thirteen self-assessed emotions with over 90%.

Well, maybe I should start the previous sentence with a spoiler alert, sorry about that. Before discussing the bQSA method in detail, it is imperative to describe the materials and methods employed in this study. The greatest tasks in this study are the datasets, the channel selection method, and bQSA signal processing, as the general diagram of this work, displayed in Fig. 3.1. The following sections provide a detailed description of each of these components.

3.1 Database description

In the first six months of life, newborns develop six basic emotions based on a stimuli-response that influence their commitment to specific goals. This study delves into the intricacies of neuroscience and emotion recognition technology. To provide a reliable and robust evaluation of the bQSA method, the V- and VII-SEED series, AMIGOS, DEAP, and FEEL datasets are

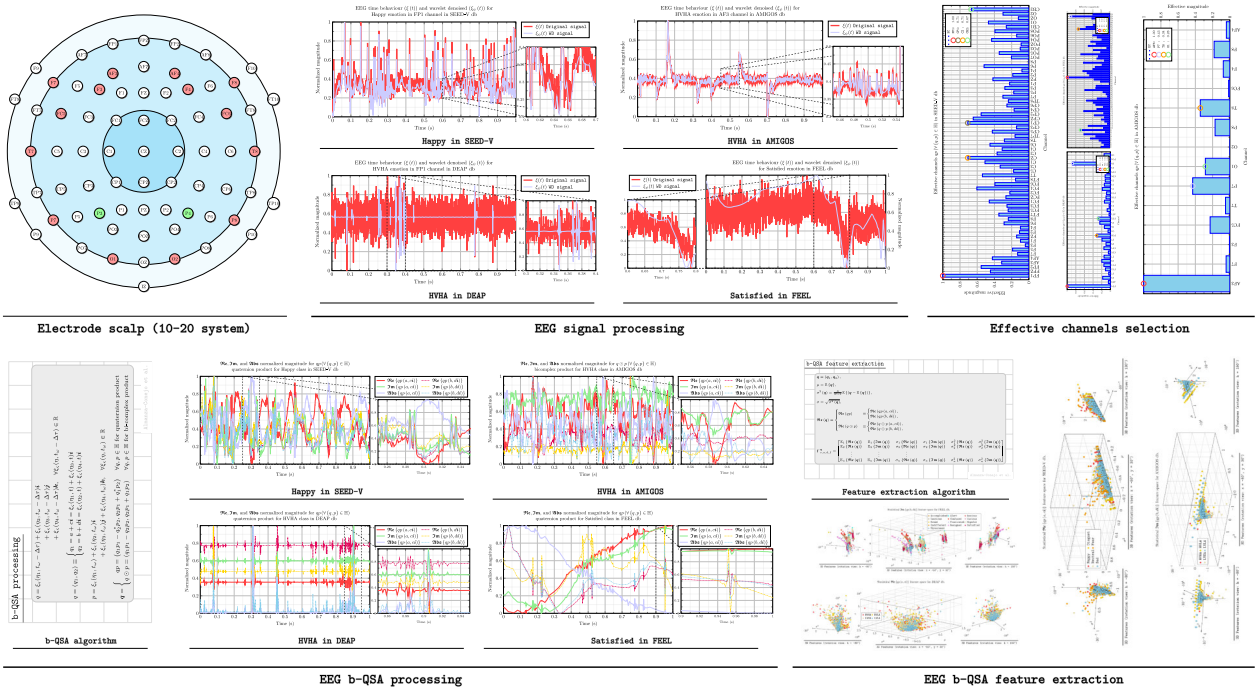

Figure 3.1: General method diagram of the bQSA signal processing.

used. The data is pre-processed with complex techniques, such as Wavelet noise reduction and bQSA, to capture the relevant information of the data. Consequently, the statistical feature extraction is applied to the bQSA signals to achieve an ML model for classifying five, four, and thirteen primary, primitive, and self-assessed emotion stimuli, respectively. The data structure per dataset is summarized as follows:

1. SEED-VII is the newest and most recent emotion recognition dataset developed by Jiang et al. (2025), the dataset accomplished the physiological impulse response of 20 subjects, where each one accomplished 4-folders of 4 tests, evoking five emotion stimuli per test, randomly choosing five out of seven emotional targets per each stimuli. EEG information was collected using a 62-electrode scalp. Same as in the SEED-V dataset, the protocol followed the same four emotion stimuli and neutral material to accomplish in the new subjects the same stimuli, completing the six primary emotions, inspired by Ekman's theory, with the anger and surprise emotions. Data storage sums a total of $\Xi_{s_{vii}} \in \mathbb{R}^{99200 \times n}$.
   (a) Twenty test subjects.
   (b) Four folders per subject.
   (c) Four times test per folder

   (d) Primary emotions: happy, surprise, sad, disgust, neutral, anger, and fear.
   (e) Sixty-two electrode scalp.
   (f) A total of $99,200$ EEG signals.
   (g) Sampling frequency, $f_s = 200$ Hz.
2. The SEED-V dataset is a data collection in which an audiovisual movie clip was used to stimulate the test subjects. The signal length varies per sample, and the brain bioelectrical potential is recorded with a 62-channel electrode scalp. This dataset stores several emotion stimuli, making it an ideal resource for this research. Sixteen subjects participated in this experiment following three different trials. Besides, each trial contains 15 different stimuli movie clips, three per emotion. In short, a total of $\Xi_{s_v} \in \mathbb{R}^{44640\times n}$ samples are recorded, where n is the signal length. Each emotion label τ stores the same number of samples, i.e., $\Xi_s^\tau \in \mathbb{R}^{8928\times n}$ is the EEG emotion dimension.
   (a) Sixteen test subjects.
   (b) Tree tests per subject.
   (c) Tree-times trial per emotion.
   (d) Primary emotions: happy, sad, disgust, neutral, and fear.
   (e) Sixty-two scalp electrodes.
   (f) A total of 44640 EEG signals.
   (g) Sampling frequency, $f_s = 1.0$ kHz.
3. AMIGOS dataset was developed as a minor data collection tool using popular movies as emotional stimuli. As in SEED-V, EEG's length differs per sample according to the duration of stimuli. In practice, AMIGOS used an EMOTIV-Epoch scalp electrodes with 14 EEG channels and 40 test subjects. The bioelectrical potential for the four primitive emotions is recorded in four different trials. In summary, a total of $\Xi_a \in \mathbb{R}^{8960\times n}$ samples is recorded for $\Xi_a^\tau \in \mathbb{R}^{2240\times n}$ per primitive emotion.
   (a) Forty test subjects.
   (b) Four times per trial.
   (c) Primitive emotions: HVHA, HVLA, LVHA, and LVLA.
   (d) Fourteen scalp electrodes.
   (e) A total of 8960 EEG signals.
   (f) Frequency sampling, $f_s = 128$ Hz.
4. DEAP is a collection of EEG signals using popular music videos as an audiovisual emotion stimuli. Scalp electrodes with 32-EEG channels records the brain's bioelectrical potential for 32 subjects and 40 music videos. Self-assessed labeling was introduced

following the SAM Mannequins to visualize ratings for Valence and Arousal (V&A) primitive emotions. DEAP contains a sum of $\Xi_d \in \mathbb{R}^{40960\times n}$ of EEG emotion stimuli samples. Classification targets and frequency sampling are the same as in AMIGOS.
   (a) Thirty-two test subjects.
   (b) Forty stimuli videos per subject.
   (c) Thirty-two scalp electrodes.
   (d) A total of 40960 EEG signals.
   (e) Frequency sampling, $f_s = 128$ Hz.
5. FEEL accomplished the EEG data recorded while subjects played video games. Geodesic Sensor Net, 64-EEG channels, read the neurological activity for an extended set of subjects' self-assessed labeled classes. Here, FEEL developers proposed timestamps with 5 seconds of duration after each timestamp to achieve the emotional stimuli. In sum, a $\Xi_f \in \mathbb{R}^{1356\times n}$ is stored in the FEEL dataset.
   (a) Sixteen test subjects.
   (b) Approx. thirteen stimuli videos per subject.
   (c) Sixty-four scalp electrodes.
   (d) Frequency sampling, $f_s = 1000$ Hz.

3.2 Channel selection method

The first part of this methodology is the noise- and lack-reduction processing. Here, the channel selection method by using the WD, Local Binary Pattern (LBP), a statistical, time-frequency, energy, and morphology feature extraction, and the mRMR is introduced. The following subsections describe these methods.

3.2.1 Wavelet decomposition noise reduction

One of the first pre-processing tasks for every scientist who works with non-periodical signals is noise and artifact reduction. In this regard, Dadebayev et al. (2022) suggested that the most common techniques are based on the FT and WT. Moreover, Torres et al. (2020) conducted a comprehensive study from 2015 to 2020, evaluating several spectral analysis techniques for feature extraction, yielding FT and WT as the top ones. In particular, Xie and Oniga (2020) mentioned the contribution of wavelet transform and decomposition of EEGs overates the Fourier-based noise reduction techniques. Those examples remark the wavelet advantage in

non-periodical signals. Assuming an $x(t) \in \mathbb{R}$ as input signal, which in this case could be any input signal from any of the datasets described above, the wavelet noise-reduction method can be applied by

$$W(s,\tau) = \frac{1}{\sqrt{s}} \int_{-\infty}^{\infty} \overline{\psi\left(\frac{t-\tau}{s}\right)} x(t)\, dt. \tag{3.1}$$

where $\overline{\psi\left(\frac{t-\tau}{s}\right)}$ represents the complex conjugate kernel transform; s and τ represents the scales and time shift factor. Based on the proposals of this document, the wavelet noise reduction is performed with the `wdenoise` MATLAB-wavelet toolbox function. According to the documentation, the algorithm outperforms the

$$s(n) = f(n) + \sigma e(n), \tag{3.2}$$

where n is the dimention space of the $f(n)$ input signal; $e(n)$ is the Gaussian white noise $N(0,1)$ and σ is the noise level. The denoising procedure consists of three steps:

- Decomposition: Select a mother wavelet and a decomposition level σ. Perform a wavelet decomposition of the $s(n)$ signal at σ level.
- Detail Coefficients Thresholding: For each level from $[1, \sigma]$ choose a denoising method for detail coefficients (see documentation for possible `args`).
- Reconstruction: Reconstruct the signal using the original approximation coefficients from level σ and the modified detail coefficients from levels 1 to σ.

Then, by using the wavelet kernel, the wavelet filters are split into several scales to outperform the σ-th decomposition level, computed by the $\sigma = \lfloor \log_2(n) \rfloor$ criteria, based on the f_s scalar — $[4, 2)$ Hz, $[8, 4)$ Hz, and suchlike until $[1000, 500)$ Hz for $f_s = 1000$ Hz — as shown in Fig. 3.2a. Additionally, a representation of the EEG wavelet decomposition is shown in Fig. 3.2b — a `wdenoise(x, σ, NoiseEstimation = LevelDependent)` criteria is employed for each decomposition.

3.2.2 The local binary pattern

Following the WD, the One Dimensional Local Binary Pattern (1D-LBP) algorithm is adapted to input data. According to Khan et al. (2020), the combination of EEG-WD-1D-LBP preprocessing techniques produced an accurate performance in ML models. Similarly, in Kılıç et al. (2021), a multimodal input data is processed by computing histograms and features

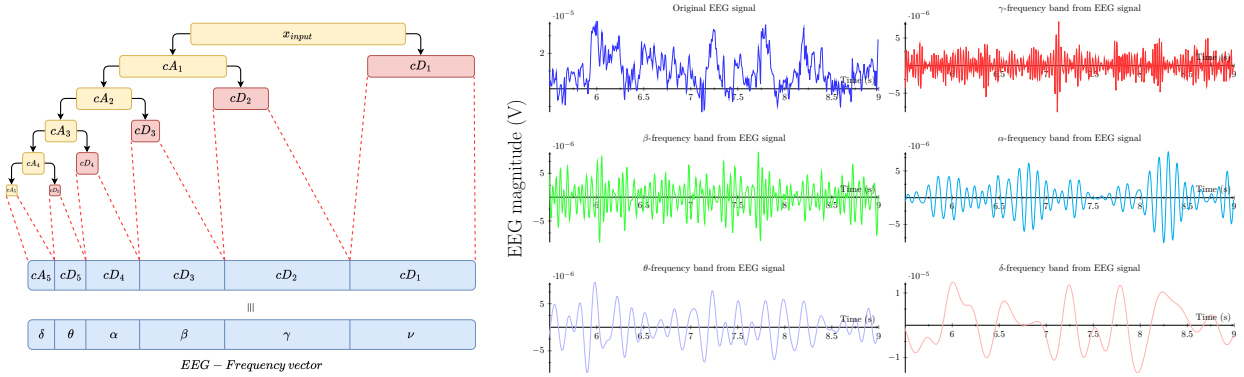

(a) Decomposition level. (b) EEG wavelet decomposition.

Figure 3.2: Wavelet decomposition.

from the resulting 1D-LBP. In this order of ideas, the 1D-LBP can be expressed as

$$LBP(t) = \sum_{p=1}^{\tau} s\left(\delta\right) * 2^{p-1}, \tag{3.3}$$

$$s(\delta) = \begin{cases} 1, & \text{if } \xi\left(t+\tau\right) \geq \xi\left(\left\lceil \frac{t+\tau}{2} \right\rceil\right) \\ 0, & \text{otherwise} \end{cases}, \tag{3.4}$$

where in this context τ is the window's lenght for analysis the 1D-LBP, taking the $\xi\left(\left\lceil \frac{t+\tau}{2} \right\rceil\right)$ central value of the $\xi\left(t+\tau\right)$ current window as threshold. The 1D-LBP maximum and minimum values will be dependent on the τ length. For the purposes of this study, the classical 8-bit configuration; therefore, min = 0 and max = 255 is computed. This process is repeated for each window in the input tensor. An example of the 1D-LBP processing is shown in Fig. 3.3.

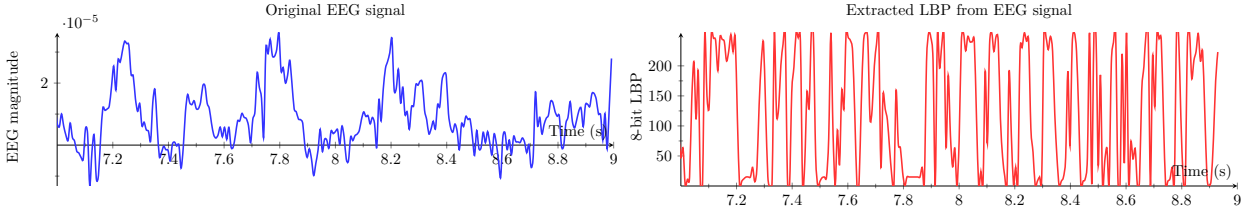

Figure 3.3: EEG 1D-LBP processing.

3.2.3 The 1D-LBP feature extraction

Following the 1D-LBP processing, a statistical, time-frequency, energy, and morphologic feature extraction is computed for each $x_i \equiv LBP(t)$ produced per input tensor as defined in Table 3.1.

Table 3.1: 1D-LBP Feature extraction.

Name	Function	Name	Function	Name	Function	Name	Function
μ	$\frac{1}{n}\sum_{i=1}^{n} x_i$	ABS	$\sum_{i=1}^{n} \lvert x_i \rvert$	NRE	$-\frac{1}{2}\log_2\left(\sum_{i=1}^{n}\left(\frac{x_i}{n\cdot\bar{x}}\right)^3\right)$	AAC	$\frac{1}{n-1}\sum_{i=1}^{n-1} \lvert x_{i+1}-x_i \rvert$
σ^2	$\frac{1}{n-1}\sum_{i=1}^{n}(x_i-\bar{x})^2$	MOB	$\frac{\sigma(\Delta x)}{\sigma(x)}$	FLX	$\sum_{i=1}^{n-1}(x_{i+1}-x_i)$	MAV	$\frac{1}{n-1}\sum_{i=1}^{n-1} \lvert x_{i+1}-x_i \rvert$
ς	$\frac{1}{n}\sum_{i=1}^{n}\left(\frac{x_i-\bar{x}}{\sigma}\right)^3$	EC	$\left(\sum_{i=1}^{n}\sqrt{\lvert x_i \rvert}\right)^2$	MAD	$\frac{1}{n}\sum_{i=1}^{n} \lvert x_i-\bar{x} \rvert$	HMO	$\frac{1}{n-1}\sum_{i=1}^{n-1}\frac{1}{1+\lvert x_{i+1}-x_i \rvert}$
κ	$\frac{1}{n}\sum_{i=1}^{n}\left(\frac{x_i-\bar{x}}{\sigma}\right)^4$	RMS	$\sqrt{\frac{1}{n}\sum_{i=1}^{n} x_i^2}$	CLR	$\frac{\max(x)-\min(x)}{\text{EC}}$	GME	$\exp\left\{\frac{1}{n}\sum_{i=1}^{n}\log\left(\lvert x_i \rvert+\varepsilon\right)\right\}$
SPE	$0.85\sum_{i=1}^{n} x_i$	SF	$\text{RMS}/\frac{1}{n}\sum_{i=1}^{n} \lvert x_i \rvert$	CF	$\frac{\max(x)-\min(x)}{\text{RMS}}$	GHO	$\left(1+\sum_{i=1}^{n-1} \lvert x_{i+1}-x_i \rvert\right)^{-1}$

μ (mean), σ^2 (variance), ς (skewness), κ (kurtosis), MAD (mean absolute deviation), RMS (root mean square), MAV (mean absolute value), HMO (Homogeneity), SPE (spectral power energy), NRE (nonlinear energy operator), EC (energy concentration), FLX (signal flux), and GHO (Hjorth complexity). The n is the number of samples in the input tensor x_i.

Then, $\digamma \equiv [n \times f] \in \mathbb{R}$ is the produced feature matrix, where in this context n and f are the number of samples and features extracted, respectively. Then $\digamma$ is resized to $\digamma_\varsigma \equiv [\rho \times \eta] \in \mathbb{R}$ where ρ is the number of features times the number of samples per dataset and η the number of channels or input sources per dataset, e.g. for SEED-V dataset the initial $\{\digamma \equiv [44640 \times 13]\} \Rightarrow \{\digamma_\varsigma \equiv [4320 \times 62]\}$.

3.2.4 The minimum redundancy maximum relevance algorithm (mRMR)

After data management and performing pre-processing to get the $\digamma$ feature matrix, the mRMR algorithm (see Ding and Peng (2005)) is adapted to obtain the most relevant input sources based on the extracted features, e.g., the electrode signals in EEG input tensor per dataset collection. The mRMR introduces the

$$I(a,b) = \sum_{\{i,j\}\in\digamma} p(a_i,b_j)\log\frac{p(a_i,b_j)}{p(a_i)\,p(b_j)} \tag{3.5}$$

criteria, where in this context, $p(a_i, b_j)$ represents the joint probability distribution, while $p(a_i)$ and $p(b_j)$ denote the marginal probabilities for each feature in the matrix $\digamma$. In consequence, the mRMR criterion is computed by

$$\max_{i \in \Omega_{\digamma}} \left[I(i, \mathbf{h}) - \frac{1}{|\digamma|} \sum_{i \in \digamma} I(i, j) \right], \tag{3.6}$$

where $\mathbf{h} = [h_1, h_2, \ldots, h_k]^{\intercal}$ is the target class and $|\digamma|$ is the cardinality of the input feature matrix $\digamma$. The $\boldsymbol{\eta}_{\zeta} \in \mathbb{R}^{\eta \times 1}$ resulting relevance vector estimates a relevance scalar coefficient per input source (e.g. EEG channels). Once the relevance vector is obtained, the top-four references are used to compute the quaternion processing as described below. An example of the produced mRMR scores is plotted in Fig. 3.4 bar chart.

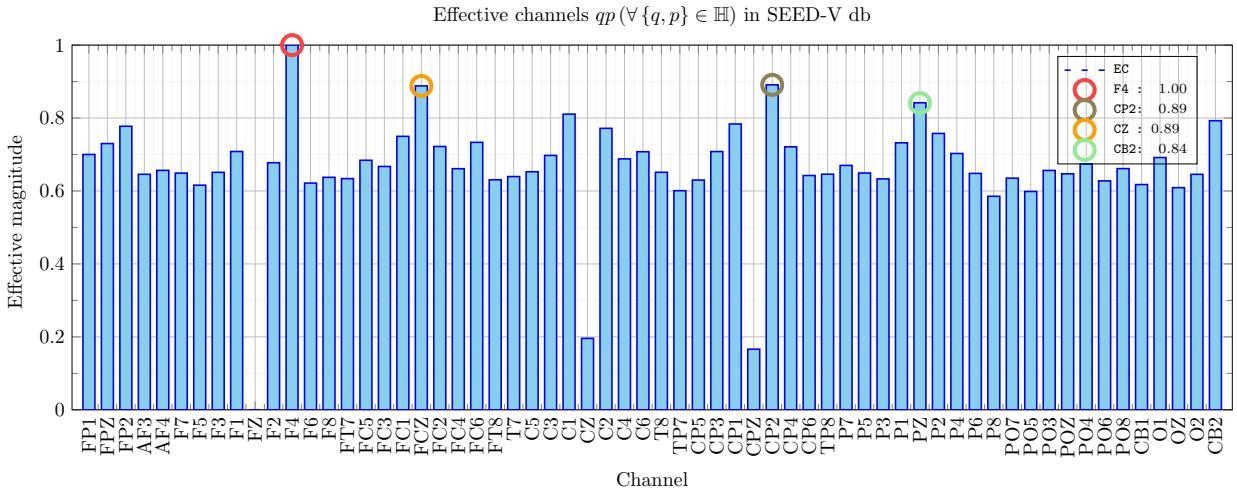

Figure 3.4: mRMR scores according to each channel in the SEED-V dataset.

3.3 The bQSA method

The channel selection is a very robust method to find the top-four references to construct a quaternion. Before of the bQSA introduction, once the top-four effective channels are selected, a translation offset is applied to the denoised signal (ξ_{ψ}). The translation offset is computed as

$$\xi_{\varsigma}(t) = \xi_{\psi}(t) - \frac{\min(\xi_{\psi}(t))}{\max(\xi_{\psi}(t)) - \min(\xi_{\psi}(t))}, \tag{3.7}$$

transforming the $\xi_{\psi}(t) \rightarrow \xi_{\varsigma}(t)$ in order to reduce outliers and the bias generated by the WD effect and preserving relative scales without compressing data spread as with $\min - \max$ normalization. As a very important fact, for this experimental protocol, the EEG channels are used in order of the acquisition magnitude. Datasets as SEED and AMIGOS in the MATLAB management-reading yields magnitude values in the order of $\xi(t) \times 10^{0}$; however the documentation details that values are in the order of $\times 10^{-6}$. For this experimentation, each channel magnitude is returned to μV values by applying a $\xi(t) \times 10^{-6}$ scalar. This process is made in order to accomplish all computations as close as the raw files as possible. The following step is to compute the quaternion representation, denoted by

$$q = a + b\boldsymbol{i} + c\boldsymbol{j} + d\boldsymbol{k},\ q \in \mathbb{H}, \tag{3.8}$$

where q encompasses scalar and vectorial components, expressed as $\{q = S(q) + \boldsymbol{V}(q)\,|\,S(q) \in \mathbb{R}, \boldsymbol{V}(q) \in \mathbb{H}\}$. Therefore, the (3.8) form can change to a new expression consistent with the effective channels proposal and the achieved top-four references as

$$q = \xi_{\varsigma}(\eta_1, t) + \xi_{\varsigma}(\eta_2, t)\boldsymbol{i} + \xi_{\varsigma}(\eta_3, t)\boldsymbol{j} + \xi_{\varsigma}(\eta_4, t)\boldsymbol{k},\ \{\forall \xi_{\varsigma}(\eta_k, t) \in \mathbb{R}\}, \tag{3.9}$$

where $\xi_{\varsigma}(\eta_k, t) \in \mathbb{R}$. Then, (3.9) is addapted to bicomplex quaternion form

$$q = (q_1, q_2) \equiv \begin{cases} q_1 = a + c\boldsymbol{i} = \xi_{\varsigma}(\eta_1, t) + \xi_{\varsigma}(\eta_3, t)\boldsymbol{i}, \\ q_2 = b + d\boldsymbol{i} = \xi_{\varsigma}(\eta_2, t) + \xi_{\varsigma}(\eta_4, t)\boldsymbol{i}. \end{cases} \tag{3.10}$$

Following this processing, a second quaternion is declared by applying a time shifting to the first one. The time-shift follows a 250ms criteria as $x(t - \tau)$ where $\tau = \frac{f_s}{4}$. This criteria is justified based on the low- and high-road pathway response (see Chapter 2). For instance, Guex et al. (2020) found that the emotional stimuli response is observed between 100 and 200 ms, indicating an early amygdala activation. Alternatively, Šimić et al. (2021) established a low-road pathway with activation occurring between 40-140 ms, which bypasses the level of consciousness and directly reaches the amygdala response. As consequence, the q quaternion is rewritten as

$$q = \xi_{\varsigma}(\eta_1, t - \Delta\tau) + \xi_{\varsigma}(\eta_2, t - \Delta\tau)\boldsymbol{i} + \xi_{\varsigma}(\eta_3, t - \Delta\tau)\boldsymbol{j} + \xi_{\varsigma}(\eta_4, t - \Delta\tau)\boldsymbol{k},\ \{\forall \xi_{\varsigma}(\eta_k, t - \Delta\tau) \in \mathbb{R}\}, \tag{3.11}$$

rewritting Equation (3.10) as

$$q = (q_1, q_2) \equiv \begin{cases} q_1 = a + c\boldsymbol{i} = \xi_\varsigma(\eta_1, t-\tau) + \xi_\varsigma(\eta_3, t-\tau)\boldsymbol{i}, \\ q_2 = b + d\boldsymbol{i} = \xi_\varsigma(\eta_2, t-\tau) + \xi_\varsigma(\eta_4, t-\tau)\boldsymbol{i}. \end{cases} \tag{3.12}$$

and yielding p quaternion as

$$p \;=\; \xi_\varsigma(\eta_1, t) + \xi_\varsigma(\eta_2, t)\boldsymbol{i} + \xi_\varsigma(\eta_3, t)\boldsymbol{j} + \xi_\varsigma(\eta_4, t)\boldsymbol{k},\;\; \{\forall \xi_\varsigma(\eta, t) \in \mathbb{R}\}\,, \tag{3.13}$$

equally represented in the bicomplex form, yielding

$$p = (p_1, p_2) \equiv \begin{cases} p_1 = a + c\boldsymbol{i} = \xi_\varsigma(\eta_1, t) + \xi_\varsigma(\eta_3, t)\boldsymbol{i}, \\ p_2 = b + d\boldsymbol{i} = \xi_\varsigma(\eta_2, t) + \xi_\varsigma(\eta_4, t)\boldsymbol{i}. \end{cases} \tag{3.14}$$

The Cayley-Dixon form presented in Ell et al. (2014) introduces a dual approach by considering both q and p quaternions to achieve a bicomplex $\mathbf{q}$ form and proposing the quaternion product and the bicomplex product for signal processing, as:

$$\mathbf{q} \equiv (\boldsymbol{q}_1, \boldsymbol{q}_2) \equiv \begin{cases} qp & = (q_1p_1 - q_2^*p_2, q_2p_1 + q_1^*p_2)\,, \\ q \odot p & = (q_1p_1 - q_2p_2, q_2p_1 + q_1p_2)\,, \end{cases} \tag{3.15}$$

where $\{p, q\} \in \mathbb{H}$, $\{q_1, q_2, p_1, p_2\} \in \mathbb{C}$, and * denotes the complex conjugated. Here, an example plot of the quaternion and bicomplex product time-behaviour is shown in Figs. 3.5a and 3.5b.

3.4 Feature extraction

The computational feature extraction method is based only on statistics. Once that bQSA is computed, the mean, standard deviation, and variance are computed per $\mathbf{q}$ quaternion product selection. The $\mathfrak{Re}(\mathbf{q})$ and $\mathfrak{Im}(\mathbf{q})$ are used to compute the basic statistical features. In this study, the unbiased variance σ^2 for N elements is computed by

$$\sigma^2(\mathbf{q}) = \frac{N}{N-1}\mathbb{E}\left((\mathbf{q} - \mathbb{E}(\mathbf{q}))^2\right), \tag{3.16}$$

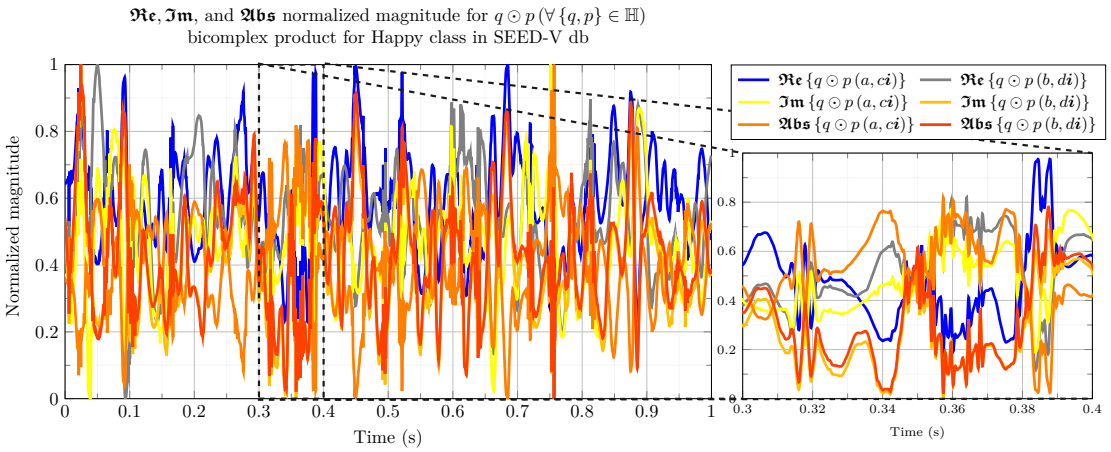

(a) Bicomplex product for a happy input EEG signal using the top-four EC.

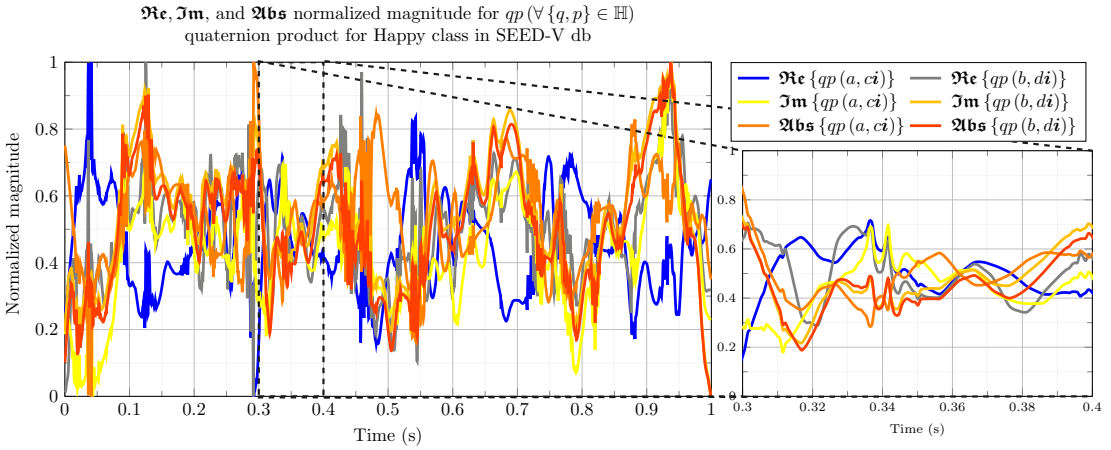

(b) Quaternion product for a happy input EEG signal using the top-four EC.

Figure 3.5: Comparison of quaternion and bicomplex products for a happy input EEG signal using the top-four EC.

where $E(\mathbf{q})$ is the expected value of $\mathbf{q}$, denoted by μ. A single feature matrix, as the one obtained for the SEED-V dataset, is computed by the following expression

$$\digamma^{\mathfrak{q}} = \left[\digamma_1^{\mathfrak{q}}, \ \digamma_2^{\mathfrak{q}}, \ \ldots, \ \digamma_N^{\mathfrak{q}}\right]^{\intercal} \tag{3.17}$$

where $\digamma_i^{\mathfrak{q}}$ is the feature matrix for the i-th sample, and N is the number of samples in the dataset. The feature matrix $\digamma_i^{\mathfrak{q}}$ is computed by

$$\digamma_i^{\mathfrak{q}} = \left[\mathbb{E}\left(\mathfrak{Re}(\mathbf{q}_{i,j})\right) \ \ \mathbb{E}\left(\mathfrak{Im}(\mathbf{q}_{i,j})\right) \ \ \sigma\left(\mathfrak{Re}(\mathbf{q}_{i,j})\right) \ \ \sigma\left(\mathfrak{Im}(\mathbf{q}_{i,j})\right) \ \ \sigma^2\left(\mathfrak{Re}(\mathbf{q}_{i,j})\right) \ \ \sigma^2\left(\mathfrak{Im}(\mathbf{q}_{i,j})\right)\right] \tag{3.18}$$

where i indexes the dataset samples, and j refers to the number of observations per second in the bicomplex vector $\mathbf{q}_{i,j}$. Finally, the feature matrices $\digamma_s^{\mathfrak{q}} \in \mathbb{R}^{456736\times 12}$, $\digamma_a^{\mathfrak{q}} \in \mathbb{R}^{222248\times 12}$, $\digamma_d^{\mathfrak{q}} \in \mathbb{R}^{302080\times 12}$, and $\digamma_f^{\mathfrak{q}} \in \mathbb{R}^{5424\times 12}$ are used as the input data for the proposed ML classifier. The feature extraction method employed is straightforward and statistically based, significantly enhancing computational efficiency and reducing processing time. In this study, the classification results achieved are sufficiently robust, avoiding the need for a more complex set of features.

Chapter 4

Numerical results

Over the past ten years, EEG signal analysis has increasingly supported recognition tasks and artificial intelligence applications aimed at diagnosing neurological disorders such as epilepsy, Parkinson's disease, and Alzheimer's disease. In affective computing, EEG has emerged as a pivotal tool for elucidating brain activity related to emotional states. Then, the non-invasive properties of EEG's enable the effective capture in CNS and ANS activities, particularly the emotion-related brain regions like the amygdala, hippocampus, and thalamus. Additionally, multimodal studies examine physiological indicators such as variations in temperature, heart rate, and skin conductance, reflecting ANS responses associated with emotional experiences. Previous studies have indicated that brain bioelectrical potentials are good indicators of emotional processing despite their complexity and interpretation to classify challenges. As introduced in the previous chapters, preprocessing typically involves noise reduction, channel selection, and feature extraction. In this document, recognizing the refined methodologies reported in the state-of-the-art, a mathematical model based on the Cayley-Dixon theory that uses both real and imaginary components for EEG signal processing is explored. However, before getting there, it is essential to explore how the previous research results influence this study. The following sections introduce a short overview of the published works.

4.1 Background

4.1.1 Emotion recognition in EEG signals using the continuous wavelet transform and CNNs

This approach addresses a methodology based on the Continuous Wavelet Transform (CWT), an spectral distribution images, to feed a CNN (GoogLeNet) architechture to classify VA (see Fig. 4.1a) and VAD (see Fig. 4.1b) emotion space. In here, authors suggested the possibility to get four and eight discrete emotion classes for both VA and VAD, respectively. Each EEG signal is transformed to a 2D image spectral distribution (as showed in the input images example in Fig. 4.1c) by using the CWT method and the wavelet Morlet as mother wavelet. The produced feature maps per class is shown in Figs. 4.1d and 4.1e. Here, the performance exceed the 80%, however, the authors improve the performance by increasing the number of images per class using a data augmentation method by adding white Gaussian noise to the original images. The data augmentation method is a common technique used in DL to increase the number of training samples by applying random transformations to the original images, such as rotation, scaling, and flipping. This approach helps to improve the generalization ability of the model and reduce overfitting.

This approach was our first step to understand how complex and difficult is to create an overview to classify the EEG signals. From here, authors explored the idea to used another dataset that as closely related to primary emotions instead of using a primitive one and apply a discretization to the self-assessed labels to approximate to a primary one. As introduced before, primitive datasets as DEAP, which this first approach was based on, presents a lack of reliability if the idea is to classify a primary emotion model. As consequence, the authors found the SEED-series as an option to avoid the self-assessed labels and increase the reliability of the study.

4.1.2 A channel selection method to find the role of the amygdala in emotion recognition avoiding conflict learning in EEG signals

This paper was our first approach to two main tasks: (1) the channel selection process to reduce the computational cost and the lack produced by noise and (2) the conflict learning. The conflict learning is a re-labeling methodology for machine learning labels (see Ledesma

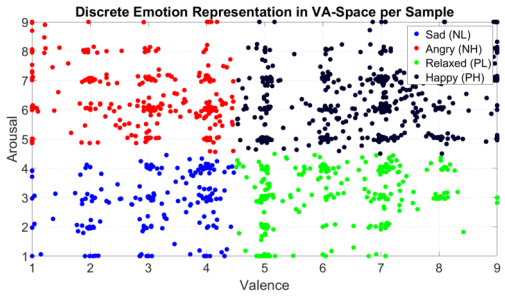

(a) Sad, Angry, Relaxed, and Happy discrete classes produced by the acva primitive emotion space.

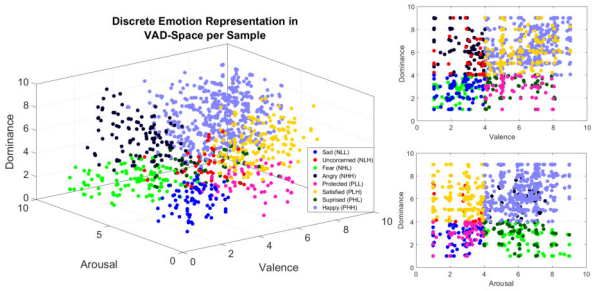

(b) Sad, Uncorcerned, Fear, Angry, Protected, Satisfied, Suprised, and Happy discrete classes produced by the VAD primitive emotion space.

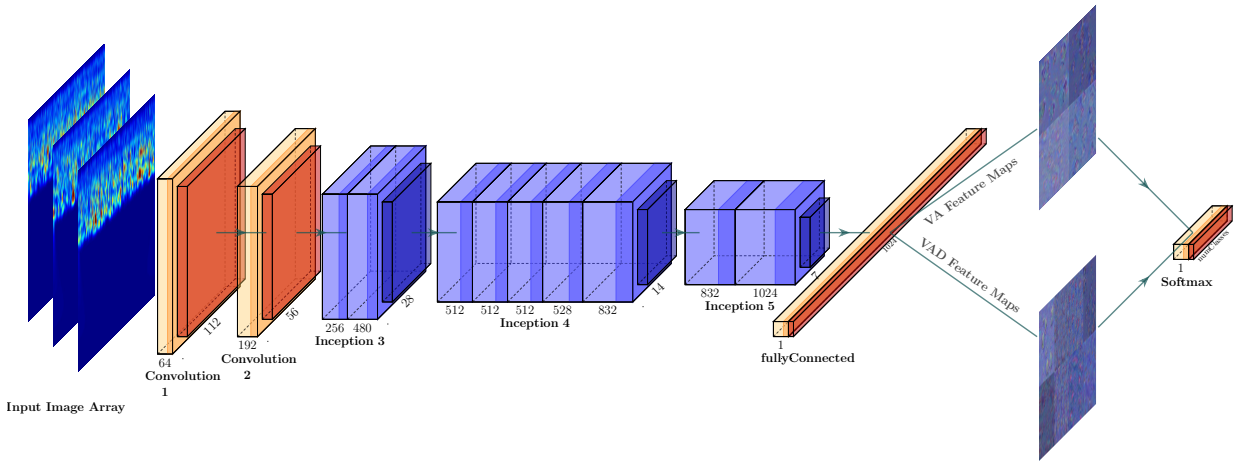

(c) GoogLeNet architechture to extract feature maps and classify the entry tensor of spectral distributions images.

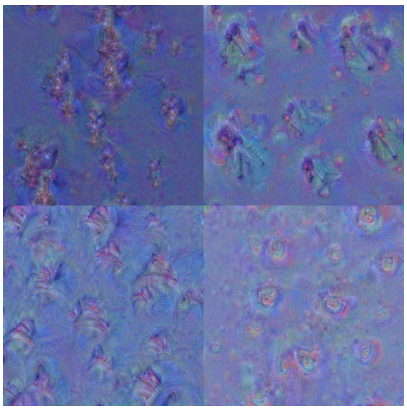

(d) The feature map produced by the GoogLeNet architechture for the four labels produced by the VA emotion space.

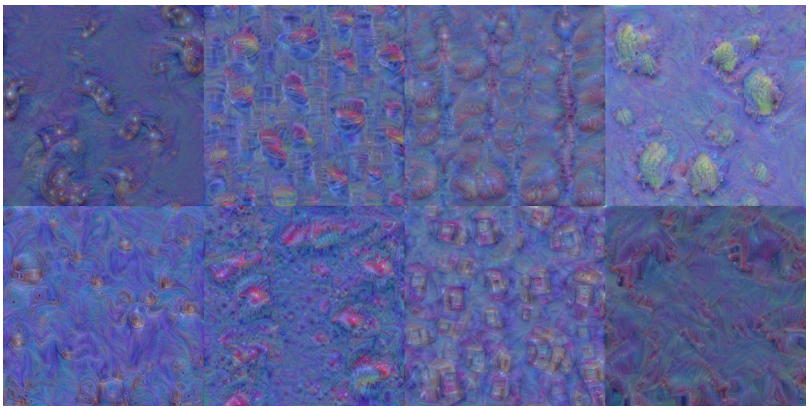

(e) The feature map produced by the GoogLeNet architechture for the eight labels produced by the VAD emotion space.

Figure 4.1: The main performed tasks in our first published paper work to develop the VA and VAD classification task in a multi-class model performance.

et al. (2018) for details). As consequence of the channel selection, the authors found that the top-two effective channels (FCZ and CP4) are the closest ones to those the literature established as the most effective in capturing the amygdala activity (FC1 and CZ, according to Albert et al. (2010)). In here, it is important to highlight that the channel selection method is the same that is used in this study, as seeing in Sect. 3.2. The conflict learning method is a re-labeling process where labels are redefined based on three metrics: (1) the Hamming, (2) Tanimoto (see Rogers and Tanimoto (1960)), and (3) Dixon-Koehler (see Dixon and Koehler (1999)). The conflict learning metrics follows the criteria:

$$\mathbb{D}(\theta_2,\theta_2) = \begin{cases} \delta^H_{i,j}(\theta_1,\theta_2) = \frac{1}{N}\sum_{i=1}^{N}(\theta_1 \oplus \theta_2) \\ \delta^T_{i,j}(\theta_1,\theta_2) = \begin{cases} 1 & \text{if } \theta_1 = \theta_2 = 0 \\ 1 - \frac{\sum \theta_1 \cap \theta_2}{\sum \theta_1 \cup \theta_2} & \text{otherwise} \end{cases} \\ \delta^{DK}_{i,j}(\theta_1,\theta_2) = \delta^H_{i,j}(\theta_1,\theta_2) \times \delta^T_{i,j}(\theta_1,\theta_2) \end{cases}, \tag{4.1}$$

where θ_1 and θ_2 are the current and displacement windows of the 1D-LBP pattern (the displacement is performed only for a single sample in the input vector), as the one presented in Equation (3.3). Once the entire input vector has been processed, a vector of $\delta^H_{i,j}(\bullet)$, $\delta^T_{i,j}(\bullet)$, and $\delta^{DK}_{i,j}(\bullet)$ is generated. From this vector, the max and μ magnitudes of the δ vector are computed, yielding:

$$\mathbb{D}(\theta_2,\theta_2) = \left[\max\left(\delta^H_{i,j}(\bullet)\right) \quad \mu\left(\delta^H_{i,j}(\bullet)\right) \quad \max\left(\delta^T_{i,j}(\bullet)\right) \quad \mu\left(\delta^T_{i,j}(\bullet)\right) \quad \max\left(\delta^{DK}_{i,j}(\bullet)\right) \quad \mu\left(\delta^{DK}_{i,j}(\bullet)\right)\right]. \tag{4.2}$$

Additionally, the conflict learning levels are achieved by $c_{i,j} = T_{i,j}W(\delta_{i,j})$ criteria, where $T_{i,j} = |\tau_i - \tau_j|$, being τ the normalized targets per sample, and $\sigma = 0.01$, following the description given in Ledesma et al. (2018). Next, the weighted function is defined by

$$W(\delta_{i,j}) = \exp\left(-\frac{\delta_{i,j}}{2\sigma^2}\right), \tag{4.3}$$

where $\delta_{i,j}$ could take all values from the μ and max coefficient per distance metric. Then, the $c_{i,j}$ is computed as

$$c_{i,j} = |\tau_i - \tau_j| \exp\left(-\frac{\delta_{i,j}}{2\sigma^2}\right), \tag{4.4}$$

and the conflict coefficient per sample is represented by

$$C_i = \frac{1}{N} \sum_{\substack{j=1 \\ i \neq j}}^{N} c_{i,j}. \tag{4.5}$$

Finally, the full matrix $\mathbb{C}$ is obtained as

$$\mathbb{C} = \begin{bmatrix} {C_1}_{\max}^{H} & {C_1}_{\mu}^{H} & {C_1}_{\max}^{T} & {C_1}_{\mu}^{T} & {C_1}_{\max}^{DK} & {C_1}_{\mu}^{DK} \\ {C_2}_{\max}^{H} & {C_2}_{\mu}^{H} & {C_2}_{\max}^{T} & {C_2}_{\mu}^{T} & {C_2}_{\max}^{DK} & {C_2}_{\mu}^{DK} \\ \vdots & \vdots & \vdots & \vdots & \vdots & \vdots \\ {C_i}_{\max}^{H} & {C_i}_{\mu}^{H} & {C_i}_{\max}^{T} & {C_i}_{\mu}^{T} & {C_i}_{\max}^{DK} & {C_i}_{\mu}^{DK} \end{bmatrix}, \tag{4.6}$$

The authors first reported numerical results by taking the full set of EEG channels and processed with the 1D-LBP and the feature extraction (see paper for math details attributes). The classification result reached a 89.83% of accuracy rate in 10-CV and a $\approx$ 90.00% in LOSO-CV cross validation. However, the channel selection showed that a single channel (FCZ) was enough to classify these five primary emotions with 79.03 of accuracy. Then, the top-two effective channels (FCZ and CP4) outperformed a 87.36%, the following performances of effective channels are shown in Fig. 4.2a. Then, the mRMR algorithm is applied to get the top of the features in the whole channels set, the results achieved the homogeneity, spectral roll-off, and normalized Renyi entropy, which are the most effective features to classify the five primary emotions. In conflict learning, the conflicts generated with the computed results in $\mathbb{C}$ were removed, the classification performance improved for each conflict metric, however the ${C_i}_{\max}^{T}$ was the top one. Classification stats can be seen in Fig. 4.2b, where the spatial top-three features distribution are shown in Fig. 4.2c. As seen, the algorithm is able to remove some correct features in the 3D images that are spliced with another class features (the big gray circle). However, this method shows an aggressive removal of features as can be seen in the bottom-left side of the image.

This framework proposes two main goals: (1) the top-two effective channels performed with the channel selection are consistent with the information found in literature about the reflection of the amygdala's activity (see Table 4.1 for the complete order of scores per channel in SEED-V dataset) and (2)stimuli conflict learning shows an outperformed classification, however the metric trends to be agressive in some classes. Even so, the reduction produced

by conflict learning does not suggested a great number of outliers (see paper for details). Notably, these results are highly dependent of the feature extraction process. The research performed in this paper introduces the influence of CNS to the emotion recognition task for our future applications.

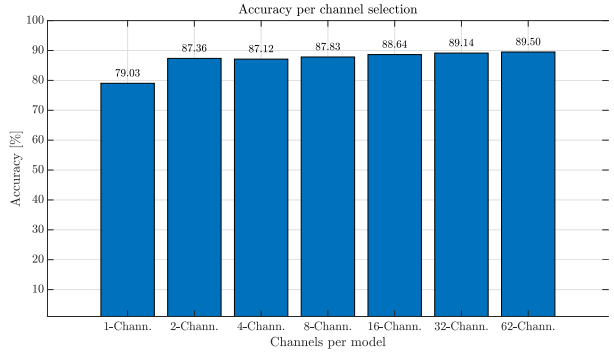

(a) The channel selection recognition performance for five primary emotions.

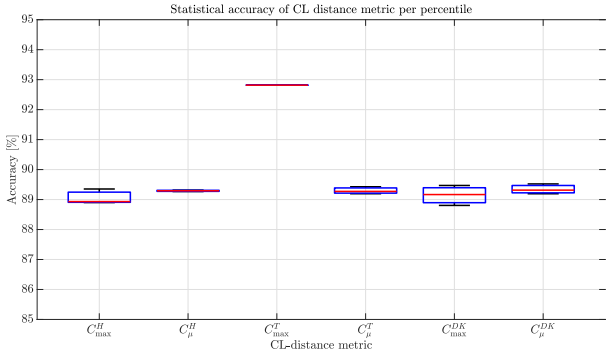

(b) The statistical accuracy performance per conflict learning metric by using .

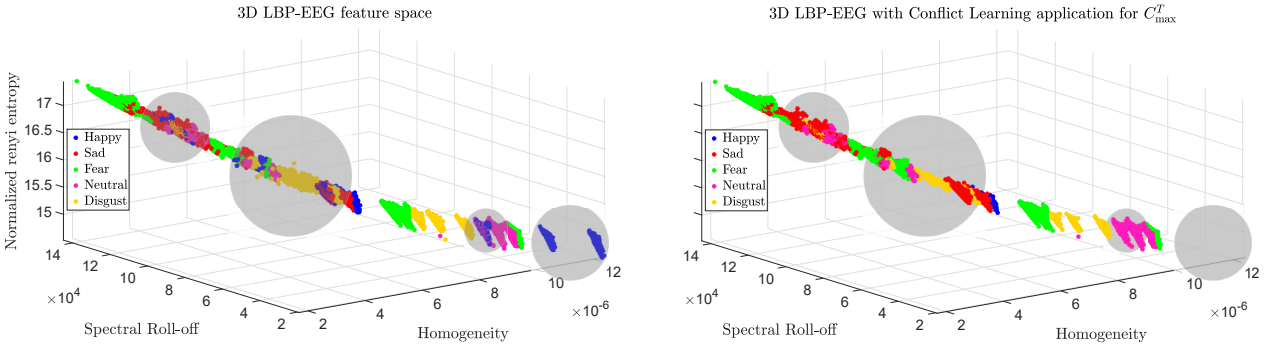

(c) The spatial top-three features distribution. The top of features is computed with the mRMR algorithm. The comparation is shown to see the conflict learning performance.

Figure 4.2: The channel selection process and the conflict learning performance.

4.1.3 Emotion Recognition in Gaming Dataset to Reduce Artifacts in the Self-Assessed Labeling Using Semi-Supervised Clustering

This work was developed to explore the performance of the FEEL (see Cang et al. (2024)) dataset. This multimodal dataset contains the electroencephalogram and motor joystick pression information for 20 subjects. Initially, the dataset proposed a set of 13 labels (emotional stimuli) for the study, however the subjects reported a full set of 45 classes in order of their subjective interpretation of the felt stimuli. Here, the same conflict learning

idea was applied to the data to find the index of the conflict labels and remove them. Authors performed this idea to see the impact of the self-assessed subject's labels. In the first trail, the spatial distribution of features, shown in Figs. 4.3a and 4.3b, reduced the labels dimension to 22. This context is important to highlight the influence of the subject's self-assessed lack of reliability in identifying their own emotions or feelings. As in our previous work, the conflict learning using the $\max_{C_i}{}^{T}$ metric outperformed as the best classification performance. Then, the initial 45 labels were manually reduced to 30 due to the subjects reported a similar label with the same suffixes. Then, authors applied conflict learning to these set of 30 labels, yielding a reduced set of 19 labels. Then, a second task is a semi-supervised dendrogram technique to cluster the complete set of targets. The main limitation of this work is that the original targets are missed in the clustering of samples. Clustering results yield a seven-clustering groups by $\delta_1 = 2.6914$ standardized Euclidean distance threshold, as seeing in Fig. 4.3c. Here, the authors infer that this work outperforms an approximation to Ekman's primary emotions theory, and assess an approach that primary emotions are linked to secondary emotions, which are generated by the previous experiences and ANS feedback.

Table 4.1: MRMR channel selection normalized scores. Here is shown only the scores for the first 16 channels, the rest of them are lower than the O1 score.

Single channel		2-Channels		4-Channels		8-Channels		16-Channels	
Channel	Score	Channel	Score	Channel	Score	Channel	Score	Channel	Score
FCZ	1.000	CP4	0.8779	FC5	0.8734	C2	0.8425	CP3	0.7821
				P1	0.8619	CP1	0.8084	FC2	0.7156
						FC1	0.8047	CPZ	0.2324
						F2	0.7914	CZ	0.1862
								FP2	0.1746
								TP8	0.1384
								T7	0.1334
								O1	0.1319

4.1.4 REGEEG: A Regression-based EEG Signal Processing in Emotion Recognition

This study introduces A Regression-based EEG Signal Processing in Emotion Recognition (REGEEG), a regression-based signal processing technique incorporating rotation matrices, directional vectors, polynomial transformations, and statistical feature extraction. It is

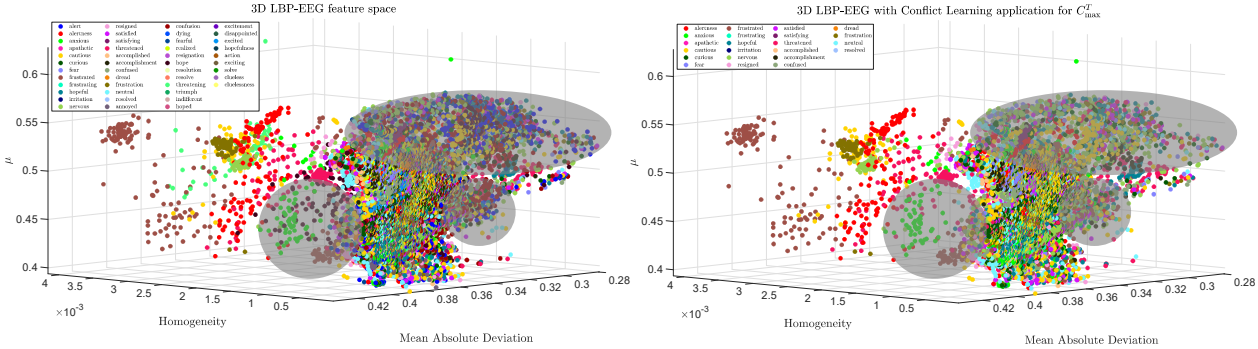

(a) The spatial distribution of the features in the FEEL dataset. The top-three features are shown in the 3D image. The conflict learning removal of samples is shown in gray circles.

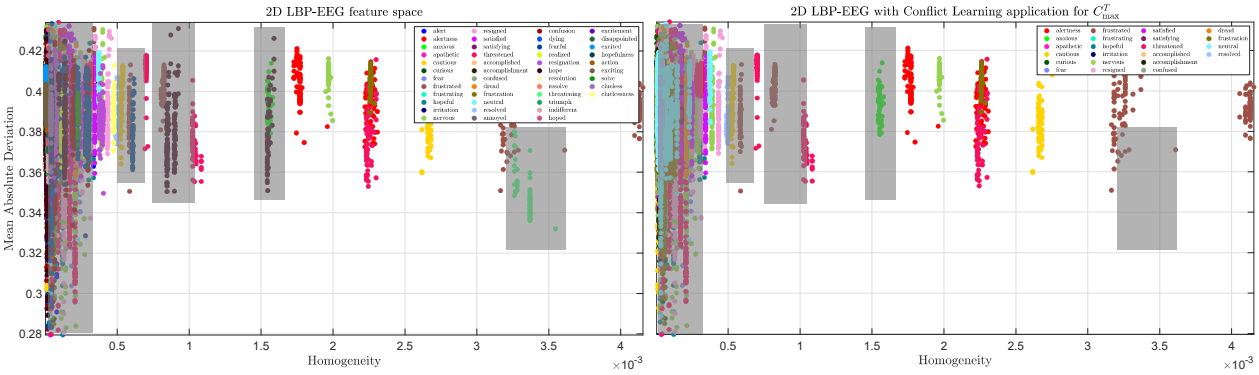

(b) The spatial distribution of the features in the FEEL dataset after remove the suffixes and applied the conflict learning. The conflict learning removal of samples is shown in gray circles.

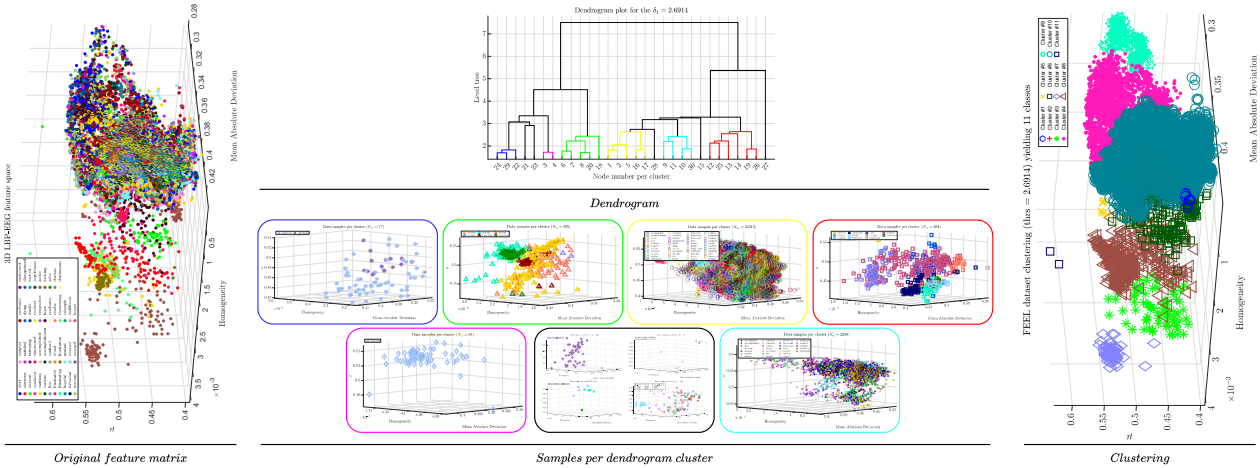

(c) The clustering of labels in the FEEL dataset that outperforms eleven different clusters by applying a dendrogram technique.

Figure 4.3: The three main contributions of this work: (1) the application of the conflict learning to the initial full set of 45 labels, yielding a reduced set if 22, (2) the removal of suffixes and application of the conflict learning achieving 19 labels, and (3) the clustering of labels to find similarities in the self-assessed labels.

evaluated using a robust EEG dataset to classify four distinct emotional stimuli: "Boring," "Calm," "Happy," and "Fear." Specifically, REGEEG employs a set of pairs of EEG electrode configurations based on orthogonality to map significant brain activity near the amygdala and hippocampus—regions critical for emotional processing—during game-playing sessions recorded in the GAMEEMO dataset. Initially, the extracted feature matrix assesses a set of 28 machine learning classifiers, where the Subspace k-NN algorithm exhibited superior performance, exceeding an average classification accuracy of 95%, verified through both 30-fold cross-validation and the LOSO-CV technique. The outperformed effectiveness of REGEEG in noise reduction and improved feature discriminability highlights its potential for EEG-based emotional analytics and manifold signal-processing applications. Although REGEEG was initially developed for emotion recognition, suggesting that it can effectively generalize to any signal-processing task involving at least a pair of related signals by modifying the original input pattern and extracting polynomial and statistical features from the Singular Value Decomposition (SVD) matrix. The methodology diagram is shown in Fig. 4.4.

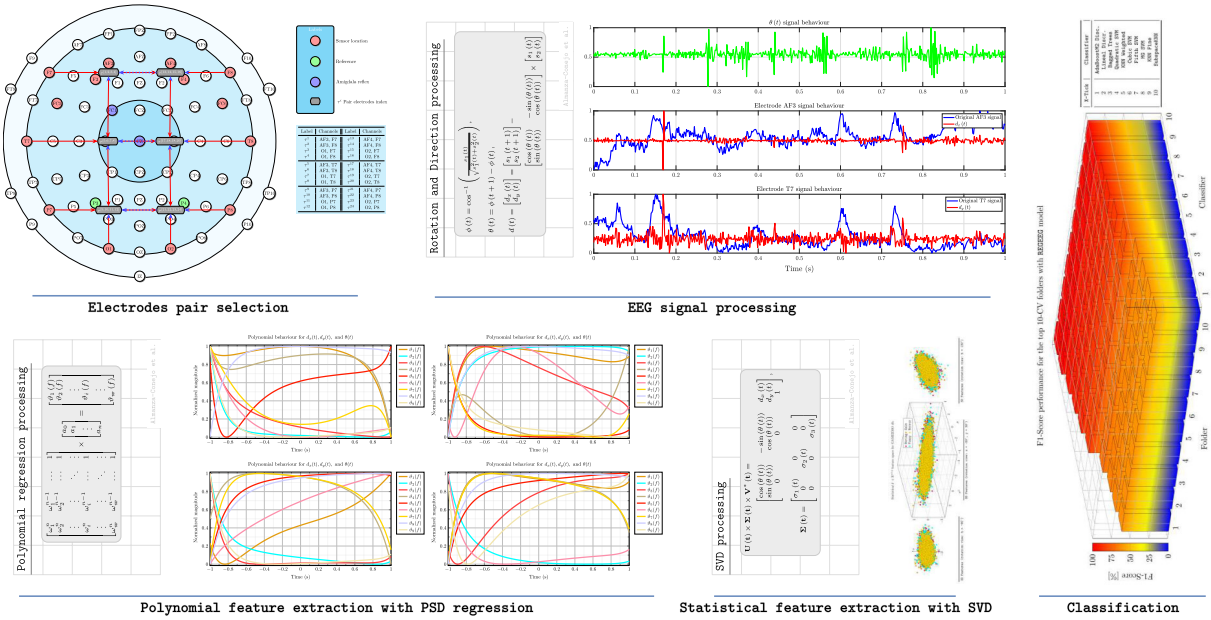

Figure 4.4: REGEEG general methodology.

This work aims to explore signal processing based on an orthogonality approach. In the context of the bQSA algorithm, imaginary numbers represent rotations of 90°. Thus, while the REGEEG method employs physical orthogonality —pairs of EEG channels arranged orthogonally— this work also explores theoretical connections between physical orthogonality

and orthogonality as represented by complex-number rotations.

4.2 bQSA method

Previous studies have demonstrated that ML methods typically achieve lower performance compared to DL techniques. However, this study investigates a methodology based on the hypothesis that the bQSA method, a digital signal processing approach applied to five EEG datasets, can yield an ML-based classification model superior to existing primary and primitive models. Accordingly, three ML classifiers — (1) Ensemble Trees, (2) k-Nearest Neighbors (k-NN), and (3) Decision Trees — are employed to evaluate the performance of the proposed feature matrix $F_{\Phi}^{\mathbf{q}}$. To validate the robustness of results avoiding overfitting, experiments are performed following a 10-fold Cross-Validation (10-CV) and Hold-Out (80 : 20 ratio) strategies. Computations were conducted on hardware consisting of a Mac Mini M2Pro processor (10 digital cores at 3.5GHz) with 16GB of RAM, running on MacOS 15. Algorithm development and tuning were carried out using MATLAB's Machine Learning toolbox (version 2024b). Visual representations and figures were coded by using the Ti*k*Z and PGFplots libraries in LaTeX.

4.2.1 The channel selection process

As described in the previous chapter, the bQSA method requires four-channel inputs for processing. The initial step involves selecting these channels according to the theory presented in Sect. 3.2. Subsequently, the bQSA is independently applied to each pair of channels resulting from EC. It is essential to note, for example, that if channels AF3, AF4, F7, and F8 are identified by the mRMR method as the top four channels, they will be arranged as follows: $q_1 = a + c\boldsymbol{i} = \xi_{\varsigma}(\eta_1, t) + \xi_{\varsigma}(\eta_3, t)\boldsymbol{i}$, and $q_2 = b + d\boldsymbol{i} = \xi_{\varsigma}(\eta_2, t) + \xi_{\varsigma}(\eta_4, t)\boldsymbol{i}$, where AF3 $= a = \xi_{\varsigma}(\eta_1, t)$, AF4 $= b = \xi_{\varsigma}(\eta_2, t)$, F7 $= c = \xi_{\varsigma}(\eta_3, t)$, and F8 $= d = \xi_{\varsigma}(\eta_4, t)$. The statistical feature extraction is produced after each Sect. 4.2 pre-procesing task. Finally, a robust set of ML algorithms are used to classify the produced feature matrix $F_{\Phi}^{\mathbf{q}}$. The following sections will detail the numerical and graphical results.

The noise reduction in the SEED-V dataset

Each dataset contains different properties, like the number of channels, sampling frequency, number of subjects and trials, and, of course a different EEG produced pattern because

"cada cabeza es un mundo" (each head is a world). This last property is more related to the hardware acquisition instead of the neural pattern; according to Ekman's theory, the neural pattern must be prevalent for the six basic emotions, avoiding the culture variance. Lots of factors can affect the signal acquisition: research bias, the subject's state of mind, environmental noise, and the equipment used. In consequence, if optimal hardware and environment conditions are considered, the noise added by the EEG scalp electrodes is negligible. This is why the datasets perform a notch filter or a Butterworth filter, removing the frequency of 50 Hz (60 Hz in the American continent) and a band pass filter between 0.5 Hz and 50 Hz.

The SEED-V dataset is a very useful dataset that accomplishes a set of four primary emotions, with a neural class as a fifth class. The dataset consisted of a set of 16 subjects, where each one of them performed the experiment 15 times (3 rounds per each of the 5 classes). The acquisition data was performed with a 62 scalp electrodes and a sampling frequency of 1000 Hz. Since this point, a noise reduction algorithm is applied to each one of the produced EEG signals. The wavelet-based noise reduction is introduced in Sect. 3.2.1, as produced pattern, the Fig. 4.5.

The 1D-LBP pattern behaviour and feature extraction

As introduced in the previous chapter, one of the most important tasks to outperform the EC selection is the feature extraction of the 1D-LBP produced pattern. This signal behaviour outperforms the "periodicity" of a signal. A single example of the 1D-LBP produced is shown in Fig. 3.3. The produced feature matrix contains a set of statistical and time-frequency attributes. If the mRMR is applied to the LBP feature matrix, a relevance scores vector per feature can be assessed. Then, according to the scores of relevances computed per dataset, the Figs. 4.6a to 4.6d showed the spatial behaviour using the top-three relevance features per dataset.

The channel selection

After achieving each feature matrix per dataset showed in Fig. 4.6, the $\digamma$ matrix is resized in the $\digamma_\eta = [n \times \eta]$ where in this context n is the number of samples in the dataset and η the number of channels per dataset, e.g. the SEED-V dataset acomplished a

$$\{\digamma \equiv [44640 \times 13]\} \Rightarrow \{\digamma_\eta \equiv [4320 \times 62]\}\,, \tag{4.7}$$

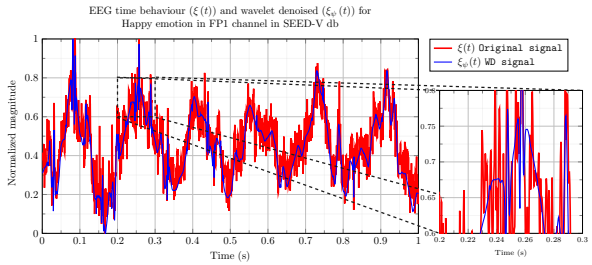

(a) The wavelet-based noise reduction in the SEED-V dataset for Happy class (randomly selected).

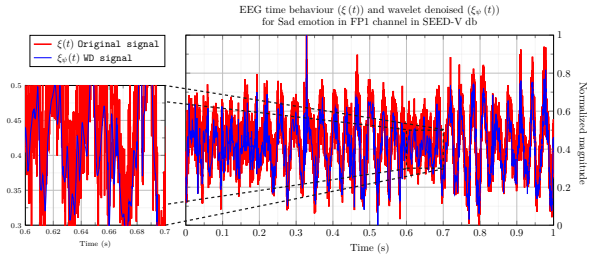

(b) The wavelet-based noise reduction in the SEED-V dataset for Sad class (randomly selected).

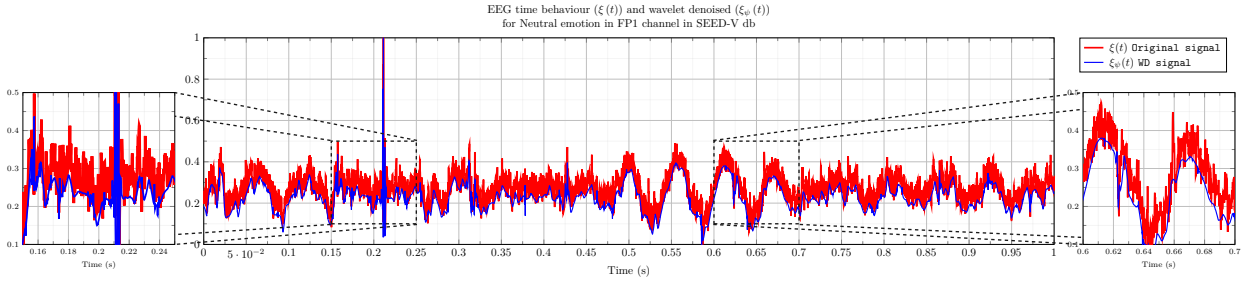

(c) The wavelet-based noise reduction in the SEED-V dataset for Neutral class (randomly selected).

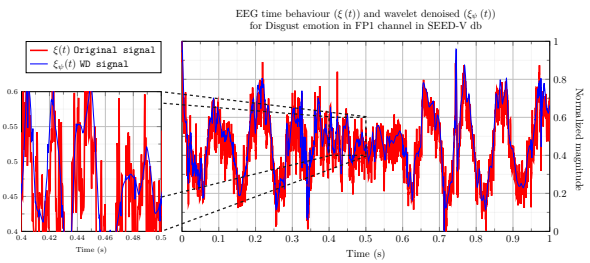

(d) The wavelet-based noise reduction in the SEED-V dataset for Disgust class (randomly selected).

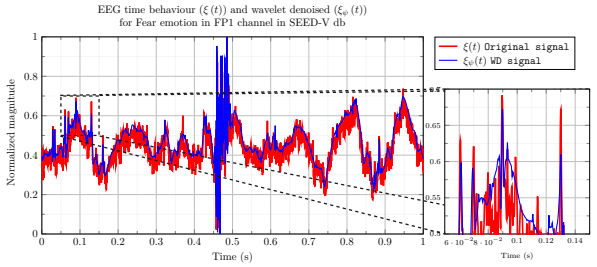

(e) The wavelet-based noise reduction in the SEED-V dataset for Fear class (randomly selected).

Figure 4.5: The wavelet-based noise reduction in the SEED-V dataset. In the top the (a) Happy and (b) Sad classes, at the middle the (c) Neutral. In the bottom, the (d) Disgust, and (e) Fear classes. The original time behavior of the EEG is plotted as red line and blue line the wavelet-based noise reduction.

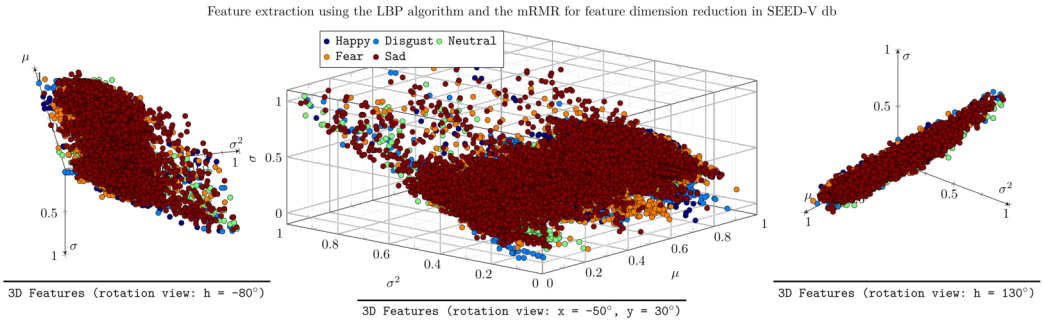

(a) LBP feature extraction using the (1) inverse difference moment, (2) power spectral estimate, and (3) kurtosis features by the mRMR algorithm in SEED-V dataset.

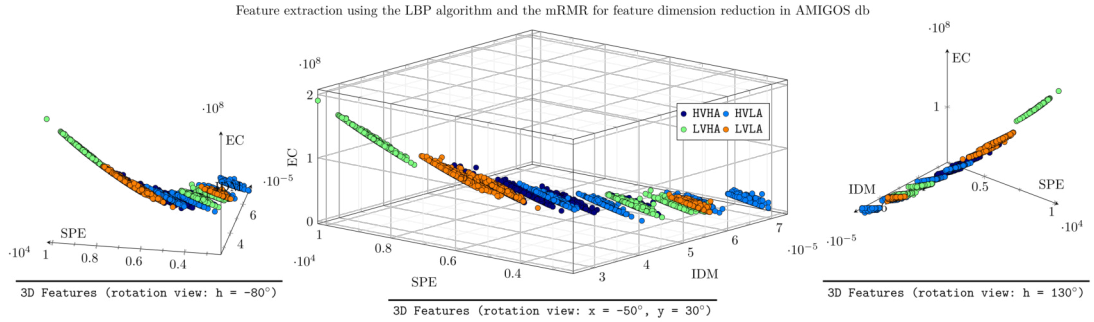

(b) LBP feature extraction using the (1) inverse difference moment, (2) power spectral estimate, and (3) energy concentration features by the mRMR algorithm in AMIGOS dataset.

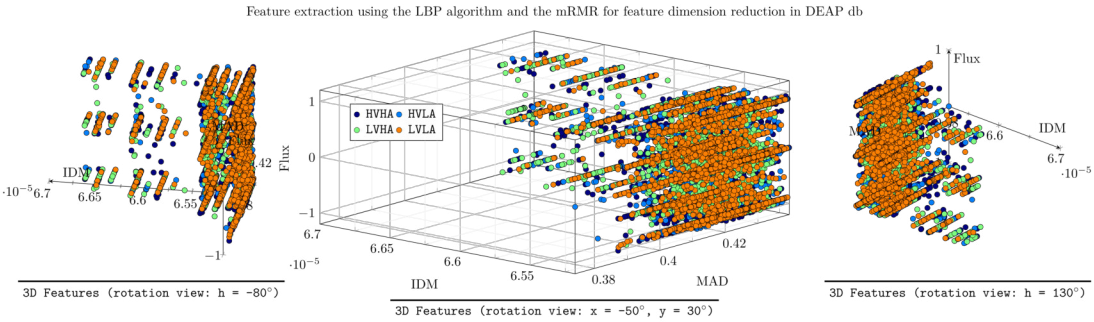

(c) LBP feature extraction using the (1) mean absolute deviation, (2) inverse difference moment, and (3) flux features by the mRMR algorithm in DEAP dataset.

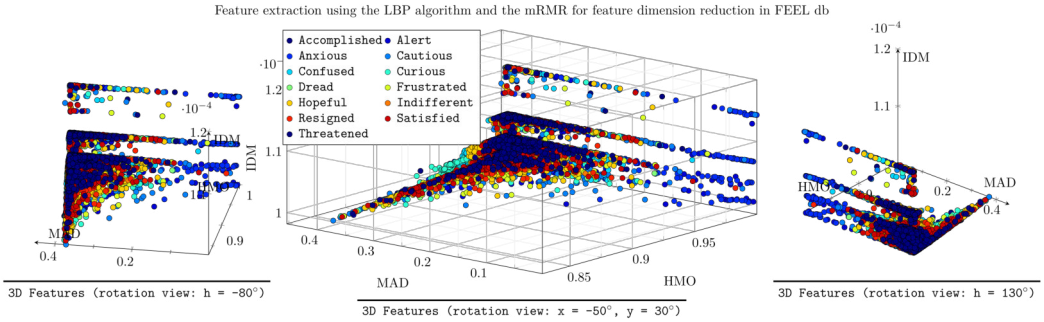

(d) LBP feature extraction using the (1) harmonic mean oscillation, (2) mean absolute deviation, and (3) inverse difference moment features by the mRMR algorithm in FEEL dataset.

Figure 4.6: Feature extraction to compute the most effective channels.

matrix dimension. As achivement, this F_η feature matrix feeds the mRMR algorithm to compute the relevance score per channel. The four-top effective channels can be seeing in Fig. 4.7 and table 4.2.

Table 4.2: Effective channels per dataset.

Dataset	Effective channels				Predominant lobe
	a	*b*	*c*	*d*	
SEED-VII	TP8: 1.00	CPZ: 0.65	FPZ: 0.62	CP2: 0.55	Fronto-parietal
SEED-V	F4 : 1.00	CP2: 0.89	CZ : 0.89	CB2: 0.84	Fronto-parietal
AMIGOS	F8 : 1.00	P7 : 0.31	AF3: 0.29	P8 : 0.26	Fronto-temporal
DEAP	P7 : 1.00	C4 : 0.84	P3 : 0.84	OZ : 0.78	Tempo-parietal
FEEL	17 : 1.00	07 : 0.92	34 : 0.89	41 : 0.87	Fronto-parietal

4.2.2 bQSA

The aim of the previously outlined protocol was to select four optimal EEG channels to form the bicomplex representation employed by the bQSA, described in Sect. 4.2. A significant disadvantage of this channel selection approach is its dependency on the specific features extracted in this protocol, particularly 1D-LBP and those features described in Table 3.1. Consequently, altering these feature extraction methods significantly influences the resultant relevance vectors for each dataset. Nevertheless, by following the methodology introduced here, the channel selection has consistently provided accurate results, as demonstrated by the classification performances detailed in subsequent sections. In order to assess the bQSA approach, after the noise reduction, a translation offset is applied, the pattern behaviour is qualitatively similar to the one achieved by the WD (see Fig. 4.5), however, the numerical array suggested a change in the amplitude of the signal. The translation offset criteria follows the function

$$\xi_\varsigma(t) = \xi_\psi(t) - \frac{\min\left(\xi_\psi(t)\right)}{\max\left(\xi_\psi(t)\right) - \min\left(\xi_\psi(t)\right)}. \tag{4.8}$$

The bQSA algorithm that results by the (3.15), both quaternion and bicomplex product, produced a bQSA pattern as those are shown in Fig. 4.8. Here, the $\mathbf{q}_{\text{happy}}^{\text{seed-v}}$ and $\mathbf{q}_{\text{hvha}}^{\text{amigos}}$ presents a higher frequency pattern than those in $\mathbf{q}_{\text{hvha}}^{\text{deap}}$ and $\mathbf{q}_{\text{satisf}}^{\text{feel}}$. However, the former two achieved a higher accuracy rate than the latter two, as introduced in the following section. The feature space for the $\mathbb{E}\left(\mathfrak{Re}\left(\mathbf{q}\right)\right) \equiv \left[\mathbb{E}\left(\mathfrak{Re}\left(qp\right)\right), \mathbb{E}\left(\mathfrak{Re}\left(q \odot p\right)\right)\right]$, and so on for

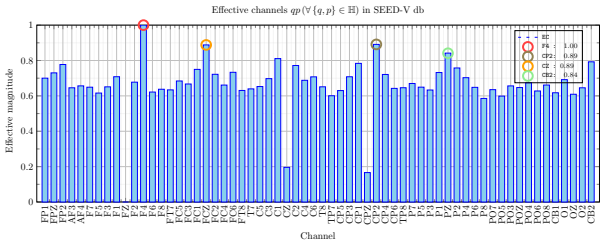

(a) The relevance computed by the mRMR algorithm using the $\digamma_\eta$ as input features in the SEED-V dataset.

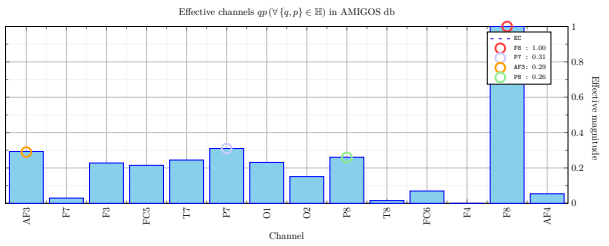

(b) The relevance computed by the mRMR algorithm using the $\digamma_\eta$ as input features in the AMIGOS dataset.

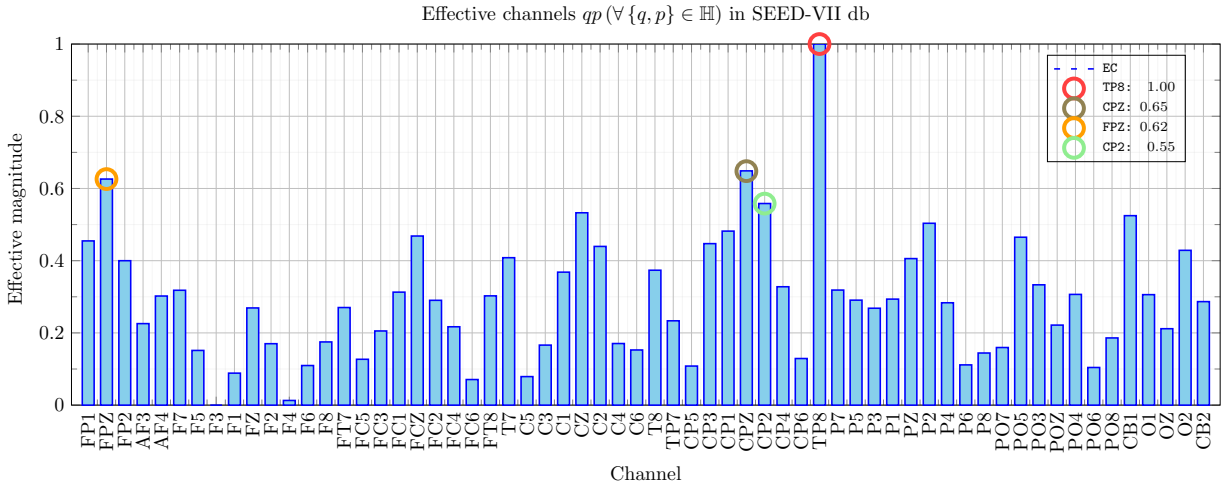

(c) The relevance computed by the mRMR algorithm using the $\digamma_\eta$ as input features in the SEED-VII dataset.

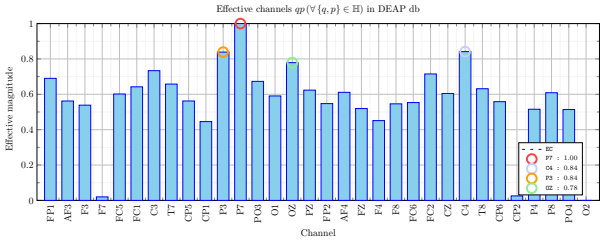

(d) The relevance computed by the mRMR algorithm using the $\digamma_\eta$ as input features in the DEAP dataset.

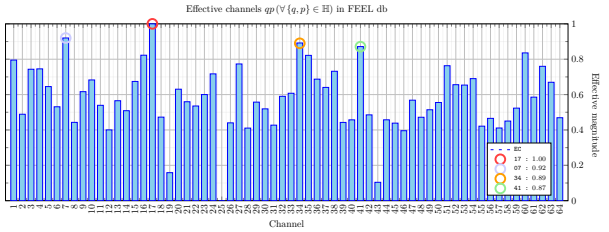

(e) The relevance computed by the mRMR algorithm using the $\digamma_\eta$ as input features in the FEEL dataset.

Figure 4.7: Bar chart of the scores computed by the mRMR algorithm per dataset used.

the $\sigma^2(\bullet)$ and $\sigma(\bullet)$ statistical features are computed and plotted in the Fig. 4.9. Notably, here only the 3D feature space for the $\mathfrak{Re}(\mathbf{q}_1)$ is shown; however following (3.18) the feature space per samples is a vector of twelve elements. That is why the statistics to the $[\mathfrak{Re}(\mathbf{q}_1), \mathfrak{Re}(\mathbf{q}_2), \mathfrak{Im}(\mathbf{q}_1), \mathfrak{Im}(\mathbf{q}_2)]$ are applied to quaternion product. Then, the following section introduces the ML training-validation performance. Training and validation tests are performed following a 10-fold cross-validation and a $(80:20)$ training ratio in hold-out technique.

4.2.3 bQSA performance

The classification technique involves the performance of feeding a ML algorithm with a $F_i^{\mathbf{q}}$ feature matrix, where each sample is composed of 12 statistical features, as introduced previously. In order to carry out a robust classification method, this method proposed the use of several ML kernels to achieve the top-three best performing models. In this order of ideas, a 25-ML kernels for the FEEL in bicomplex product dataset are tested. The performance is shown in Fig. 4.10 where notably the Ensamble-Tree, kNN, and Tree kernels are the top-performance ones. Then, these ML kernels are used to test the feature classification task.

The cross-validation results

As the main objective of this research is to provide a context of the performance of bQSA algorithm, the time and spatial behaviour of the $\mathfrak{Re}(\bullet)$ and $\mathfrak{Im}(\bullet)$ on the figures above are used to feed a 10-fold cross-validation technique, where the model is trained, validated, and tested by using the ML toolbox of MATLAB.

The global classification results per dataset and quaternion product type is showed in the Fig. 4.11 where performance was sorted as ascending. Classification results outperforms DEAP as the low-performance and the SEED-V as the higher one. Analyzing the performance in the context of the dataset, DEAP was achieved as the weaker in emotion recognition over the three kernels, reaching only more than 50% of correct predictions in the Ensamble-Tree kernel. Moreover, this DEAP performance is very similar in the quaternion and bicomplex product.

As can be noticed in Fig. 4.11 the DEAP is the lower performance dataset. The Figs. 4.12a and 4.12b reports the performance per class in this model, yielding the HVHA-class as the best predicted one (almost 50%); however, this performance is very poor to any future

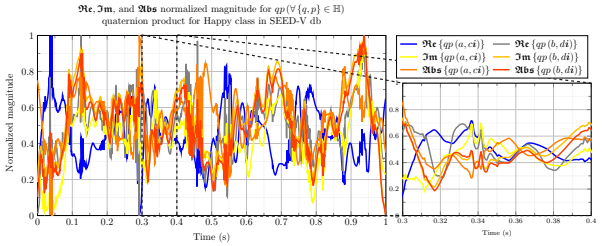

(a) The $\mathbf{q}_{\text{happy}}^{\text{seed-v}} \equiv (\boldsymbol{q}_1, \boldsymbol{q}_2) \equiv qp$ pattern following the (3.15).

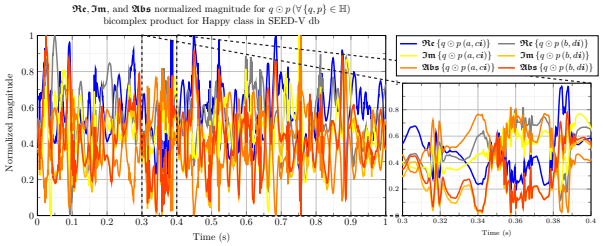

(b) The $\mathbf{q}_{\text{happy}}^{\text{seed-v}} \equiv (\boldsymbol{q}_1, \boldsymbol{q}_2) \equiv q \odot p$ pattern following the (3.15).

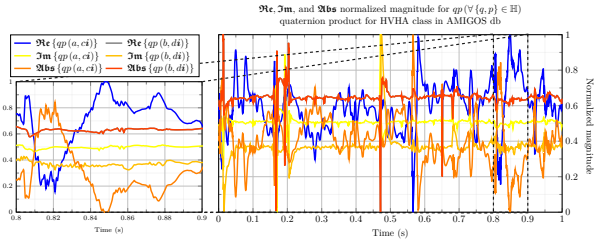

(c) The $\mathbf{q}_{\text{hvha}}^{\text{amigos}} \equiv (\boldsymbol{q}_1, \boldsymbol{q}_2) \equiv qp$ pattern following the (3.15).

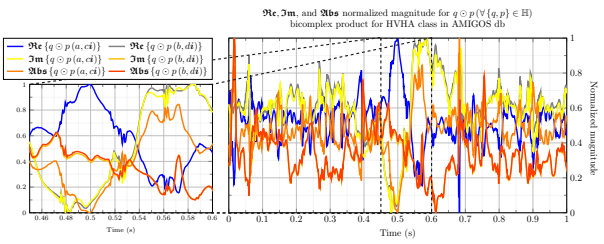

(d) The $\mathbf{q}_{\text{hvha}}^{\text{amigos}} \equiv (\boldsymbol{q}_1, \boldsymbol{q}_2) \equiv q \odot p$ pattern following the (3.15).

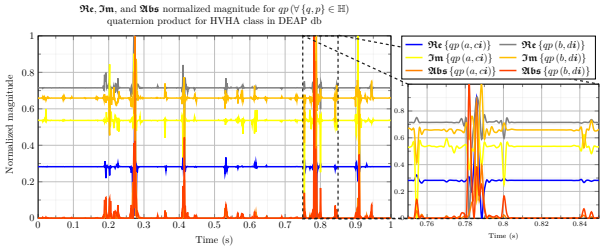

(e) The $\mathbf{q}_{\text{hvha}}^{\text{deap}} \equiv (\boldsymbol{q}_1, \boldsymbol{q}_2) \equiv qp$ pattern following the (3.15).

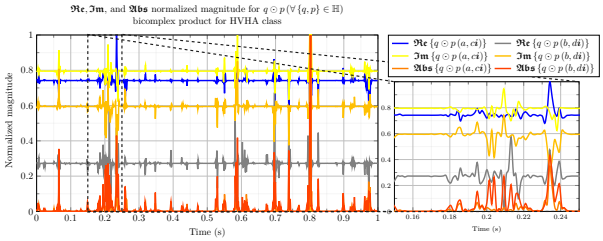

(f) The $\mathbf{q}_{\text{hvha}}^{\text{deap}} \equiv (\boldsymbol{q}_1, \boldsymbol{q}_2) \equiv q \odot p$ pattern following the (3.15).

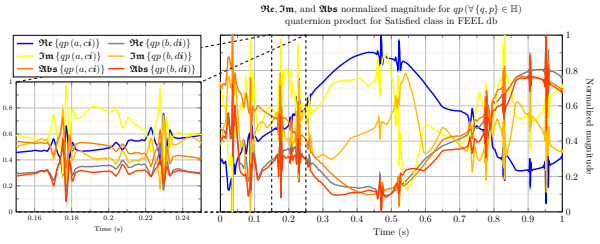

(g) The $\mathbf{q}_{\text{satisf}}^{\text{feel}} \equiv (\boldsymbol{q}_1, \boldsymbol{q}_2) \equiv qp$ pattern following the (3.15).

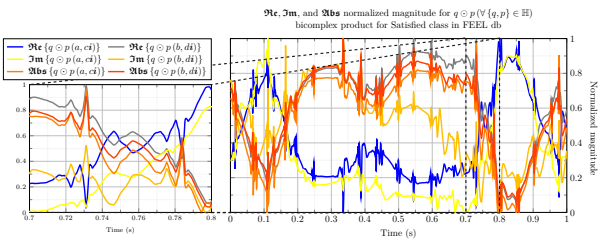

(h) The $\mathbf{q}_{\text{satisf}}^{\text{feel}} \equiv (\boldsymbol{q}_1, \boldsymbol{q}_2) \equiv q \odot p$ pattern following the (3.15).

Figure 4.8: Computed bQSA pattern achieved from the $\mathbf{q} = \text{bQSA}\left(\xi_\varsigma(\eta, t)\right)$.

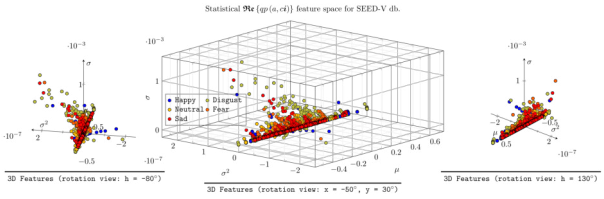

(a) The $\underset{\text{seed-v}}{F} = \text{fextract}\,(qp)$ statistical feature extraction space following the (3.18).

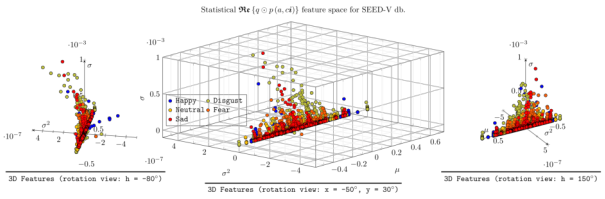

(b) The $\underset{\text{seed-v}}{F} = \text{fextract}\,(q \odot p)$ statistical feature extraction space following the (3.18).

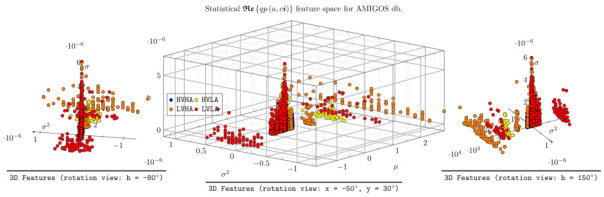

(c) The $\underset{\text{amigos}}{F} = \text{fextract}\,(qp)$ statistical feature extraction space following the (3.18).

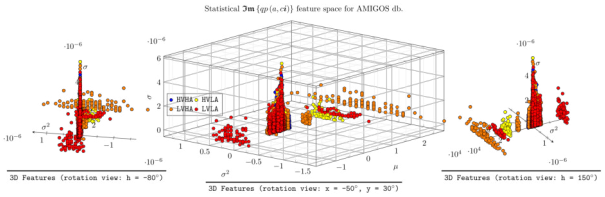

(d) The $\underset{\text{amigos}}{F} = \text{fextract}\,(q \odot p)$ statistical feature extraction space following the (3.18).

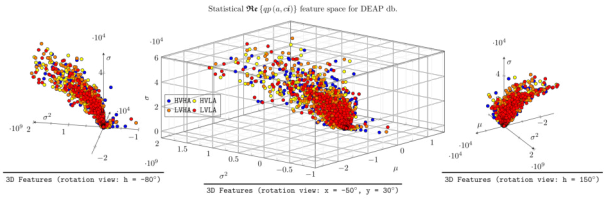

(e) The $\underset{\text{deap}}{F} = \text{fextract}\,(qp)$ statistical feature extraction space following the (3.18).

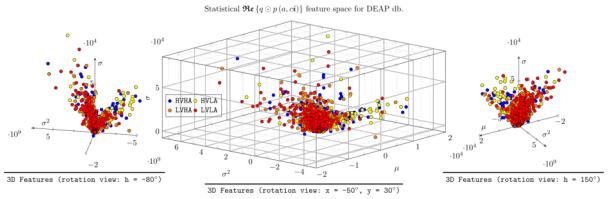

(f) The $\underset{\text{deap}}{F} = \text{fextract}\,(q \odot p)$ statistical feature extraction space following the (3.18).

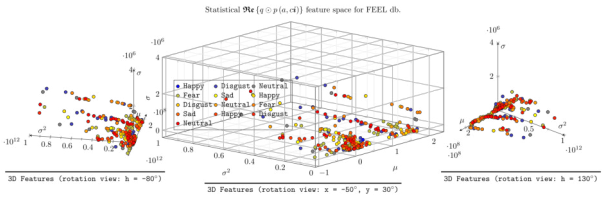

(g) The $\underset{\text{feel}}{F} = \text{fextract}\,(qp)$ statistical feature extraction space following the (3.18).

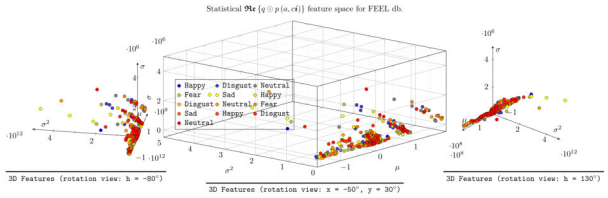

(h) The $\underset{\text{feel}}{F} = \text{fextract}\,(q \odot p)$ statistical feature extraction space following the (3.18).

Figure 4.9: Computed bQSA statistical feature extraction.

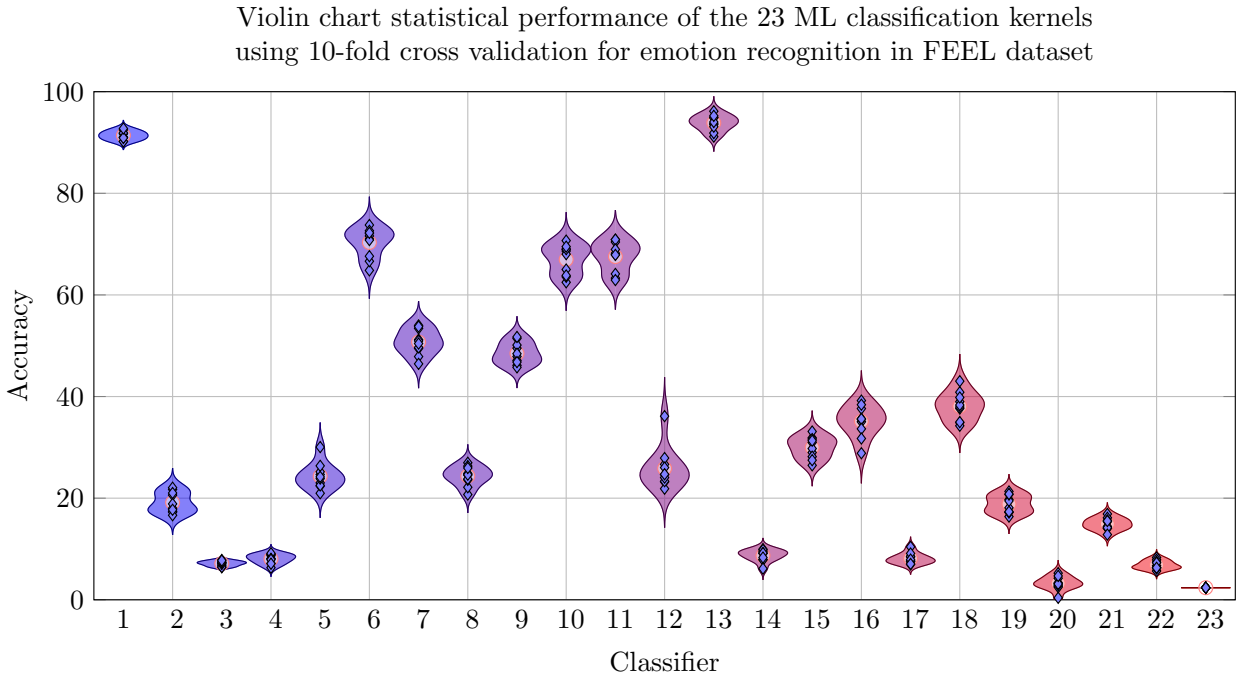

Tick	Classifier	Tick	Classifier	Tick	Classifier	Tick	Classifier
1	Tree Fine	7	k-NN Medium	13	Ensemble Trees	19	Cubic SVM
2	Tree Medium	8	k-NN Coarse	14	Subspace Discriminant	20	Fifth SVM
3	Coarse Tree	9	k-NN Cosine	15	Subspace k-NN	21	Fine Gaussian SVM
4	Naive Bayes G	10	k-NN Minkowski	16	RUSBoosted Trees	22	Medium Gaussian SVM
5	Naive Bayes K	11	k-NN Weighted	17	Linear SVM	23	Coarse Gaussian SVM
6	k-NN Fine	12	Boosted Trees	18	Quadratic SVM		

Figure 4.10: Violin statistical performance of 23-ML classification kernels using the F_{feel} datset.

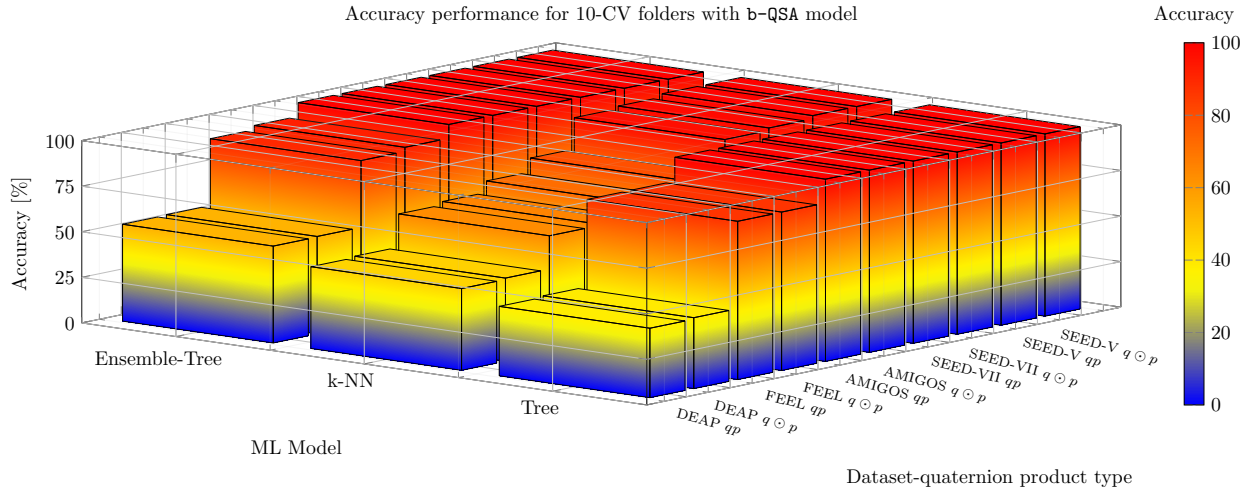

Figure 4.11: The ML performance per dataset for each classification kernel and product type.

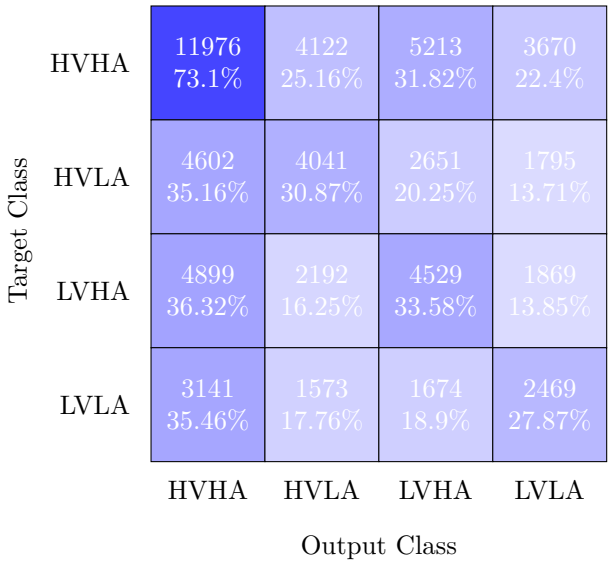

(a) Confussion Matrix (CM) of the testing task in quaternion product following the 10-fold cross-validation criteria for the DEAP.

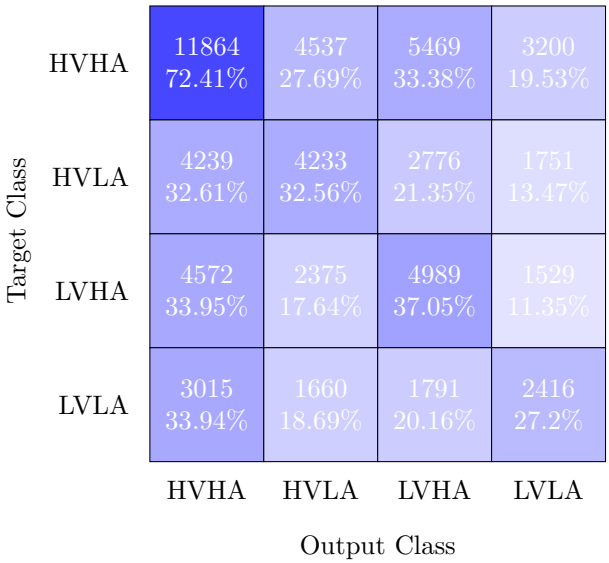

(b) Confussion Matrix (CM) of the testing task in bicomplex product following the 10-fold cross-validation criteria for the DEAP.

application. In consequence, an experimental protocol performed by the AMIGOS research team can be performed if the principal aims follows the context of the primitive recognition — see Miranda-Correa et al. (2021) for details. Analyzing the Confussion Matrix (CM) of the DEAP dataset, the dispersion of the samples presented in the Tree model, corresponding to the displayed CMs, tends to the high valence classes. According to the feature space distribution, Figs. 4.9e and 4.9f, the statistical features derived from quaternion or bicomplex representations may fail to encapsulate the key emotional or affective distinctions in DEAP, which often has high inter-subject variability.

The FEEL one achieved globally a better classification behaviour in the bicomplex product; however, the kNN model persists as the weaker kernel (and so on for the AMIGOS and SEED-series datasets). Here, Ensemble-Tree showed a difference of $\approx 2\%$ between bicomplex and quaternion product, yielding quaternion as the lower-performance and higher variability one; hence, both achieved more than 90% of accuracy rate. Then, the Tree kernel yields a $\approx 88\%$, yielding Ensemble as the top one with an approximate difference of 4% between both kernels. According to the CM, indifferent and dread are the classes with the lower number of examples in the testing task. In context, the dead is the lower precision class due to five over 22 samples wrongly predicted. In contrast, the lower sample class is indifferent. In the context of time-accuracy performance, the FEEL presents a higher classification performance

Table 4.3: Average and std of the training time and F1 score per dataset, product criteria, and ML kernel using 10-fold cross-validation.

Product	**Classes**	**Ensemble**		**k-NN**		**Tree**	
Type	N	Time [s] ($\mu \pm \sigma$)	F1 ($\mu \pm \sigma$)	Time [s] ($\mu \pm \sigma$)	F1 ($\mu \pm \sigma$)	Time [s] ($\mu \pm \sigma$)	F1 ($\mu \pm \sigma$)
$F_{s-v}^{q\odot p}$	5	363.45 ± 8.76	100 ∓ 0.00	0.46 ± 0.01	$99.99 \mp 2.0 \times 10^{-3}$	09.12 ± 0.15	$99.99 \mp 1.5 \times 10^{-3}$
F_{s-v}^{qp}	5	365.13 ± 5.09	100 ∓ 0.00	0.45 ± 0.01	$99.99 \mp 2.0 \times 10^{-3}$	09.16 ± 0.12	$99.99 \mp 1.5 \times 10^{-3}$
$F_{s-vii}^{q\odot p}$	7	1332.68 ± 18.69	100 ∓ 0.00	1.00 ± 0.06	96.86 ± 0.07	27.27 ± 0.79	$99.99 \mp 2.8 \times 10^{-3}$
F_{s-vii}^{qp}	7	1499.97 ± 62.04	100 ∓ 0.00	0.99 ± 0.01	98.21 ± 0.04	35.23 ± 0.85	$99.99 \mp 2.0 \times 10^{-3}$
$F_{a}^{q\odot p}$	4	110.91 ± 6.11	100 ∓ 0.00	0.31 ± 0.09	79.53 ± 0.09	03.49 ± 0.07	$99.99 \mp 5.5 \times 10^{-3}$
F_{a}^{qp}	4	095.15 ± 3.19	100 ∓ 0.00	0.23 ± 0.01	71.58 ± 0.16	02.82 ± 0.07	100 ∓ 0.00
$F_{f}^{q\odot p}$	13	003.79 ± 0.07	92.90 ± 0.68	0.04 ± 0.00	64.20 ± 1.83	00.19 ± 0.00	88.81 ± 1.55
F_{f}^{qp}	13	003.83 ± 0.13	90.94 ± 0.83	0.04 ± 0.01	62.81 ± 1.98	00.19 ± 0.01	87.30 ± 1.21
$F_{d}^{q\odot p}$	4	355.40 ± 5.64	46.70 ± 0.20	0.34 ± 0.02	43.00 ± 0.22	185.94 ± 3.34	36.02 ± 0.24
F_{d}^{qp}	4	361.59 ± 6.48	45.34 ± 0.24	0.32 ± 0.01	42.24 ± 0.22	190.97 ± 3.28	34.98 ± 0.23

over $\approx 4\%$. However, the ratio is $\approx 20.06\times$ training time for Ensemble Tree against Tree in the FEEL dataset, where real-time applications make a difference. The bQSA algorithm performance in the FEEL dataset achieved good performance considering the 13 classes that the models had to predict. The CM validation data is displayed in Figs. 4.13a and 4.13b where both product types outperform 100% in indifferent class and more than 90% in large subsets of classes, suggesting that both Ensemble and Tree kernels, in combination with bQSA, outperforms accurately for small and large sample subsets of predicted classes.

This study found that both products yield similar average accuracy; however, bicomplex product shows slightly higher performance consistency across a broader range of classes. Moreover, the bicomplex product enhances classification for ambiguous or less distinctive emotions, such as dead, frustrated, resigned, and satisfied. Both CM exhibit indifferent as the accurate class; meanwhile, dread, frustrated, and satisfied outperforms the wider confused classes in the quaternion-based model. The most significant finding in both FEEL models if that qp product-type outperforms as fewer off-diagonal elements with non-zero values, indicating more focused predictions. In contrast, $q \odot p$ outperforms as a stronger model for minority classes. In short, the bicomplex product might capture more nuanced dynamics of emotionally similar classes (e.g., "alert" vs "anxious"), leading to better classification in certain contexts but at the cost of more false positives; in contrast, quaternion-based is more stable across diverse classes and are better at minimizing broad confusion. In this order of ideas, further tuning combining both representations could leave that may use quaternion for general emotion space and bicomplex for local discriminations.

In the same context than before, the bQSA signal processing in AMIGOS is totally

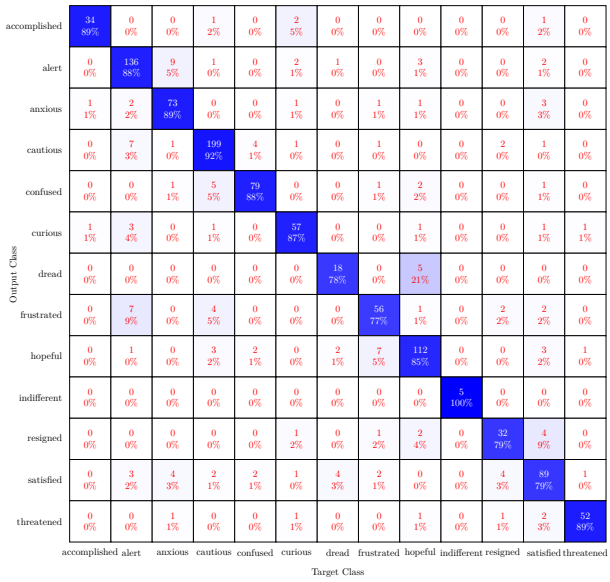

(a) CM of the testing task in quaternion product following the 10-fold cross-validation criteria for the FEEL.

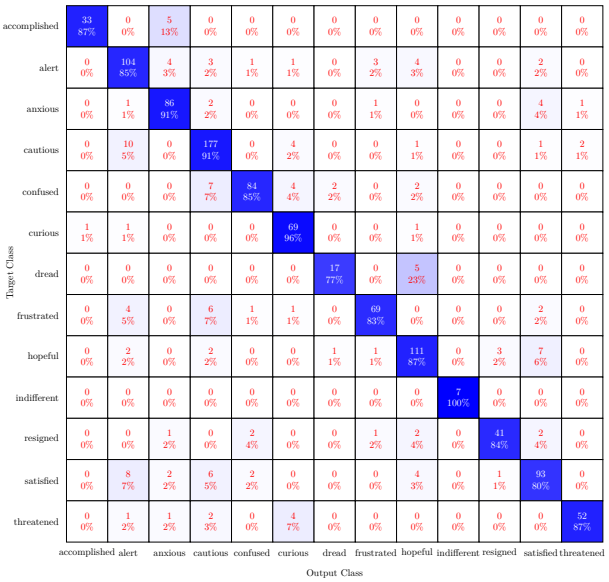

(b) CM of the testing task in bicomplex product following the 10-fold cross-validation criteria for the FEEL.

different than the DEAP one, even if both are developed in a primitive ER context. This dataset achieved a 100% of accuracy rate in a single multiclass model. Both CM highlights that $q \odot p$ product outperforms slightly better than the qp one. The ER in a primitive context is a very complex task, having a tendency to the development of a single binary class model per primitive emotion (two for VA and three for VAD). Here, a single and accurate model for amigos dataset is introduced, where taking advantage of the bQSA algorithm, the four out of six trained and validated models outperform close to 100% (see Table 4.3). In both product criteria models, same as the FEEL above, bicomplex product ($\digamma_a^{q\odot p}$) takes a few seconds more to train and is slightly more variable in time-accuracy performance; however is also slightly accurate than the quaternion product ($\digamma_a^{qp}$). The resulting CM for both product types are shown in Figs. 4.14a and 4.14b. Here, CM results are consistent with the average information provided by the Table 4.3, where it is noticed that bicomplex is 0.001% less accurate than the quaternion product in the tree kernel, which is displayed as outliers in the Fig. 4.14b.

Interestingly, the quaternion product emerged as the best in training and validation performance, surpassing the bicomplex product, but both achieve 100% performance in ML metrics. The main limitation of this model, as well as the following SEED-series models datasets, is the training time performance; taking time as the discriminative factor, the

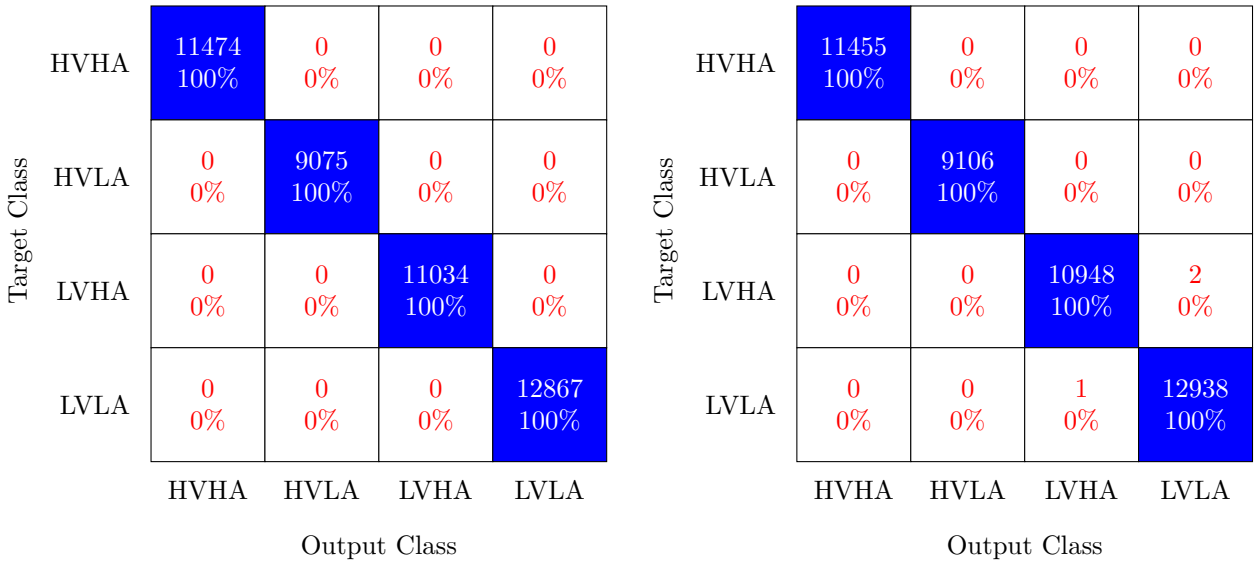

(a) CM of the testing task in quaternion product. (b) CM of the testing task in bicomplex product.

Figure 4.14: CM of the AMIGOS datasets in the quaternion and bicomplex product following the 10-fold cross-validation criteria.

bicomplex in the Tree kernel is the best choice for real-time applications. The average training time-performance ratio between Ensemble and Tree classifiers for the AMIGOS dataset (across both product types) is $\approx 32.76\times$ longer. An advantage of this model is the single model recognition; in ER, a very considerable amount of models are developed following the binary multi-models classification task, achieving a single model per primitive emotion. However, hierarchical models are not the best choice for real-time applications. If time-consuming is considered, security, psychological, and medical-related applications require an outperforming and faster model. In this order of ideas, the bQSA algorithm is an optimal solution to primitive ER tasks. As a disadvantage, a strict signal acquisition protocol is needed to replicate the results, as the bQSA algorithm is very sensitive to the signal noise and artifacts.

The SEED-series is one of the most popular datasets in ER in the primary emotion space. The dataset was developed in a controlled environment, where Chinese participants were asked to watch a series of audio-visual material to elicit five basic emotions: disgust, fear, happy, neutral, and sad in the SEED-V dataset. Developers and researchers have been working on this project for more than a decade, achieving different datasets approaches and multimodal material in order to the emotion recognition. In this study, the bQSA approach

only considers the V and VII SEED-series datasets. The former was published in 2019, and the latter in 2025; a very recent dataset. The latter is the closer material to Ekman (1992a) basic emotions theory, accomplishing a set of seven emotional stimuli: disgust, fear, happy, neutral, sad, and surprise multimodal material. According to Jiang et al. (2025), the SEED-V audiovisual stimuli were reused in the SEED-VII dataset, suggesting a controlled stimuli detection in different subjects. In this order of ideas, the bQSA is applied to both datasets, achieving 100% of accuracy rate for both V and VII material. The CM in the former dataset is shown in Figs. 4.15a and 4.15b, where no outliers are detected in both product types. This only suggested that the SEED-V dataset is a very controlled and well-designed dataset, where in a single and multiclass model the bQSA outperforms perfectly. However, training time-performance is very expensive. In the Ensemble kernel, the bicomplex product is slightly faster than the quaternion product one, however the average ratio is $\approx 3.00\times$ longer than the AMIGOS one and $\approx 100\times$ longer than the FEEL dataset. This ratio could be attributed to the great number of samples of difference between the SEED-series datasets and the FEEL dataset, e.g. the fewer subset of samples in the SEED-V dataset is 15554 for the happy class, in contrast lower one in FEEL dataset is indifferent with less than 10 samples in the class.

As introduced above, the SEED-VII dataset is one of the most recent and complete datasets in the ER material. The dataset was developed following a four-session study, where each session contained four different folders of a combination of five out of seven basic emotions stimuli recorded using 62-channels scalp electrodes. The 20-subjects material achieved a sum of $[20 \times 4 \times 4 \times 5 \times 62] = 99200$ samples, for details see Jiang et al. (2025). Two main differences between both SEED-series datasets are the number of samples and the number of classes; the former cardinality is $|S_{s-v}| = 468,096$ samples, and $|S_{s-vii}| = 1,120,316$ for the latter. With more than twice of the number of samples the latter is a more robust and complex dataset. The relation bewteen time-accuracy performance is the more complex one due to Ensemble kernel takes ≈ 1500 seconds to train a model that is only ≈ 1.8 percent accurate than the kNN model; which takes only ≈ 0.99 seconds to train using the quaternion product as base (see Table 4.3).

As Fig. 4.16 shows, AMIGOS, V- and VII-SEED remains as the higher performance datasets. Probably, the FEEL one achieved $\approx 9\%$ points less than the previous mentioned ones due to the small number of samples ($|S_f| = 5424$) and the large number of targets. Now, the reasons behind the notably low accuracy achieved by the DEAP dataset remains unclear, particularly considering its large cardinality ($|S_d| = 302,080$), similar to the AMIGOS dataset

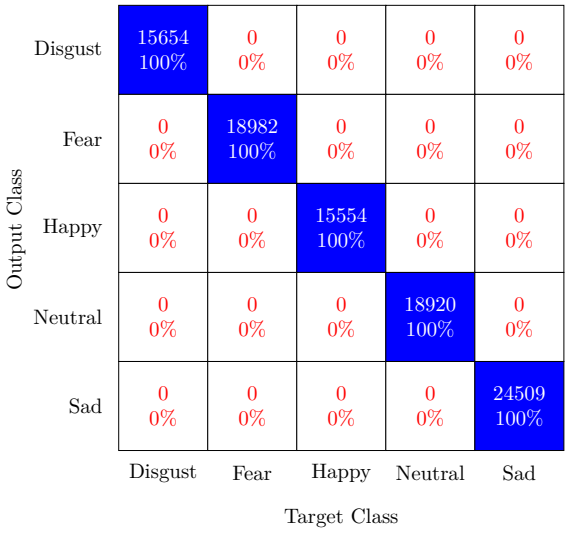

(a) CM of the testing task in quaternion product using the Tree-kernel in SEED-V dataset.

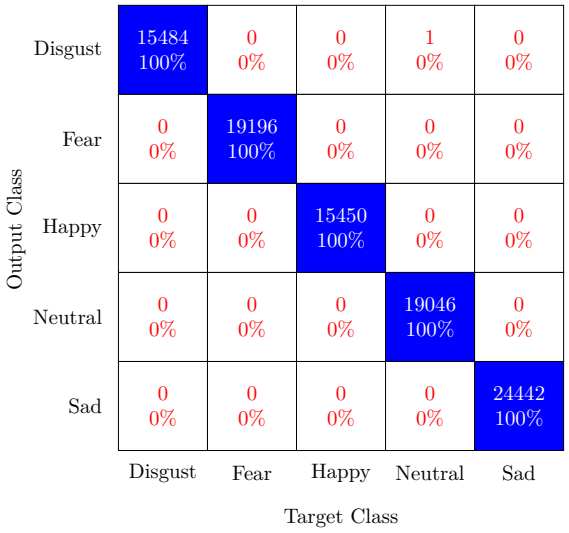

(b) CM of the testing task in bicomplex product using the Tree-kernel in SEED-V dataset.

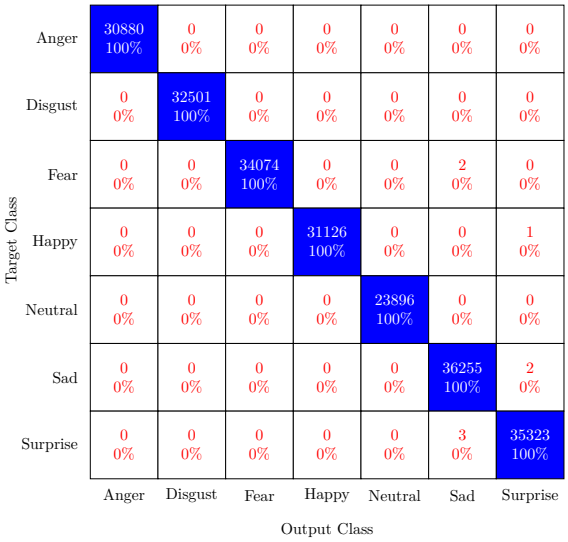

(c) CM of the testing task in quaternion product using the Tree-kernel in SEED-VII dataset

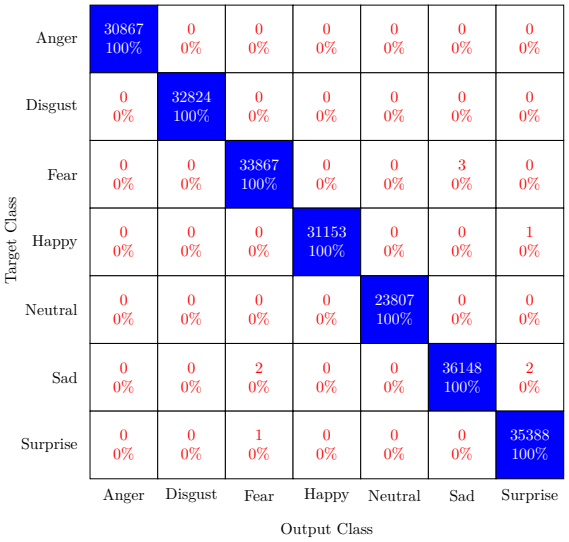

(d) CM of the testing task in bicomplex product using the Tree-kernel in SEED-VII dataset.

Figure 4.15: CM of the V and VII SEED-series datasets in the quaternion and bicomplex product following the 10-fold cross-validation criteria.

($|S_a| = 222,248$). The analysis of Figs. 4.8e and 4.8f indicates that the temporal behavior of the DEAP-bQSA dataset differs from the other datasets. Specifically, the observed patterns of $\mathfrak{Re}(\bullet)$, $\mathfrak{Im}(\bullet)$, and $\mathfrak{Abs}(\bullet)$ exhibit a constant and linear patterns, not found in the other cases. This suggests a potential incompatibility between the data acquisition methods of DEAP and the processing requirements of the bQSA technique. Despite this, four out of the five datasets demonstrate a strong compatibility with the bQSA method for emotion recognition applications.

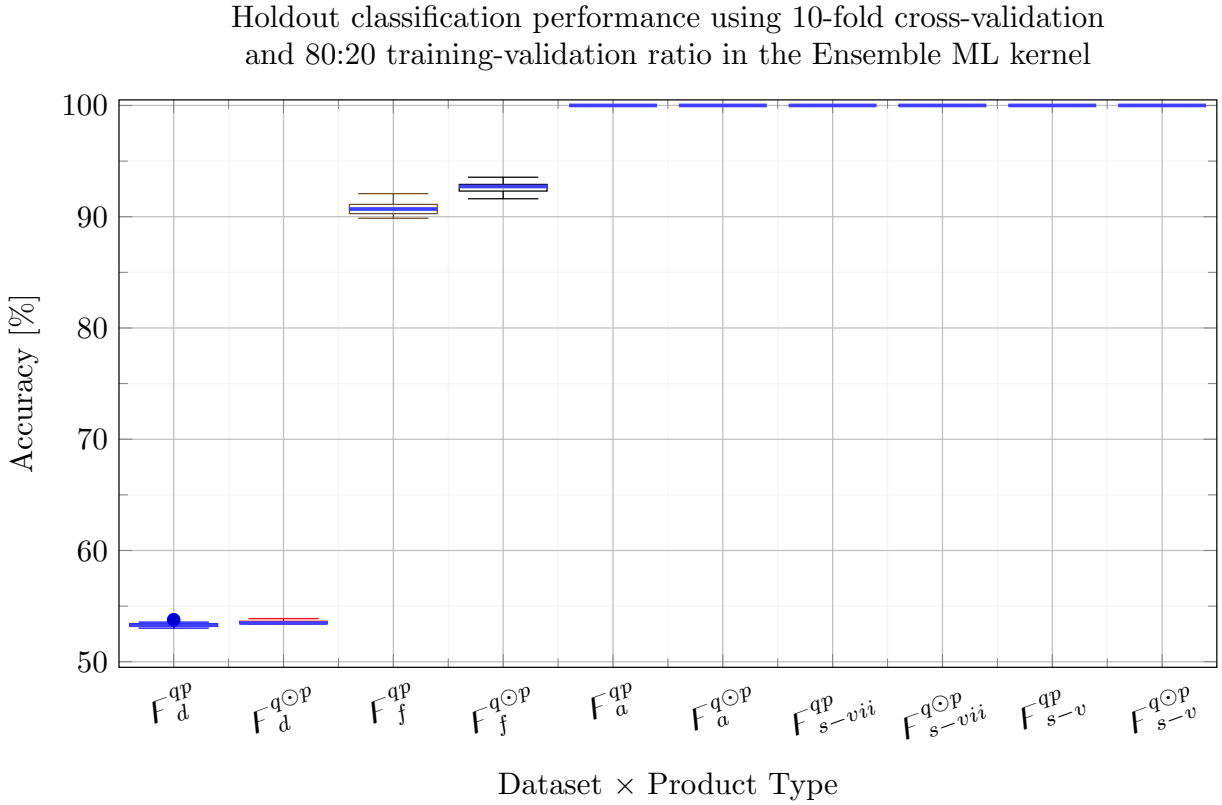

Figure 4.16: Boxplot of the validation normalized score per dataset and product criteria using the Ensemble ML kernel by 10-fold cross-validation.

4.2.4 Analysis of Variance (ANOVA) performance

In order to the 10-fold cross-validation, a three-way ANOVA was performed to analyze the performance of the bQSA algorithm across datasets (five levels), product types (two levels), and ML kernels (three levels). On average, the dataset, product type, and ML kernel

significantly affects the bQSA performance, as shown in Table 4.4. There are significant main effects between the classifier kernel ($p < 0.0001$), product type ($p < 0.0001$), and dataset ($p < 0.0001$). Moreover, the effect between Classifier × Product type suggested that the best ML kernel depends on the product type used ($p < 0.0001$). This is consistent with the reported performance in Table 4.3, where in most of the cases $q \odot p$ product is the reliable one. In addition, the relation between Classifier × Dataset ($p < 0.0001$) concluding that SEED-series and AMIGOS achieved the best performance and, as discussed previoulsly, yielding DEAP as the lower one. In Product Type × Dataset criteria, ANOVA results interpretation suggested that the effectiveness of the product type is highly dependent on the dataset used ($p < 0.0001$). At last, based on the three-way interaction, the inference where Classifier × Product type × Dataset interaction is significant based on the bQSA method is supported. Here, even if six out of ten models achieved 100% in performance metrics, a deeper analysis is needed based on another physiological or non-physiological datasets.

One of the most important findings in this work is the slightly better performance of the bicomplex product over the quaternion one. Noticing that (3.15) the Cayley-Dixon quaternion form in the bicomplex product does not introduce the complex conjugate element to the equation, which p value (P:D) is the middle one in the significance of the two-way ANOVA performance.

Table 4.4: Three-way ANOVA results for the bQSA performance across datasets, product types, and ML kernels.

Source	**F-value**	***p*-value**	**Significance**
Classifier	11184.42	2.13×10^{-260}	Classifier type significantly affects accuracy.
Product type	139.68	2.95×10^{-26}	Quaternion vs. Bicomplex has a significant impact.
Dataset	83897.63	0	Accuracy varies a lot depending on the dataset used.
C:P	34.71	3.84×10^{-14}	The best classifier depends on the product type used.
C:D	3704.17	4.29×10^{-271}	Classifier behavior changes drastically across datasets.
P:D	61.18	9.66×10^{-37}	Product type effectiveness depends on dataset.
C:P:D	65.98	3.77×10^{-59}	Interaction between C, P, and D is significant.

C: Classifier, P: Product type, D: Dataset. The p-values indicate the significance of each factor and their interactions. A p-value less than 0.05 is considered statistically significant.

4.2.5 Previous works and research gaps

Previous studies have shown their own effectiveness in EEG-ER task based on different fusion or novel techniques in the signal pre- and post-processing. As discussed in Chapter 2, no

evidence of quaternion and ER fusion techniques has been found in the literature. However, the Digital Signal Processing (DSP) and quaternion fusion techniques have been used in other materials, such as the proposed by Batres-Mendoza et al. (2016); Contreras-Hernandez et al. (2019); the former processed EEG signals in the motor imagining process, the latter one introduced the quaternion theory to detect broken rotor bars in induction motor. In this order of ideas, a strong evidence of the quaternion performance in ML applications with periodic and non-periodic signals was found; however, none of these explored the bicomplex product or the Cayley-Dixon quaternion processing. Even if the performance metrics for both studies is consistent with a good experimental protocol, the introduction of bQSA algorithm in another engineering areas is needed.

Prior studies have noted the importance of a single model that classify multi-targets in emotion recognition tasks, where Doma and Pirouz (2020); Işık et al. (2023) achieved a single model per primitive emotion in binary target's space using the DEAP dataset as input data. Both studies achieved a superior performance in contrast to the bQSA algorithm; however they had to feed the ML model with the use of the hole electrodes information, which can present noise and artifacts related to non-optimal feature extraction. Also, and consistent with their approaches results, an inference where bQSA algorithm needs a more robust input matrix based on the use of more than four electrodes information is proposed; nevertheless, this contrast with our main approach where a reduced subset of electrodes is used to process the bQSA. Furthermore, DEAP have presented a good performance in DL techniques; as those porposed by Fang et al. (2021); Islam et al. (2021). Both approaches achieved a $70 - 80\%$ of accuracy rate. The former employed a binary classification task, yielding a trained and validated model per primitive above; menawhile the latter one achieved a single multiclass model discretizing the VA space into four primary emotions and a neutral class. In addition, ML techniques used by Topic and Russo (2021); V. and Bhat. (2022) achieved a good performance in the amigos dataset where the latter achieved a superior performance in VAD space developing a single binary classification model per primitve emotion (see Chapter 2 for a deeper introduction). Furthermore, Wu et al. (2022); Zhang et al. (2022) chose to use the SEED-V and AMIGOS datasets as input data to their research in fusion with DL techniques. Authors in Zhang et al. (2022) reported a very close classification rate to the one in this approach (the bQSA) for the DEAP dataset and a slightly superior performance to the 70% in the SEED-V data. By the other hand, Wu et al. (2022) used a subject dependent classification technique to achived a 72.63 ± 08.25 of accuracy rate in the SEED-V dataset.

One of the limitations of a single and multiclass classification model in ER is their complex

and noisy nature of electroencephalogram signals. Sometimes, even if a Wavelet-based algorithm to noise reduction is applied, the signal is still with artifacts, which can lead to a misclassification for both primary and primitive classification. In addition, if a larger targets space is introduced (as the one in SEED-V dataset), the classification task became harder. That's why some methodologies prefer to use a binary classification model to increase the reliability of their results and, in consequence, the performance metrics. As example, authors in Jiang et al. (2025) outperform a single model classification technique applied to their SEED-VII data and concluding that different emotions activate different neural patterns and regions. In consequence, following their own classification approach (which is a multilayer adaptive and mixture transformer), classification results achieved a 33.98%, 50.70%, and 58.24% of accuracy rate performance using ML, DL, and transformer-based kernels, respectively. The complete comparation performance between close related works and the bQSA is reported in the Table 4.5; moreover, an extension and highlights of the state-of-the-art is presented in Chapter 2.

4.2.6 Discussion

Advantages

The bQSA algorithm performance is slightly consistent with previous QSA approaches, such as the one proposed by Batres-Mendoza et al. (2016); Contreras-Hernandez et al. (2019). Both approaches, and the one introduced in this document, are trained using ML kernels for the classification task, which shows a common pattern performance in the quaternion signal processing, increasing the reliability of the method. In fact, binary and ternary classification tasks were performed, respectively, in the former and latter approaches, achieving results close to the 100%; however, the bQSA beats a more robust targets space, specially in SEED-VII and FEEL. In addition, the reported results in Table 4.3 shows that Tree-based kernels were the most reliable ones, even for a large number of emotions classification.

In early observations, the performance in Sect. 4.1.2 used only a subset of four channels in the SEED-V dataset (five targets), achieving 87.12% of accuracy rate, following the channels selection technique of noise reduction, feature extraction, and mRMR channel and feature selection. Hence, the main hypothesis of this work introduced in Chapter 1 theorized that the combination between the DSP and quaternion algebra could improve the classification in ER, where, based on the previous section results, the inference is justified. This hypothesis was validated by outperforming the bQSA algorithm and using only three

statistical features per complex signal (the bicomplex pattern) applied to the $\mathfrak{Re}(\bullet)$ and $\mathfrak{Im}(\bullet)$ pattern. Moreover, Chapter 2 has shown that even with a reduced subset of channels, performance metrics can be equal or even slightly better than using the whole set of channels available. In consequence, the method is superior to all of those reported in Chapter 2 and sect. 4.1, even tested in several EEG datasets.

Table 4.5: Performance comparison between the state-of-the-art relevant results and the proposed method, SPER b-QSA.

ER works in the state-of-the-art							
Reference	Dataset	IA Approach	EC	Classes	Accuracy [%]	F1-measure [%]	Kappa-score
Doma and Pirouz (2020)	DEAP	SI[1]-SVM-PCA	32	V & A	63.43, 73.75	77.62, 84.73	-
Fang et al. (2021)	DEAP	SI-DF[2]	32	AHSPN[3]	71.05	-	-
Islam et al. (2021)	DEAP	SI-CNN	32	V & A	78.22, 74.92	-	-
Işık et al. (2023)	DEAP	SI-kNN	32	VAD	98.94	98.9	-
Topic and Russo (2021)	AMIGOS	SD[4]-SVM	14	V & A	79.54 ± 01.26 85.07 ± 02.04	-	-
V. and Bhat. (2022)	AMIGOS	SI-EBT[5]	4	V, A, & D	94.20, 98.71, 94.53 per PE	92.50, 98.61, 94.37 per PE	-
Zhang et al. (2022)	AMIGOS SEED-V	SI-PARSE[6]	14 62	V & A DFHNS[7]	$\approx 58.77 \pm 10.80$ 71.50 ± 14.05	-	-
Wu et al. (2022)	SEED-V	SD-DCCA	18	DFHNS	72.63 ± 08.26	-	-
Ma et al. (2025)	SEED-V		62	DFHNS	71.86 ± 10.90	-	-
Jiang et al. (2025)	SEED-VII	kNN RGNN MAET	62	ADFHNSS[8]	33.98 50.70 58.24	32.86 49.55 58.08	-
Our approach	SEED-V $q \odot p$	SI-10CV-Ensem	4	DFHNS	100.00 ± 0.00	100.00 ± 0.00	1.00 ∓ 0.00
		SI-10CV-Tree	4	DFHNS	$99.99 \pm 1.60 \times 10^{-3}$	$99.99 \pm 1.54 \times 10^{-3}$	$0.99 \mp 2.01 \times 10^{-5}$
	SEED-V qp	SI-10CV-Ensem	4	DFHNS	100.00 ∓ 0.00	100.00 ∓ 0.00	1.00 ∓ 0.00
		SI-10CV-Tree	4	DFHNS	$99.99 \pm 1.60 \times 10^{-3}$	$99.99 \pm 1.54 \times 10^{-3}$	$0.99 \mp 2.01 \times 10^{-5}$
	SEED-VII $q \odot p$	SI-10CV-Ensem	4	ADFHNSS	100.00 ∓ 0.00	100.00 ∓ 0.00	1.00 ∓ 0.00
		SI-10CV-Tree	4	ADFHNSS	$99.99 \pm 2.83 \times 10^{-3}$	$99.99 \pm 2.84 \times 10^{-3}$	$0.99 \mp 3.31 \times 10^{-5}$
	SEED-VII qp	SI-10CV-Ensem	4	ADFHNSS	100.00 ∓ 0.00	100.00 ∓ 0.00	1.00 ∓ 0.00
		SI-10CV-Tree	4	ADFHNSS	$99.99 \pm 2.01 \times 10^{-3}$	$99.99 \pm 1.93 \times 10^{-3}$	$0.99 \mp 2.35 \times 10^{-5}$
	AMIGOS $q \odot p$	SI-10CV-Ensem	4	(H/L)V(H/L)A	100 ∓ 0.00	100.00 ∓ 0.00	1.00 ∓ 0.00
		SI-10CV-Tree	4	(H/L)V(H/L)A	$99.99 \mp 6.00 \times 10^{-3}$	$99.99 \mp 5.54 \times 10^{-3}$	$0.99 \mp 8.04 \times 10^{-5}$
	AMIGOS qp	SI-10CV-Ensem	4	(H/L)V(H/L)A[9]	100.00 ∓ 0.00	100.00 ∓ 0.00	1.00 ∓ 0.00
		SI-10CV-Tree	4	(H/L)V(H/L)A	100.00 ∓ 0.00	100.00 ∓ 0.00	1.00 ∓ 0.00
	FEEL $q \odot p$	SI-10CV-Ensem	4	13	92.64 ± 0.51	92.89 ± 0.68	$0.92 \pm 5.90 \times 10^{-3}$
		SI-10CV-Tree	4	13	88.22 ± 1.79	88.81 ± 1.55	$0.87 \pm 2.04 \times 10^{-2}$
	FEEL qp	SI-10CV-Ensem	4	13	90.82 ± 0.67	90.93 ± 0.83	$0.89 \pm 7.50 \times 10^{-3}$
		SI-10CV-Tree	4	13	87.04 ± 1.34	87.30 ± 1.21	$0.85 \pm 1.49 \times 10^{-2}$
	DEAP $q \odot p$	SI-10CV-Ensem	4	(H/L)V(H/L)A	53.57 ± 0.17	46.69 ± 0.19	$0.29 \pm 2.36 \times 10^{-3}$
		SI-10CV-Tree	4	(H/L)V(H/L)A	39.16 ± 0.33	36.01 ± 0.24	$0.14 \pm 3.26 \times 10^{-3}$
	DEAP qp	SI-10CV-Ensem	4	(H/L)V(H/L)A	53.34 ± 0.21	45.33 ± 0.24	$0.28 \pm 2.79 \times 10^{-3}$
		SI-10CV-Tree	4	(H/L)V(H/L)A	38.28 ± 0.37	34.97 ± 0.23	$0.13 \pm 2.85 \times 10^{-3}$

[1]Subject Independent, [2]Deep Forest, [3]Angry, Happy, Sad, Pleasant, and Neutral, [4]Subject Dependent, [5]AdaBoost Decision Tree, [6]Pairwise Alignment of Representations for Semi-Supervised EEG Learning, [7]Disgust, Fear, Happy, Neutral, and Sad, [8]Anger, Disgust, Fear, Happy, Neural, Sad, and Surprise, [9]High Valence - High Arousal, High Valence - Low Arousal, Low Valence - High Arousal, Low Valence - Low Arousal.

Principal findings

As discussed previously, the qp and $q \odot p$ product are different only for the complex conjugate in the quaternion product criteria. This little and important difference makes bicomplex product suitable in three out of five datasets (even if the difference is only sensible in the FEEL and DEAP datasets). Even more, the conclusion that Tree is highlighted as the outperforming kernel due to its time-improvement in comparison with the Ensemble one is justified with the information presented in Table 4.3 where 10-fold of Cross-Validation (CV) was performed. Now, the effects of kNN kernel are noticed, however its advantages are only noticed in SEED-V and VII datasets; for the rest of the datasets the performance remains limited, yielding Tree as the best choice.

In the channel selection process, a set of four different effective channels were found, according to statistical, time, frequency, and morphologic features. Based on these kind of features, see Table 3.1, four out of five datasets presents a fronto-parietal effective lobes, only AMIGOS achieved fronto-temporal information, which is consistent with the information analyzed in Chapter 2. According to several authors, frontal and temporal lobes are those commonly used with a high performance in ER, being T7 and T8 those used more frequently. However, our channel selection results do not included any of both temporal channels, see Table 4.2. Summarizing, the frequency of occurrence per brain lobe is: frontal (5), temporal (5), parietal (8), and occipital (2), where parietal occurrence is presented two times per dataset — except in AMIGOS. According to the discussion of He et al. (2021) an strong evidence of emotional processing was found in the frontal, temporal, parietal, and occipital lobe by eliciting positive and negative emotional faces in subjects. Moreover, Spence et al. (1996), and more recently Hartikainen (2021), support the philosophy that establishes an overall right hemispheric dominance for emotion, attention, and arousal. Hence, our experiment is consistent with this theory, achieving nine out of sixteen electrodes located at the right hemisphere, three at the central line, and four out of sixteen at the left hemisphere (FEEL is not considered in this analysis due to the channel location information is private). In sum, it can be assumed that 12 out of 16 channels are located at the right hemisphere. A channel location per brain lobe can be seen in Fig. 4.17.

Limitations

A major advantage of this study is its superior performance using a single-model multiclass approach compared to current state-of-the-art methods. Nevertheless, despite the primary

hypothesis of this research being centered on emotion recognition, additional testing is necessary to ensure the method's reliability. Furthermore, prior successful implementations of similar methodologies, such as QSA applied to motor imagery and induction motor fault diagnosis, enhance confidence in the robustness of the proposed approach. Now, the discussion of the channel selection method is a "double-edged sword" due to the sensitivity of the method to the feature extraction and the main advantage of the reduction of the whole set of channels per dataset. If one is taken off, the model changes the relevance weights, and the effective channels will change. However, in order to complete the objectives of this work, several changes were made off and, at least for the SEED-series and AMIGOS datasets, only slightly changes were noticed. However, FEEL and DEAP presented a more aggressive misclassification performance, achieving $\approx$ 37% of accuracy rate in the DEAP dataset. Furthermore, in those test bicomplex product remains as the outperforming product type model. Finally, it is important to explore the bQSA limitations in deeper analysis with another type of data and even try to explore its performance even in image processing tasks; however, that will accomplish a more robust work and future approaches.

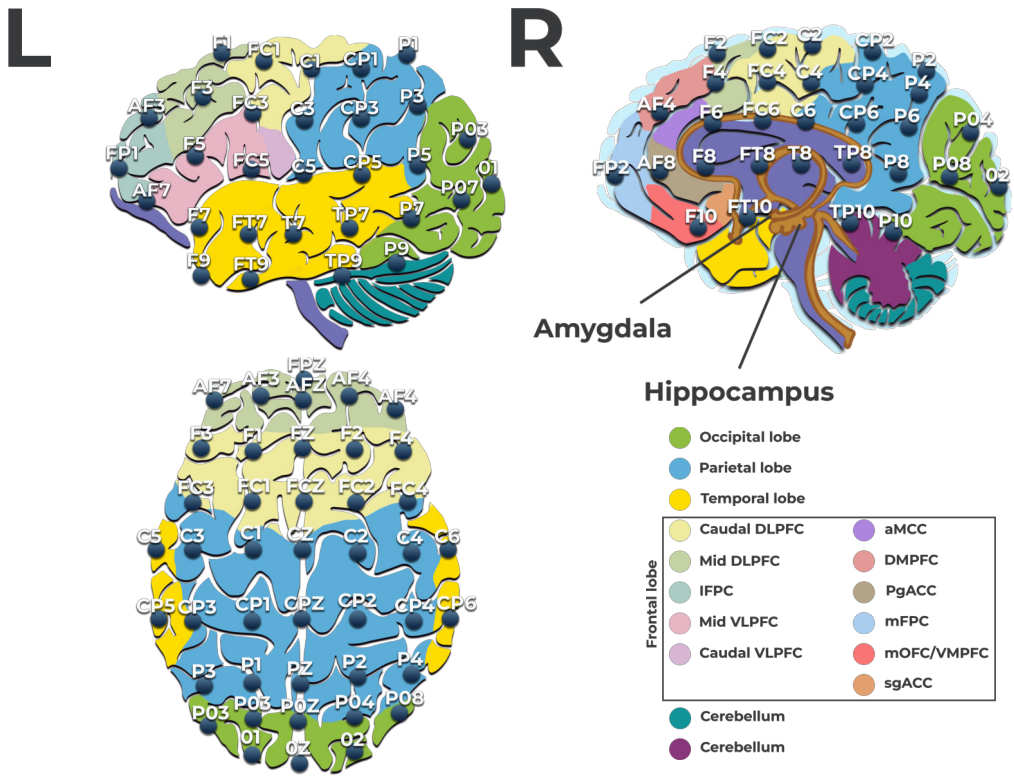

Figure 4.17: EEG electrodes distribution according to the brain lobes location.

Chapter 5

Conclusion

In this study, an introduction to the Hilbert space in order of the quaternion algebra is explored following the bicomplex Cayley-Dixson form of the quaternion processing applied to electroencephalogram signals to increase the performance of the emotion recognition. To explore the reliability of this method, the bicomplex Quaternion Signal Analysis (bQSA) algorithm was tested in five different and multimodal datasets for emotion recognition that includes the primary and primitive emotion space. The SEED-V, SEED-VII, AMIGOS, FEEL, and DEAP datasets were used as input data to perform the bQSA proposed algorithm. Each dataset presents a unique signal acquisition method, which includes the number of subjects, age, gender, among others, and environment, which increases the robustness and complexity of the proposed task.

In order to accomplish the use of the quaternion algebra in electroencephalogram signals, a channel selection method was applied to the raw EEG signals by using the wavelet noise reduction, local binary pattern, and feature extraction to achieved four discriminant electrodes information to construct the bicomplex quaternion form and increase the emotion recognition performance. This effective channels protocol achieved four different and relevant channels per used dataset, yielding that effective information is concentrated in the fronto-tempo-parietal lobes, which is consistent with the literature. Then, the bicomplex quaternion form is constructed by following the Cayley-Dixon theory and using statistical features ($\mu, \sigma,$ and σ^2) to each $\mathfrak{Re}\,(\bullet)$ and $\mathfrak{Im}\,(\bullet)$ part of each component of the bicomplex form.

Experimental results highlights the bicomplex product as the accurate bQSA form, showing a slightly increase in performance metrics in contrast with the quaternion product form ($\pm 0.001\%$). Moreover, the three-way ANOVA test suggested that (1) the best classifier is

dependent on the dataset used, (2) the classifier performance metrics change significantly per dataset, and (3) that the product type (bicomplex or quaternion form) effectiveness depends on the dataset. In addition, the 10-fold cross-validation increases the reliability of bQSA effectiveness; however, only three- and kNN-kernels were concluded as the accurate ones in the recognition process, whereas contrary to the state-of-the-art SVM is weaker for this approach.

In summary, the bQSA algorithm was initially proposed as a signal processing method for EEG-based emotion recognition. This constituted our hypothesis, which is supported and justified by the obtained classification results. Moreover, the channel selection method showed to include the fronto-temporal dependencies as the most relevant information about the brain lobes and 75% of the electrodes located at the right hemisphere of the brain, which is consistent with the evoking of the emotions in the literature. Finally, the bQSA construction and temporal displacement showed a high performance using ML algorithms to validate the method.

As future work, the bQSA methodology will be extended to analyze 2D and 3D pulse patterns identified within each windowed segment, as accomplished in this study. A deeper understanding of these pulses is required; however, preliminary analysis suggests that emotion pulse responses are presented once or twice per second in the electroencephalogram activity. Analyzing these patterns is pivotal for emotional processing theories. Furthermore, integrating oculogram information captured by using a frontal camera could enable artificial intelligence systems to detect physiological ocular responses and correlate these with specific neural patterns, enhancing the accuracy and robustness of AI models in real-world applications and providing an accurate psychological, psychiatric, and human behaviour understanding.

Acronyms

1D-LBP One Dimensional Local Binary Pattern
AC Affective Computing
AI Artificial Intelligence
AMIGOS Affect, Personality, and Mood Research on Individuals and Groups
ANOVA Analysis of Variance
ANS Autonomic Nervious System
bQSA Bicomplex Quaternion Signal Analysis
CM Confussion Matrix
CNN Convolutional Neural Network
CNS Central Nervious System
CV Cross-Validation
CWT Continuous Wavelet Transform
db Daubechies
DE Differential Entropy
DEAP Database for Emotion Analysis Using Physiological Signals
DL Deep Learning
dlPFC dorsolateral Prefrontal Cortex
DNN Deep Neural Network
DSP Digital Signal Processing
DWT Discrete Wavelet Transform
EC Effective Channels
ECG Electrocardiogram
EEG Electroencephalogram
EMD Empirical Mode Decomposition
EMG Electromyogram
EMODB Berlin Database of Emotional Speech

ENP EEG based Network Patterns
EOG Electrooculogram
ER Emotion Recognition
FAWT Functional Analytic Wavelet Transform
FEEL Force, EEG and Emotion-Labelled
FER Facial Emotion Recognition
FL Fussion Learning
FT Fourier Transform
GBA Gamma Band Activity
GSR Galvanic Skin Response
HHT Hilbert-Huang Transform
IEMOCAP Interactive emotional dyadic motion capture database
IMFs Intrinsic Mode Functions
LBP Local Binary Pattern
LOSO-CV Leave-One-Subject-Out Cross-Validation
MANHOB-HCI A Multimodal Database for Affect Recognition and Implicit Tagging
ML Machine Learning
MPED Multi-Modal Physiological Emotion Database
mRMR Minimum Redundancy Maximum Relevance
OFC Orbitofrontal Cortex
PCA Principal Component Analysis
PFC Prefrontal Cortex
PLV Phase Locking Value
PNN Positive, Negative, and Neutral
PNS Peripheral Nervious System
PSO Particle Swarm Optimization
QSA Quaternion Signal Analysis
RAVDESS The Ryerson Audio-Visual Database of Emotional Speech and Song
REGEEG A Regression-based EEG Signal Processing in Emotion Recognition
RF Random Forest
SEED SJTU Emotion EEG Dataset
SER Speech Emotion Recognition
SMH Somatic Maker Hypothesis
SSWT Synchosqueezing Wavelet Transform

SVM Support Vector Machine
TER Textual Emotion Recognition
VA Valence-Arousal
VAD Valence-Arousal-Dominance
vmPFC ventromedial Prefrontal Cortex
WD Wavelet Decomposition
WOS Web of Science Core Collection
WT Wavelet Transform

Bibliography

F. Ahmed, A. S. M. H. Bari, and M. L. Gavrilova. Emotion recognition from body movement. *IEEE Access*, 8:11761–11781, 2020. ISSN 2169-3536. doi: 10.1109/access.2019.2963113.

T. B. Alakus, M. Gonen, and I. Turkoglu. Database for an emotion recognition system based on EEG signals and various computer games – GAMEEMO. *Biomedical Signal Processing and Control*, 60:101951, July 2020. ISSN 1746-8094. doi: 10.1016/j.bspc.2020.101951.

J. Albert, S. López-Martín, and L. Carretié. Emotional context modulates response inhibition: Neural and behavioral data. *NeuroImage*, 49(1):914–921, Jan. 2010. ISSN 1053-8119. doi: 10.1016/j.neuroimage.2009.08.045.

S. Bagherzadeh, M. R. Norouzi, S. Bahri Hampa, A. Ghasri, P. Tolou Kouroshi, S. Hosseininasab, M. A. Ghasem Zadeh, and A. M. Nasrabadi. A subject-independent portable emotion recognition system using synchrosqueezing wavelet transform maps of EEG signals and resnet-18. *Biomedical Signal Processing and Control*, 90:105875, Apr. 2024. ISSN 1746-8094. doi: 10.1016/j.bspc.2023.105875.

A.-M. Bao and D. F. Swaab. The human hypothalamus in mood disorders: The HPA axis in the center. *IBRO Reports*, 6:45–53, June 2019. ISSN 2451-8301. doi: 10.1016/j.ibror.2018.11.008.

P. Batres-Mendoza, C. Montoro-Sanjose, E. Guerra-Hernandez, D. Almanza-Ojeda, H. Rostro-Gonzalez, R. Romero-Troncoso, and M. Ibarra-Manzano. Quaternion-based signal analysis for motor imagery classification from electroencephalographic signals. *Sensors*, 16(3):336, Mar. 2016. ISSN 1424-8220. doi: 10.3390/s16030336.

A. Bechara and A. R. Damasio. The somatic marker hypothesis: A neural theory of economic decision. *Games and Economic Behavior*, 52(2):336–372, Aug. 2005. ISSN 0899-8256. doi: 10.1016/j.geb.2004.06.010.

Z. Ben-Zion, N. Korem, N. B. Fine, S. Katz, M. Siddhanta, M. C. Funaro, O. Duek, T. R. Spiller, S. K. Danböck, I. Levy, and I. Harpaz-Rotem. Structural neuroimaging of hippocampus and amygdala subregions in posttraumatic stress disorder: A scoping review. *Biological Psychiatry Global Open Science*, 4(1):120–134, Jan. 2024. ISSN 2667-1743. doi: 10.1016/j.bpsgos.2023.07.001.

S. Berboth and C. Morawetz. Amygdala-prefrontal connectivity during emotion regulation: A meta-analysis of psychophysiological interactions. *Neuropsychologia*, 153:107767, Mar. 2021. ISSN 0028-3932. doi: 10.1016/j.neuropsychologia.2021.107767.

N. Bhagavan and C.-E. Ha. *Endocrine Metabolism II*, pages 545–557. Elsevier, 2015. ISBN 9780124166875. doi: 10.1016/b978-0-12-416687-5.00029-4.

M. Y. Bhat, A. H. Dar, I. Nurhidayat, and S. Pinelas. Uncertainty principles for the two-sided quaternion windowed quadratic-phase fourier transform. *Symmetry*, 14(12):2650, Dec. 2022. ISSN 2073-8994. doi: 10.3390/sym14122650.

F. Burkhardt, A. Paeschke, M. Rolfes, W. F. Sendlmeier, and B. Weiss. A database of german emotional speech. In *Interspeech 2005*, pages 1517–1520, 2005. doi: 10.21437/Interspeech.2005-446.

C. Busso, M. Bulut, C.-C. Lee, A. Kazemzadeh, E. Mower, S. Kim, J. N. Chang, S. Lee, and S. S. Narayanan. IEMOCAP: interactive emotional dyadic motion capture database. *Language Resources and Evaluation*, 42(4):335–359, Nov. 2008. ISSN 1574-0218. doi: 10.1007/s10579-008-9076-6.

X. L. Cang, R. R. Guerra, B. Guta, P. Bucci, L. Rodgers, H. Mah, Q. Feng, A. Agrawal, and K. E. MacLean. FEELing (key)pressed: Implicit touch pressure bests brain activity for modeling emotion dynamics in the space between stressed & relaxed. *IEEE Transactions on Haptics*, 17(3):310–318, July 2024. ISSN 2334-0134. doi: 10.1109/toh.2023.3308059.

A. Celeghin, M. Diano, A. Bagnis, M. Viola, and M. Tamietto. Basic emotions in human neuroscience: Neuroimaging and beyond. *Frontiers in Psychology*, 8, Aug. 2017. ISSN 1664-1078. doi: 10.3389/fpsyg.2017.01432.

J. L. Contreras-Hernandez, D. L. Almanza-Ojeda, S. Ledesma-Orozco, A. Garcia-Perez, R. J. Romero-Troncoso, and M. A. Ibarra-Manzano. Quaternion signal analysis algorithm for

induction motor fault detection. *IEEE Transactions on Industrial Electronics*, 66(11): 8843–8850, Nov. 2019. ISSN 1557-9948. doi: 10.1109/tie.2019.2891468.

D. Dadebayev, W. W. Goh, and E. X. Tan. EEG-based emotion recognition: Review of commercial EEG devices and machine learning techniques. *Journal of King Saud University - Computer and Information Sciences*, 34(7):4385–4401, July 2022. ISSN 1319-1578. doi: 10.1016/j.jksuci.2021.03.009.

A. Damasio and G. B. Carvalho. The nature of feelings: evolutionary and neurobiological origins. *Nature Reviews Neuroscience*, 14(2):143–152, Jan. 2013. ISSN 1471-0048. doi: 10.1038/nrn3403.

A. R. Damasio. The somatic marker hypothesis and the possible functions of the prefrontal cortex. *Philosophical Transactions of the Royal Society of London. Series B: Biological Sciences*, 351(1346):1413–1420, Oct. 1996. ISSN 1471-2970. doi: 10.1098/rstb.1996.0125.

A. R. Damasio. *The Feeling of What Happens: Body and Emotion in the Making of Consciousness*. Houghton Mifflin Harcourt, Boston, MA, 1st edition, 1999. ISBN 0151003696.

A. De Silva, V. Salem, P. M. Matthews, and W. S. Dhillo. The use of functional MRI to study appetite control in the CNS. *Experimental Diabetes Research*, 2012:1–13, 2012. ISSN 1687-5303. doi: 10.1155/2012/764017.

M. R. Delgado, K. I. Nearing, J. E. LeDoux, and E. A. Phelps. Neural circuitry underlying the regulation of conditioned fear and its relation to extinction. *Neuron*, 59(5):829–838, Sept. 2008. ISSN 0896-6273. doi: 10.1016/j.neuron.2008.06.029.

J. Deng and F. Ren. A survey of textual emotion recognition and its challenges. *IEEE Transactions on Affective Computing*, 14(1):49–67, Jan. 2023. ISSN 2371-9850. doi: 10.1109/taffc.2021.3053275.

C. Ding and H. Peng. Minimum redundancy feature selection from microarray gene expression data. *Journal of Bioinformatics and Computational Biology*, 03(02):185–205, Apr. 2005. ISSN 1757-6334. doi: 10.1142/s0219720005001004.

S. L. Dixon and R. T. Koehler. The hidden component of size in two-dimensional fragment descriptors: Side effects on sampling in bioactive libraries. *Journal of Medicinal Chemistry*, 42(15):2887–2900, July 1999. ISSN 1520-4804. doi: 10.1021/jm980708c.

V. Doma and M. Pirouz. A comparative analysis of machine learning methods for emotion recognition using EEG and peripheral physiological signals. *Journal of Big Data*, 7(1), Mar. 2020. ISSN 2196-1115. doi: 10.1186/s40537-020-00289-7.

Y. Dong, C. Jing, M. Mahmud, M. K.-P. Ng, and S. Wang. Enhancing cross-subject emotion recognition precision through unimodal EEG: a novel emotion preceptor model. *Brain Informatics*, 11(1), Dec. 2024. ISSN 2198-4026. doi: 10.1186/s40708-024-00245-8.

M. Egger, M. Ley, and S. Hanke. Emotion recognition from physiological signal analysis: A review. *Electronic Notes in Theoretical Computer Science*, 343:35–55, May 2019. ISSN 1571-0661. doi: 10.1016/j.entcs.2019.04.009.

P. Ekman. Are there basic emotions? *Psychological Review*, 99(3):550–553, 1992a. ISSN 0033-295X. doi: 10.1037/0033-295x.99.3.550.

P. Ekman. An argument for basic emotions. *Cognition and Emotion*, 6(3–4):169–200, May 1992b. ISSN 1464-0600. doi: 10.1080/02699939208411068.

A. D. Ekstrom and P. F. Hill. Spatial navigation and memory: A review of the similarities and differences relevant to brain models and age. *Neuron*, 111(7):1037–1049, Apr. 2023. ISSN 0896-6273. doi: 10.1016/j.neuron.2023.03.001.

T. A. Ell, N. L. Bihan, and S. J. Sangwine. *Quaternion Fourier Transforms for Signal and Image Processing*. John Wiley & Sons, 2014. ISBN 978-1-118-64792-9.

U. K. A. Elvira, S. Seoane, J. Janssen, and N. Janssen. Contributions of human amygdala nuclei to resting-state networks. *PLOS ONE*, 17(12):e0278962, Dec. 2022. ISSN 1932-6203. doi: 10.1371/journal.pone.0278962.

A. Etkin, C. Büchel, and J. J. Gross. The neural bases of emotion regulation. *Nature Reviews Neuroscience*, 16(11):693–700, Oct. 2015. ISSN 1471-0048. doi: 10.1038/nrn4044.

M. R. Ezilarasan and M.-F. Leung. An efficient EEG signal analysis for emotion recognition using FPGA. *Information*, 15(6):301, May 2024. ISSN 2078-2489. doi: 10.3390/info15060301.

Y. Fang, H. Yang, X. Zhang, H. Liu, and B. Tao. Multi-feature input deep forest for EEG-based emotion recognition. *Frontiers in Neurorobotics*, 14, Jan. 2021. ISSN 1662-5218. doi: 10.3389/fnbot.2020.617531.

S. Farashi and R. Khosrowabadi. EEG based emotion recognition using minimum spanning tree. *Physical and Engineering Sciences in Medicine*, 43(3):985–996, July 2020. ISSN 2662-4737. doi: 10.1007/s13246-020-00895-y.

G. Ghous, S. Najam, M. Alshehri, A. Alshahrani, Y. AlQahtani, A. Jalal, and H. Liu. Attention-driven emotion recognition in EEG: A transformer-based approach with cross-dataset fine-tuning. *IEEE Access*, 13:69369–69394, 2025. ISSN 2169-3536. doi: 10.1109/access.2025.3561137.

H. Guerdelli, C. Ferrari, W. Barhoumi, H. Ghazouani, and S. Berretti. Macro- and micro-expressions facial datasets: A survey. *Sensors*, 22(4):1524, Feb. 2022. ISSN 1424-8220. doi: 10.3390/s22041524.

R. Guex, C. Méndez-Bértolo, S. Moratti, B. A. Strange, L. Spinelli, R. J. Murray, D. Sander, M. Seeck, P. Vuilleumier, and J. Domínguez-Borràs. Temporal dynamics of amygdala response to emotion- and action-relevance. *Scientific Reports*, 10(1), July 2020. ISSN 2045-2322. doi: 10.1038/s41598-020-67862-1.

V. Gupta, M. D. Chopda, and R. B. Pachori. Cross-subject emotion recognition using flexible analytic wavelet transform from EEG signals. *IEEE Sensors Journal*, 19(6):2266–2274, Mar. 2019. ISSN 2379-9153. doi: 10.1109/jsen.2018.2883497.

W. R. Hamilton. Ii. on quaternions; or on a new system of imaginaries in algebra. *The London, Edinburgh, and Dublin Philosophical Magazine and Journal of Science*, 25(163): 10–13, July 1844. ISSN 1941-5974. doi: 10.1080/14786444408644923.

F. Hansen. Distinguishing between feelings and emotions in understanding communication effects. *Journal of Business Research*, 58(10):1426–1436, Oct. 2005. ISSN 0148-2963. doi: 10.1016/j.jbusres.2003.10.012.

K. M. Hartikainen. Emotion-attention interaction in the right hemisphere. *Brain Sciences*, 11(8):1006, July 2021. ISSN 2076-3425. doi: 10.3390/brainsci11081006.

H. He, Y. Tan, J. Ying, and W. Zhang. Strengthen EEG-based emotion recognition using firefly integrated optimization algorithm. *Applied Soft Computing*, 94:106426, Sept. 2020. ISSN 1568-4946. doi: 10.1016/j.asoc.2020.106426.

Z. He, K. Yang, N. Zhuang, and Y. Zeng. Processing of affective pictures: A study based on functional connectivity network in the cerebral cortex. *Computational Intelligence and Neuroscience*, 2021(1), Jan. 2021. ISSN 1687-5273. doi: 10.1155/2021/5582666.

M.-P. Hosseini, A. Hosseini, and K. Ahi. A review on machine learning for EEG signal processing in bioengineering. *IEEE Reviews in Biomedical Engineering*, 14:204–218, 2021. ISSN 1941-1189. doi: 10.1109/rbme.2020.2969915.

M. R. Islam, M. M. Islam, M. M. Rahman, C. Mondal, S. K. Singha, M. Ahmad, A. Awal, M. S. Islam, and M. A. Moni. EEG channel correlation based model for emotion recognition. *Computers in Biology and Medicine*, 136:104757, Sept. 2021. ISSN 0010-4825. doi: 10.1016/j.compbiomed.2021.104757.

Ü. Işık, A. Güven, and T. Batbat. Evaluation of emotions from brain signals on 3d vad space via artificial intelligence techniques. *Diagnostics*, 13(13):2141, June 2023. ISSN 2075-4418. doi: 10.3390/diagnostics13132141.

J. C. Jackson, J. Watts, T. R. Henry, J.-M. List, R. Forkel, P. J. Mucha, S. J. Greenhill, R. D. Gray, and K. A. Lindquist. Emotion semantics show both cultural variation and universal structure. *Science*, 366(6472):1517–1522, Dec. 2019. ISSN 1095-9203. doi: 10.1126/science.aaw8160.

M. Javidan, M. Yazdchi, Z. Baharlouei, and A. Mahnam. Feature and channel selection for designing a regression-based continuous-variable emotion recognition system with two EEG channels. *Biomedical Signal Processing and Control*, 70:102979, Sept. 2021. ISSN 1746-8094. doi: 10.1016/j.bspc.2021.102979.

S. Javidi, C. C. Took, and D. P. Mandic. Fast independent component analysis algorithm for quaternion valued signals. *IEEE Transactions on Neural Networks*, 22(12):1967–1978, Dec. 2011. ISSN 1941-0093. doi: 10.1109/tnn.2011.2171362.

W.-B. Jiang, X.-H. Liu, W.-L. Zheng, and B.-L. Lu. Seed-vii: A multimodal dataset of six basic emotions with continuous labels for emotion recognition. *IEEE Transactions on Affective Computing*, 16(2):969–985, Apr. 2025. ISSN 2371-9850. doi: 10.1109/taffc.2024.3485057.

R. L. Kaplan, L. J. Levine, H. C. Lench, and M. A. Safer. Forgetting feelings: Opposite biases in reports of the intensity of past emotion and mood. *Emotion*, 16(3):309–319, Apr. 2016. ISSN 1528-3542. doi: 10.1037/emo0000127.

S. Katsigiannis and N. Ramzan. Dreamer: A database for emotion recognition through EEG and ecg signals from wireless low-cost off-the-shelf devices. *IEEE Journal of Biomedical and Health Informatics*, 22(1):98–107, Jan. 2018. ISSN 2168-2208. doi: 10.1109/jbhi.2017.2688239.

K. A. Khan, S. P. P., Y. U. Khan, and O. Farooq. A hybrid local binary pattern and wavelets based approach for EEG classification for diagnosing epilepsy. *Expert Systems with Applications*, 140:112895, Feb. 2020. ISSN 0957-4174. doi: 10.1016/j.eswa.2019.112895.

Ş. Kılıç, Y. Kaya, and İ. Askerbeyli. A new approach for human recognition through wearable sensor signals. *Arabian Journal for Science and Engineering*, 46(4):4175–4189, March 2021. ISSN 2191-4281. doi: 10.1007/s13369-021-05391-3.

C. F. Kirstein, O. Güntürkün, and S. Ocklenburg. Ultra-high field imaging of the amygdala – a narrative review. *Neuroscience & Biobehavioral Reviews*, 152:105245, Sept. 2023. ISSN 0149-7634. doi: 10.1016/j.neubiorev.2023.105245.

J. C. Klein, T. E. Behrens, and H. Johansen-Berg. *Connectivity Fingerprinting of Gray Matter*, pages 377–402. Elsevier, 2009. ISBN 9780123747099. doi: 10.1016/b978-0-12-374709-9.00017-1.

S. Koelstra, C. Muhl, M. Soleymani, J.-S. Lee, A. Yazdani, T. Ebrahimi, T. Pun, A. Nijholt, and I. Patras. Deap: A database for emotion analysis; using physiological signals. *IEEE Transactions on Affective Computing*, 3(1):18–31, Jan. 2012. ISSN 1949-3045. doi: 10.1109/t-affc.2011.15.

S. Ledesma, M.-A. Ibarra-Manzano, E. Cabal-Yepez, D.-L. Almanza-Ojeda, and J.-G. Avina-Cervantes. Analysis of data sets with learning conflicts for machine learning. *IEEE Access*, 6:45062–45070, 2018. ISSN 2169-3536. doi: 10.1109/access.2018.2865135.

J. E. LeDoux and R. Brown. A higher-order theory of emotional consciousness. *Proceedings of the National Academy of Sciences*, 114(10), Feb. 2017. ISSN 1091-6490. doi: 10.1073/pnas.1619316114.

P. Li, H. Liu, Y. Si, C. Li, F. Li, X. Zhu, X. Huang, Y. Zeng, D. Yao, Y. Zhang, and P. Xu. EEG based emotion recognition by combining functional connectivity network and local activations. *IEEE Transactions on Biomedical Engineering*, 66(10):2869–2881, Oct. 2019. ISSN 1558-2531. doi: 10.1109/tbme.2019.2897651.

P. Lian. Uncertainty principle for the quaternion fourier transform. *Journal of Mathematical Analysis and Applications*, 467(2):1258–1269, Nov. 2018. ISSN 0022-247X. doi: 10.1016/j.jmaa.2018.08.002.

R. Y. Lim, W.-C. L. Lew, and K. K. Ang. Review of EEG affective recognition with a neuroscience perspective. *Brain Sciences*, 14(4):364, Apr. 2024. ISSN 2076-3425. doi: 10.3390/brainsci14040364.

W. Liu, J.-L. Qiu, W.-L. Zheng, and B.-L. Lu. Comparing recognition performance and robustness of multimodal deep learning models for multimodal emotion recognition. *IEEE Transactions on Cognitive and Developmental Systems*, 14(2):715–729, June 2022a. ISSN 2379-8939. doi: 10.1109/tcds.2021.3071170.

W. Liu, W.-L. Zheng, Z. Li, S.-Y. Wu, L. Gan, and B.-L. Lu. Identifying similarities and differences in emotion recognition with EEG and eye movements among chinese, german, and french people. *Journal of Neural Engineering*, 19(2):026012, Mar. 2022b. ISSN 1741-2552. doi: 10.1088/1741-2552/ac5c8d.

S. R. Livingstone and F. A. Russo. The ryerson audio-visual database of emotional speech and song (RAVDESS): A dynamic, multimodal set of facial and vocal expressions in north american english. *PLOS ONE*, 13(5):e0196391, May 2018. ISSN 1932-6203. doi: 10.1371/journal.pone.0196391.

Z. Ma, A. Li, J. Tang, J. Zhang, and Z. Yin. Multimodal emotion recognition by fusing complementary patterns from central to peripheral neurophysiological signals across feature domains. *Engineering Applications of Artificial Intelligence*, 143:110004, Mar. 2025. ISSN 0952-1976. doi: 10.1016/j.engappai.2025.110004.

D. Matsumoto and P. Ekman. American-japanese cultural differences in intensity ratings of facial expressions of emotion. *Motivation and Emotion*, 13(2):143–157, June 1989. ISSN 1573-6644. doi: 10.1007/bf00992959.

K. McRae, S. Misra, A. K. Prasad, S. C. Pereira, and J. J. Gross. Bottom-up and top-down emotion generation: implications for emotion regulation. *Social Cognitive and Affective Neuroscience*, 7(3):253–262, Feb. 2011. ISSN 1749-5016. doi: 10.1093/scan/nsq103.

A. Mehrabian. Communication without words. 1968. URL https://api.semanticscholar.org/CorpusID:62098432.

J. A. Miranda-Correa, M. K. Abadi, N. Sebe, and I. Patras. AMIGOS: A dataset for affect, personality and mood research on individuals and groups. *IEEE Transactions on Affective Computing*, 12(2):479–493, Apr. 2021. ISSN 2371-9850. doi: 10.1109/taffc.2018.2884461.

J. Moini and P. Piran. *Diencephalon: Thalamus and hypothalamus*, pages 267–292. Elsevier, 2020. ISBN 9780128174241. doi: 10.1016/b978-0-12-817424-1.00008-2.

P. Naga, S. D. Marri, and R. Borreo. Facial emotion recognition methods, datasets and technologies: A literature survey. *Materials Today: Proceedings*, 80:2824–2828, 2023. ISSN 2214-7853. doi: 10.1016/j.matpr.2021.07.046.

E. F. Pace-Schott, M. C. Amole, T. Aue, M. Balconi, L. M. Bylsma, H. Critchley, H. A. Demaree, B. H. Friedman, A. E. K. Gooding, O. Gosseries, T. Jovanovic, L. A. Kirby, K. Kozlowska, S. Laureys, L. Lowe, K. Magee, M.-F. Marin, A. R. Merner, J. L. Robinson, R. C. Smith, D. P. Spangler, M. Van Overveld, and M. B. VanElzakker. Physiological feelings. *Neuroscience & Biobehavioral Reviews*, 103:267–304, Aug. 2019. ISSN 0149-7634. doi: 10.1016/j.neubiorev.2019.05.002.

Y. Peng, H. Liu, J. Li, J. Huang, B.-L. Lu, and W. Kong. Cross-session emotion recognition by joint label-common and label-specific EEG features exploration. *IEEE Transactions on Neural Systems and Rehabilitation Engineering*, 31:759–768, 2023. ISSN 1558-0210. doi: 10.1109/tnsre.2022.3233109.

L. Pessoa. A network model of the emotional brain. *Trends in Cognitive Sciences*, 21(5): 357–371, May 2017. ISSN 1364-6613. doi: 10.1016/j.tics.2017.03.002.

E. A. Phelps and J. E. LeDoux. Contributions of the amygdala to emotion processing: From animal models to human behavior. *Neuron*, 48(2):175–187, Oct. 2005. ISSN 0896-6273. doi: 10.1016/j.neuron.2005.09.025.

G. Pourtois, L. Spinelli, M. Seeck, and P. Vuilleumier. Temporal precedence of emotion over attention modulations in the lateral amygdala: Intracranial ERP evidence from a patient with temporal lobe epilepsy. *Cognitive, Affective, & Behavioral Neuroscience*, 10(1):83–93, Mar. 2010. ISSN 1531-135X. doi: 10.3758/cabn.10.1.83.

L. Quadt, H. Critchley, and Y. Nagai. Cognition, emotion, and the central autonomic network. *Autonomic Neuroscience*, 238:102948, Mar. 2022. ISSN 1566-0702. doi: 10.1016/j.autneu.2022.102948.

R. Roesler, M. B. Parent, R. T. LaLumiere, and C. K. McIntyre. Amygdala-hippocampal interactions in synaptic plasticity and memory formation. *Neurobiology of Learning and Memory*, 184:107490, Oct. 2021. ISSN 1074-7427. doi: 10.1016/j.nlm.2021.107490.

D. J. Rogers and T. T. Tanimoto. A computer program for classifying plants: The computer is programmed to simulate the taxonomic process of comparing each case with every other case. *Science*, 132(3434):1115–1118, Oct. 1960. ISSN 1095-9203. doi: 10.1126/science.132.3434.1115.

E. T. Rolls, B. J. Everitt, A. Roberts, A. C. Roberts, T. W. Robbins, and L. Weiskrantz. The orbitofrontal cortex. *Philosophical Transactions of the Royal Society of London. Series B: Biological Sciences*, 351(1346):1433–1444, 1996. doi: 10.1098/rstb.1996.0128.

D. Sander, J. Grafman, and T. Zalla. The human amygdala: An evolved system for relevance detection. *Reviews in the Neurosciences*, 14(4), Jan. 2003. ISSN 0334-1763. doi: 10.1515/revneuro.2003.14.4.303.

T. R. Scott and C. R. Plata-Salamán. Taste in the monkey cortex. *Physiology & Behavior*, 67(4):489–511, Oct. 1999. ISSN 0031-9384. doi: 10.1016/s0031-9384(99)00115-8.

A. Seal, P. P. N. Reddy, P. Chaithanya, A. Meghana, K. Jahnavi, O. Krejcar, and R. Hudak. An EEG database and its initial benchmark emotion classification performance. *Computational and Mathematical Methods in Medicine*, 2020:1–14, Aug. 2020. ISSN 1748-6718. doi: 10.1155/2020/8303465.

J. Sherfey, S. Ardid, E. K. Miller, M. E. Hasselmo, and N. J. Kopell. Prefrontal oscillations modulate the propagation of neuronal activity required for working memory. *Neurobiology of Learning and Memory*, 173:107228, Sept. 2020. ISSN 1074-7427. doi: 10.1016/j.nlm.2020.107228.

A. Siegel and H. N. Sapru. *Essential Neuroscience*. Lippincott Williams & Wilkins, Philadelphia, PA, 1st edition, 2006. ISBN 9780781750776.

A. Silard and M. T. Dasborough. Beyond emotion valence and arousal: A new focus on the target of leader emotion expression within leader–member dyads. *Journal of Organizational Behavior*, 42(9):1186–1201, Mar. 2021. ISSN 1099-1379. doi: 10.1002/job.2513.

G. Šimić, M. Tkalčić, V. Vukić, D. Mulc, E. Španić, M. Šagud, F. E. Olucha-Bordonau, M. Vukšić, and P. R. Hof. Understanding emotions: Origins and roles of the amygdala. *Biomolecules*, 11(6):823, May 2021. ISSN 2218-273X. doi: 10.3390/biom11060823.

Y. B. Singh and S. Goel. A systematic literature review of speech emotion recognition approaches. *Neurocomputing*, 492:245–263, July 2022. ISSN 0925-2312. doi: 10.1016/j.neucom.2022.04.028.

M. Soleymani, J. Lichtenauer, T. Pun, and M. Pantic. A multimodal database for affect recognition and implicit tagging. *IEEE Transactions on Affective Computing*, 3(1):42–55, Jan. 2012. ISSN 1949-3045. doi: 10.1109/t-affc.2011.25.

T. Song, W. Zheng, C. Lu, Y. Zong, X. Zhang, and Z. Cui. MPED: A multi-modal physiological emotion database for discrete emotion recognition. *IEEE Access*, 7: 12177–12191, 2019. ISSN 2169-3536. doi: 10.1109/access.2019.2891579.

S. Sonkusare, D. Qiong, Y. Zhao, W. Liu, R. Yang, A. Mandali, L. Manssuer, C. Zhang, C. Cao, B. Sun, S. Zhan, and V. Voon. Frequency dependent emotion differentiation and directional coupling in amygdala, orbitofrontal and medial prefrontal cortex network with intracranial recordings. *Molecular Psychiatry*, 28(4):1636–1646, Dec. 2022. ISSN 1476-5578. doi: 10.1038/s41380-022-01883-2.

S. Spence, D. Shapiro, and E. Zaidel. The role of the right hemisphere in the physiological and cognitive components of emotional processing. *Psychophysiology*, 33(2):112–122, Mar. 1996. ISSN 1469-8986. doi: 10.1111/j.1469-8986.1996.tb02115.x.

P. Sterling. Allostasis: A model of predictive regulation. *Physiology & Behavior*, 106(1): 5–15, Apr. 2012. ISSN 0031-9384. doi: 10.1016/j.physbeh.2011.06.004.

A. Stolicyn, M. A. Harris, L. de Nooij, X. Shen, J. A. Macfarlane, A. Campbell, C. J. McNeil, A.-L. Sandu, A. D. Murray, G. D. Waiter, S. M. Lawrie, J. D. Steele, A. M. McIntosh,

L. Romaniuk, and H. C. Whalley. Disrupted limbic-prefrontal effective connectivity in response to fearful faces in lifetime depression. *Journal of Affective Disorders*, 351:983–993, Apr. 2024. ISSN 0165-0327. doi: 10.1016/j.jad.2024.01.038.

D. P. Subha, P. K. Joseph, R. Acharya U, and C. M. Lim. EEG signal analysis: A survey. *Journal of Medical Systems*, 34(2):195–212, Dec. 2008. ISSN 1573-689X. doi: 10.1007/s10916-008-9231-z.

A. Topic and M. Russo. Emotion recognition based on EEG feature maps through deep learning network. *Engineering Science and Technology, an International Journal*, 24(6): 1442–1454, Dec. 2021. ISSN 2215-0986. doi: 10.1016/j.jestch.2021.03.012.

E. P. Torres, E. A. Torres, M. Hernández-Álvarez, and S. G. Yoo. EEG-based bci emotion recognition: A survey. *Sensors*, 20(18):5083, Sept. 2020. ISSN 1424-8220. doi: 10.3390/s20185083.

J. Turner. *On the origins of human emotions: A sociological inquiry into the evolution of human affect*. Stanford University Press, 2000.

J. H. Turner. The evolution of emotions in humans: A darwinian–durkheimian analysis. *Journal for the Theory of Social Behaviour*, 26(1):1–33, Mar. 1996. ISSN 1468-5914. doi: 10.1111/j.1468-5914.1996.tb00283.x.

P. V. and A. Bhat. Human emotion recognition based on time–frequency analysis of multivariate EEG signal. *Knowledge-Based Systems*, 238:107867, Feb. 2022. ISSN 0950-7051. doi: 10.1016/j.knosys.2021.107867.

C. E. Valderrama and A. Sheoran. Identifying relevant EEG channels for subject-independent emotion recognition using attention network layers. *Frontiers in Psychiatry*, 16, Feb. 2025. ISSN 1664-0640. doi: 10.3389/fpsyt.2025.1494369.

K. P. Wagh and K. Vasanth. Performance evaluation of multi-channel electroencephalogram signal (EEG) based time frequency analysis for human emotion recognition. *Biomedical Signal Processing and Control*, 78:103966, Sept. 2022. ISSN 1746-8094. doi: 10.1016/j.bspc.2022.103966.

Y. Wang, W. Song, W. Tao, A. Liotta, D. Yang, X. Li, S. Gao, Y. Sun, W. Ge, W. Zhang, and W. Zhang. A systematic review on affective computing: emotion models, databases,

and recent advances. *Information Fusion*, 83–84:19–52, July 2022. ISSN 1566-2535. doi: 10.1016/j.inffus.2022.03.009.

T. M. Wani, T. S. Gunawan, S. A. A. Qadri, M. Kartiwi, and E. Ambikairajah. A comprehensive review of speech emotion recognition systems. *IEEE Access*, 9:47795–47814, 2021. ISSN 2169-3536. doi: 10.1109/access.2021.3068045.

X. Wu, W.-L. Zheng, Z. Li, and B.-L. Lu. Investigating EEG-based functional connectivity patterns for multimodal emotion recognition. *Journal of Neural Engineering*, 19(1):016012, Jan. 2022. ISSN 1741-2552. doi: 10.1088/1741-2552/ac49a7.

Y. Xie and S. Oniga. A review of processing methods and classification algorithm for EEG signal. *Carpathian Journal of Electronic and Computer Engineering*, 13(1):23–29, Sept. 2020. ISSN 2343-8908. doi: 10.2478/cjece-2020-0004.

K. Yang, L. Tong, J. Shu, N. Zhuang, B. Yan, and Y. Zeng. High gamma band EEG closely related to emotion: Evidence from functional network. *Frontiers in Human Neuroscience*, 14, Mar. 2020. ISSN 1662-5161. doi: 10.3389/fnhum.2020.00089.

E. Yildirim, Y. Kaya, and F. Kilic. A channel selection method for emotion recognition from EEG based on swarm-intelligence algorithms. *IEEE Access*, 9:109889–109902, 2021. ISSN 2169-3536. doi: 10.1109/access.2021.3100638.

G. Zhang, V. Davoodnia, and A. Etemad. PARSE: Pairwise alignment of representations in semi-supervised eeg learning for emotion recognition. *IEEE Transactions on Affective Computing*, 13(4):2185–2200, Oct. 2022. ISSN 2371-9850. doi: 10.1109/taffc.2022.3210441.

Z. Zhang, S.-h. Zhong, and Y. Liu. TorchEEGEMO: A deep learning toolbox towards EEG-based emotion recognition. *Expert Systems with Applications*, 249:123550, Sept. 2024. ISSN 0957-4174. doi: 10.1016/j.eswa.2024.123550.

W.-L. Zheng and B.-L. Lu. Investigating critical frequency bands and channels for EEG-based emotion recognition with deep neural networks. *IEEE Transactions on Autonomous Mental Development*, 7(3):162–175, Sept. 2015. ISSN 1943-0612. doi: 10.1109/tamd.2015.2431497.

W.-L. Zheng, W. Liu, Y. Lu, B.-L. Lu, and A. Cichocki. Emotionmeter: A multimodal framework for recognizing human emotions. *IEEE Transactions on Cybernetics*, 49(3): 1110–1122, Mar. 2019. ISSN 2168-2275. doi: 10.1109/tcyb.2018.2797176.

X. Zheng, X. Liu, Y. Zhang, L. Cui, and X. Yu. A portable HCI system-oriented EEG feature extraction and channel selection for emotion recognition. *International Journal of Intelligent Systems*, 36(1):152–176, Oct. 2020. ISSN 1098-111X. doi: 10.1002/int.22295.

L. Zhou, Q. Mao, X. Huang, F. Zhang, and Z. Zhang. Feature refinement: An expression-specific feature learning and fusion method for micro-expression recognition. *Pattern Recognition*, 122:108275, Feb. 2022. ISSN 0031-3203. doi: 10.1016/j.patcog.2021.108275.

N. Zhuang, Y. Zeng, L. Tong, C. Zhang, H. Zhang, and B. Yan. Emotion recognition from EEG signals using multidimensional information in EMD domain. *BioMed Research International*, 2017:1–9, 2017. ISSN 2314-6141. doi: 10.1155/2017/8317357.